MECHANISTIC INVESTIGATIONS OF THE CORROSION INHIBITION OF ECO-FRIENDLY POLYMERS OF MILD STEEL IN 3% NACL

BY

AASEM MUHAMMED NOUR ZEINO

A Dissertation Presented to the
DEANSHIP OF GRADUATE STUDIES

KING FAHD UNIVERSITY OF PETROLEUM & MINERALS

DHAHRAN, SAUDI ARABIA

In Partial Fulfillment of the
Requirements for the Degree of

DOCTOR OF PHILOSOPHY

In

CHEMISTRY

November 2017

KING FAHD UNIVERSITY OF PETROLEUM & MINERALS
DHAHRAN- 31261, SAUDI ARABIA
DEANSHIP OF GRADUATE STUDIES

This thesis, written by Aasem Zeino under the direction of his thesis advisor and approved by his thesis committee, has been presented and accepted by the Dean of Graduate Studies, in partial fulfillment of the requirements for the degree of **DOCTOR OF PHILOSOPHY IN CHEMISTRY.**

10/1/2018

Dr. Abdulaziz Al-Saadi
Department Chairman

Dr. Salam A. Zummo
Dean of Graduate Studies

10/1/2018
Date

Dr. Mazen Khaled
(Advisor)

Dr. Abdullah Abulkibash
(Member)

Dr. Bassam El-Ali
(Member)

Dr. Basheer Chanbasha
(Member)

Dr. Khaled Al-Hooshani
(Member)

Dedication

My parents: who nurtured me with love and supported me in all decisions I have ever taken, with sincere prayers.

My brothers & sisters: who loved me as I am and gave me all they have to support me.

My wife: without her support, it was difficult to complete my PhD.

My kids: for their laughs, cries and to be their model in future in adoring science.

My Syrian nation: for their courage to build our country as one of the most educated nations in the history.

ACKNOWLEDGMENT

With honest due gratitude to the almighty Allah who helped me during the 22 years education to turn my dream into reality, I take this opportunity to acknowledge my university King Fahd University of Petroleum & Minerals (KFUPM) for giving me the opportunity to pursue and accomplish the doctor of philosophy degree in chemistry in their top-ranking research laboratories. Furthermore, I would like to thank the department's chairman and administrators who have contributed in this research study.

Then, I am greatly pleased to thank my dissertation committee who have guided me through the research journey to accomplish this thesis. They are warmly gratitude: My advisor, Prof. Mazen Khaled, who has guided me through the whole research period and preparation of this report. Special thanks for my master advisor and my Ph.D. thesis committee member Prof. Abdullah Abulkibash, and warmly gratitude to the other members of Ph.D. committee Prof. Bassam El-Ali, Dr. Basheer Chanbasha and Prof. Ghassan Oweimreen for their efforts to improve this thesis in many different aspects.

Furthermore, I would like to thank my company Veolia Water for their unique positive environmental workplace during my study and for the last 11 years. Special gratitude to Dr. Badr Ghawji for his unlimited support in encouraging me to complete this Ph.D. and becoming a leader in the field of water treatment. He was a role model innovative scientist for me.

TABLE OF CONTENTS

LIST OF FIGURES

LIST OF TABLES

LIST OF ABBREVIATIONS

PASP	Polyaspartic Acid
PESA	Polyepoxy Succinic Acid
EIS	Electrochemical Impedance Spectroscopy
PD	Potentiodynamic Polarization
LPR	Linear Polarization Potential
SEM	Scanning Electron Microscope
AFM	Atomic Force Microscopy
R_p	Polarization Resistance
MPY	Mili-inch Per Year
MMY	Mili-meter per Year
EDS	Energy Dispersive Spectroscopy
ATR	Attenuated total reflectance
FTIR	Fourier Transform Infrared Spectroscopy

ABSTRACT

Full Name : Aasem Muhammed Nour Zeino
Thesis Title : Mechanistic Investigations of the Corrosion Inhibition of Eco-friendly Polymers of Mild Steel in 3% NaCl
Major Field : Analytical Chemistry
Date of Degree : November 2017

Corrosion is a major industrial problem causing dramatical financial and production losses annually. A wide range of methods were utilized in corrosion mitigation such as using corrosion inhibitors, cathodic protection, and coatings. Corrosion inhibitors are considered one of the most efficient mitigation methods for corrosion at different applications. There is an increased demand for using eco-friendly inhibitors because most of the currently used inhibitors are causing negative environmental or health impacts. Therefore, two eco-friendly polymers were investigated for their corrosion inhibition behavior and mechanism in aerated 3% NaCl for mild steel.

Corrosion inhibition mechanism of Polyaspartic acid (PASP) as eco-friendly polymer on mild steel (MS) in aerated 3% NaCl media was investigated utilizing electrochemical, thermodynamic, microscopic and computational chemistry techniques. Electrochemical results confirm moderate inhibition efficiency of PASP reaching 61% at 2.0 g/L by forming an adsorption layer on the metal surface. Zinc ion addition enhanced the efficiency to 97% at 0.5 g/L of PASP through a synergistic effect mechanism. Atomic force microscopy (AFM) and Scanning electronic microscopy (SEM) micrographs revealed the morphology of adsorption layer which indicate anodic inhibition mechanism of PASP. Quantum calculation and Monte Carlo simulation provided molecular level insights into the adsorption points in PASP structure showing HOMO and LUMO orbitals can donate or accept electron from the steel surface. The outputs of this study helped in understanding the inhibitive mechanism of PASP on steel surface which were consistent with the experimental findings.

Corrosion inhibition mechanism of Polyepoxy succinic acid (PESA) as eco-friendly polymer having COOH functional groups on mild steel in aerated 3% NaCl solution was investigated utilizing electrochemical, thermodynamic, microscopic and computational chemistry techniques. Electrochemical results confirm moderate inhibition efficiency of PESA reaching 60.6% at 2.0 g/L by forming an adsorption layer on the metal surface. Zinc ions addition at 2 mg/l to the solution had enhanced the efficiency to 92.2% at 2.0 g/L of PESA through a synergistic effect mechanism. Scanning electronic microscopy (SEM) and Atomic force microscopy (AFM) micrographs revealed the morphology of adsorption layer indicates anodic inhibition mechanism of PESA with remarkably high binding energy. Quantum calculation and Monte Carlo simulation provided molecular level insights into the adsorption area of carboxylic groups in PESA through showing HOMO and LUMO orbitals can donate or accept electron from the d-orbitals in mild steel surface. The outputs showed that COOH groups are functioning efficiently in the inhibitive mechanism of PESA on steel surface with a high bonding energy, which is consistent with the experimental findings.

ملخص الرسالة

الاسم الكامل: عاصم محمد نور زينو

عنوان الرسالة: دراسة ميكانيكية وآلية منع التآكل لبوليميرات صديقة للبيئة على الحديد في محلول ٣% كلوريد الصوديوم

التخصص: كيمياء تحليلية

تاريخ الدرجة العلمية: نوفمبر ٢٠١٧

يعتبر التآكل واحداً من أهم المشاكل الصناعية التي تسبب خسارةً ماديةً وإنتاجيةً معتبرةً سنوياً، واستخدمت العديد من التقنيات والوسائل لعلاج هذه الظاهرة كمثل استخدام مانعات التآكل، الحماية الكاثودية، واستخدام الطلاء. تعتبر المواد الكيميائية مانعات التآكل واحدةً من أهم وأنجح الطرق المستخدمة في علاج التآكل في تطبيقات مختلفة، وهناك طلب متزايد لاستخدام مواد كيميائية مانعة للتآكل صديقة للبيئة حيث أن أغلب المواد المستخدمة حالياً لها آثار جانبية ضارة إما على البيئة أو الصحة. وبناءً على ذلك فقد قمنا بدراسة وتحليل نوعين من البوليمرات وتقييم أدائهم وسلوكهم وآليتهم في منع التآكل في محلول ٣% من كلوريد الصوديوم مع إدخال الهواء على معدن الحديد اللين (mild steel).

تم دراسة آلية منع التآكل لبوليمير (Poly aspartic acid – PASP) كبوليمير صديق للبيئة على الحديد في محلول ٣% من كلوريد الصوديوم باستخدام تقنيات كيميائية كهربائية، ثرموديناميكية، مجهرية وطرق كيميائية حسابية. أثبتت نتائج الدراسة الكيميائية الكهربائية بأن هذا البوليمير له قدرة على منع تآكل الحديد تصل إلى ٦١% عند جرعة ٢ غ/لتر من خلال تشكيل طبقة عازلة ممتصة على سطح المعدن، كما لوحظ أن إضافة أيونات الزنك إلى المحلول تزيد من كفاءة منع التآكل لتصل إلى ٩٧% عند جرعة ٠,٥ غ/لتر من خلال آلية التأثير التعاوني لكلا المادتين. واستطاعت صور الطرق المجهرية مثل المجهر الإلكتروني الماسح (scanning electron microscope) ومجهر القوة الذرية (atomic force microscopy) إثبات وجود طبقة من البوليمير مانع التآكل (PASP) على سطح المعدن كنوع من إثبات آليته. وأخيراً قمنا باستخدام الطرق الكيمائية الحسابية والمحاكاة من نوع (Monte Carlo) والتي قدمت تفاصيل جزيئية عميقة على ميكانيكية

وآلية الامتصاص للبوليمير على سطح المعدن وإثبات قابلية هذا البوليمير للعمل كمادة مانعة للتآكل مما يتوافق مع النتائج المقدمة من الجزء الاختبارات المخبرية.

تم دراسة آلية منع التآكل لبوليمير (Poly epoxysuccinic acid – PESA) كبوليمير صديق للبيئة على الحديد في محلول ٣% من كلوريد الصوديوم باستخدام تقنيات كيميائية كهربائية، ثرموديناميكية، مجهرية وطرق كيميائية حسابية. أثبتت نتائج الدراسة الكيميائية الكهربائية بأن هذا البوليمير له قدرة على منع تآكل الحديد تصل إلى ٦٠,٦% عند جرعة ٢ غ/لتر من خلال تشكيل طبقة عازلة ممتصة على سطح المعدن، كما لوحظ أن إضافة أيونات الزنك بتركيز ٢مغ/ لتر إلى المحلول تزيد من كفاءة منع التآكل لتصل إلى ٩٢,٢% عند جرعة ٠,٥ غ/لتر من خلال آلية التأثير التعاوني لكلا المادتين. واستطاعت صور الطرق المجهرية مثل المجهر الإلكتروني الماسح (scanning electron microscope) ومجهر القوة الذرية (atomic force microscopy) إثبات وجود طبقة من البوليمير مانع التآكل (PESA) على سطح المعدن كنوع من إثبات آليته. وأخيراً قمنا باستخدام الطرق الكيمائية الحسابية والمحاكاة من نوع (Monte Carlo) والتي قدمت تفاصيل جزيئية عميقة على ميكانيكية وآلية الامتصاص للبوليمير على سطح المعدن وإثبات قابلية هذا البوليمير للعمل كمادة مانعة للتآكل مما يتوافق مع النتائج المقدمة من الجزء الاختبارات المخبرية.

CHAPTER 1

INTRODUCTION

1.1 Corrosion of Mild Steel

Corrosion in principle can be defined in chemistry as the electrochemical reaction of a metal with its surrounding environment, causing an irreversible steady deterioration in the metal, in both physical and chemical properties [1]. From the chemistry perspective, corrosion is an electrochemical reaction involving the movement of electrons as simplified in Figure 1. Corrosion could cause remarkable losses in materials and economies due to a partial or total replacement of structure and equipment in addition to system’s shutdowns. NACE International has released a two-year study estimates the recent global cost of corrosion in 2016 to be US$2.5 trillion which is equivalent to approximately 3.4 % of the global Gross Domestic Product (GDP). This statistical study revealed also that implementing corrosion mitigation methods can result in annual savings globally between 15-35 % of the cost of damage which equals approximately US $375-875 billion annually [2].

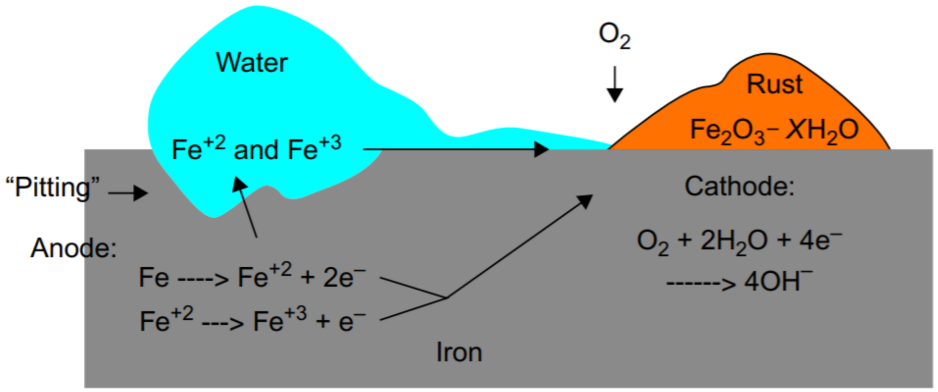

Figure 1: simple representation of corrosion cell [3]

Mild steel is the most commonly used metallurgy in our life due to its mechanical outstanding properties and low capital cost. The major drawback of mild steel is its low corrosion resistance. However, corrosion of mild steel occurs in almost all environments whether industrial or municipal. Brackish or saline waters are commonly used in different water industrial processes such as cooling systems, distribution networks, and HVAC systems. Due to the aggressiveness of brackish and saline waters, mild and carbon steels corrode harshly during in such processes [4]. Mild steel and other carbon steel metallurgies consist of two dominant phases (ferrite and pearlite) and some MnS type inclusions as shown in the SEM micrograph in Figure 2, which reflects different corrosion resistance mapping on steel surface [5].

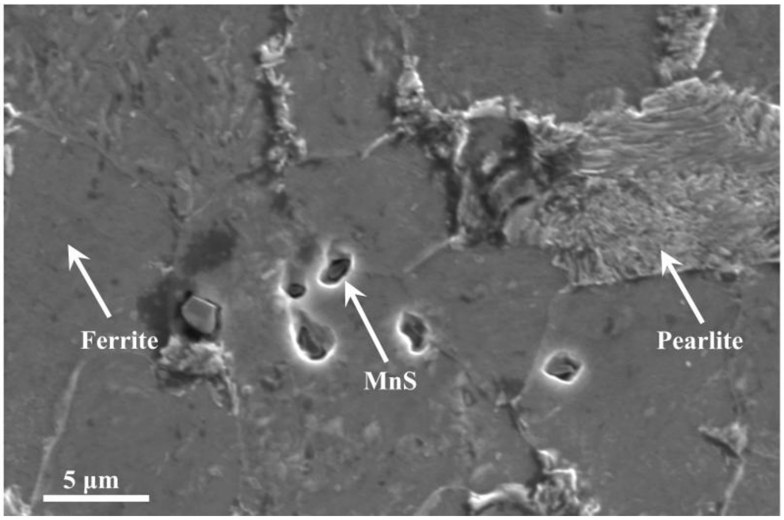

Figure 2: SEM micrograph of an etched carbon steel surface [5]

Several techniques are utilized to control corrosion in water industry such as:

a. Corrosion Inhibitors: these chemical materials are added in relatively small concentrations (mg/l) to a corrosive environment in order to decrease metal’s corrosion rate efficiently. This method is widely implemented in the industrial applications such as for pipelines, vessels and equipment and generally for all industrial applications related to water treatment [6].

b. Cathodic protection: this efficient method is used to control corrosion on steel structures either immersed or buried in water or underground soil (electrolyte).

c. Protection with the anticorrosive coating: this is principally used in order to form a physical barrier between the metal and the corrosive environment to protect the metallic part. It is widely used in steel structures subjected to open corrosive environments.

Among these mitigation methods applied to minimize corrosion, the corrosion inhibitor is considered the most commonly used and economic method to mitigate corrosion [7].

1.2 Brackish Water

Brackish water is commonly utilized water for the industrial applications especially ones related to cooling systems. Cooling towers, HVAC systems, and other industrial processes are using brackish water as a source of cooling media. Brackish water is different from seawater and potable water in its chemical composition of components. The main constituents of brackish water are Cl^-, Na^+, SO^{-2}, HCO_3^- and Ca^{+2}, where chloride and sulfate ions play a major role in pitting corrosion of mild steel structures. Therefore, many corrosion inhibition studies were conducted on 3% NaCl to represent the most dominant constituents in brackish water trigger different types of corrosion in water systems. Figure 3 shows an example of 3D analysis of steel surface having two types of corrosion take place in the non-inhibited sample [8].

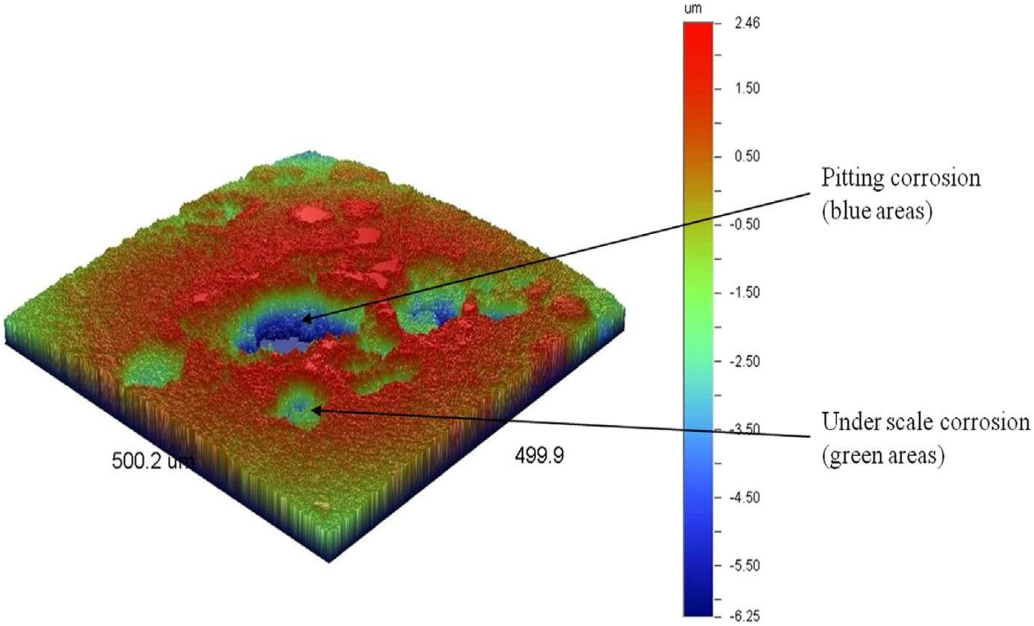

Figure 3: 3D analysis of a non-inhibited sample having two types of corrosion

1.3 Corrosion Inhibitors

As defined earlier, corrosion inhibitors are chemical formulations added in relatively small amounts to a corrosive environment to minimize the corrosion rates of the metallic corrosion. The selection of suitable inhibitors is subjected to the economic feasibility, environmental considerations, applied concentration, process temperature, water media and the type of metallurgy should be protected [9]. They can minimize corrosion rates following one of the below mechanisms [10]:

(i) decreasing or increasing the anodic and/or cathodic reaction rates

(ii) adsorption of ions or molecules onto the metal surface

(iii) decreasing the diffusion rate of the reactants to the metal surface

(iv) decreasing the electrical resistance of the metal surface.

Generally, inhibitors that can be easily applied to that corrosive environment and have in situ application are having advantages over others.

The inhibitors include inorganic inhibitors, organic inhibitors, and polymeric inhibitors.

Inorganic inhibitors are those ones based on inorganic compounds in which the active substance is an inorganic compound. These inhibitors are used to build and enhance the passive layer on a metal surface and minimize corrosion. These ions having a positive potential more than the target metal should be protected, and more positive potential to overcome the potential for discharging a proton and the surface metal will be protected [11]. The most commonly implemented in the industry of these are chromate (CrO_4^{-2}), nitrate (NO_3^-), molybdate (MoO_3^-), phosphate (PO_4^{-3}) and silicates (SiO_3^{-2}) [12].

Organic inhibitors are noticeably used in different industrial processes in respect of their tendency to build a protective layer on the metal surface at different media. Generally, organic inhibitors have heteroatoms: P, N, S, and O that having higher basicity and electron donor abilities. There are a list of these inhibitors belong to different chemical groups such as pyridines, fatty amides, imidazolines, 1,3-azoles, and polymers as a new category of organic inhibitors have shown promising performance under particular testing conditions [13]–[15].

Polymeric inhibitors are newly used in corrosion inhibition and can be applied in wide range of conditions. The most known inhibitors are polyvinyls and polyesters. Table 1 shows some examples of organic and polymeric inhibitors [16].

Table 1: Some organic and polymeric inhibitors

Name	**Structure**	**Application**
Primary amines - Alkylamines (n = 2-12)	R-NH2	Inhibitor for acid media
Primary amines - cyclic	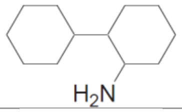	Inhibitor of acid media
Pyridines	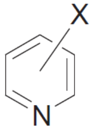 X = CH_3, Br, OR	Inhibitor of steel under acidic media
Polyvinyls	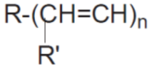 $R\text{-}(\underset{R'}{CH}=CH)_n$ R, R' = alkyl, aryl, heterocyclics	Inhibitor of carbon steel in acidic media
Polyesters	R-CO-OR'	Inhibitor of carbon steel in acidic media

Polymeric materials can act as corrosion inhibitors for mild steel through their functional groups by forming complexes with iron on the metal surface. Such chemical complexes build large surface areas, herewith blanketing the metal surface and protecting it from the corrosive environment. Both cationic polymeric inhibitors including polyacrylamide derivative, polyethyleneimine derivative, polydicyanodiamide derivative; and anionic polymeric inhibitors including polyacrylic acid derivative, polymaleic acid derivative, and polyacrylic acid were studied. They found that polymers having COOH group can function as effective corrosion inhibitors [16]. Many other studies showed that polymethacrylic acid, polyethylene oxide, amino polycarboxylic acids, polyacrylamide, and carboxymethyl cellulose (CMC) functioning as inhibitors in different corrosive media [17] [18] [19].

1.4 Green Inhibitors

These corrosion inhibitors are considered eco-friendly substances that do not contain heavy metals or organic poisonous compounds. The term green inhibitor or eco-friendly inhibitor represents the substances that have an acceptable biocompatibility with the environment and does not affect negatively the environment or its species. In the 21st century, the issue of biodegradability has been highlighted as an important parameter for limiting chemical accumulation in the environment. Biodegradability as a definition is the ability of a chemical to be broken down into small, non-toxic small components by the action of microorganisms and fungi [20]. Table 2 gives some examples of green natural corrosion inhibitors used for steel metals. However, most of these green natural inhibitors are not suitable for mass production of industrial applications and limited to research interests. Unfortunately, most of these natural inhibitors were not studied for their inhibition mechanism and only evaluated under moderate corrosive conditions.

Table 2: Examples of green corrosion inhibitors are used for corrosion

Metal	Inhibitor Source	Active Ingredient	Reference
Steel	Tea leaves	---	[21]
Steel	Eucalyptus oil	Monomtrene 1,8-cineole	[22]
Mild steel	Gum exudate	Hexuronic acid, neutral sugar residues, canaric, volatile monoterpenes, and related triterpene acids, reducing and nonreducing sugars	[23]
Mild steel	Chitosan	---	[24]
Mild steel	Caffeic acid	---	[25]

However, the green polymeric corrosion inhibitor is quite a new field of study and requires more concentration in order to find proper ones working in various corrosive environments for water treatment applications. Chapter two gives more insights on the literature review of this type of inhibitors. The polymers which will be studied in this research are polyaspartic acid (PASP) and polyepoxy succinic acid (PESA) which were proofed earlier their scale inhibition properties for different scales and other water treatment applications. These polymers were recently produced in mass quantity for different application and they could be promising green corrosion inhibitors for mild steel in water systems.

1.5 Problem Definition

Many of the traditionally used corrosion inhibitors showed either environmental or toxicological negative impacts which are leading them to ban such as chromate, nitrites, phosphonates, phosphates, and molybdate. Most of the natural green inhibitors can’t be produced in a mass quantity which could be implemented in the water industry. In addition, that these inhibitors were not evaluated under industrial water conditions in order to evaluate their real inhibitive behavior. Thus, thinking of the new generation of polymeric inhibitor could be an adopted potential solution considering green criterion of polymers and economic considerations of production and application.

The polymers PASP and PESA have been recently produced in mass quantity with cost-effective economics after they presented their effective $CaCO_3$ scale inhibition and general dispersion applications in water treatment industry. In addition, they are matching the international regulations of green chemicals and can possess multifunctional polymers in water systems.

We have a target to challenge present practices. Therefore, our target is to develop new polymeric corrosion inhibitors are able to work in strong corrosive environments and suitable for water treatment industry. Therefore, we will study the corrosion inhibition properties of two new green polymers under a strong corrosive environment of 3% NaCl solution with air bubbling using different analytical techniques. This study will draw a comprehensive understanding to elucidate the mechanism and inhibitive performance of two potential green inhibitors. The promising horizon in studying polymers that they could have multifunction in water systems such as scale inhibitor and corrosion inhibitor in parallel. This research could be a base ground for future researchers improving green polymers in order to be utilized in industrial water treatment applications.

1.6 Aims and Objectives

According to the aforementioned introduction, the aim of this work is to gain more insights about corrosion inhibition mechanism for the two newly discovered eco-friendly polymeric inhibitors in order to add new scientific values in this field. The main motivation for this study is to apply these findings directly in water treatment industrial applications. The research objectives can be organized as below:

1- Performing gravimetrical tests (weight loss methodology) of corrosion inhibitors at different inhibitor’s concentrations and temperatures in order to calculate corrosion efficiency (EI %) and corrosion rates of mild steel in 3% NaCl solution.

2- Studying corrosion properties and inhibition effect (EI %) of the polymeric inhibitors using potentiodynamic polarization (PDP) technique under various conditions of concentration and mixtures.

3- Investigating the corrosion properties and inhibition mechanism of the polymers for mild steel in aerated 3% NaCl media, utilizing electrochemical impedance spectroscopy (EIS) at different concentrations of polymers.

4- Performing the thermodynamic calculations on the inhibitive behavior of both polymers in order to get the basic thermodynamic parameters.

5- Studying the corrosion inhibition mechanism of these polymers using different techniques for surface characterization.

6- Studying the computational quantum calculations and Monte-Carlo simulation to gain molecular-level insights into the adsorption mechanism of the polymers on mild steel surface

7- Comparing the results of these inhibitors with other polymer ones recently used in mild steel corrosion inhibition at similar or different media.

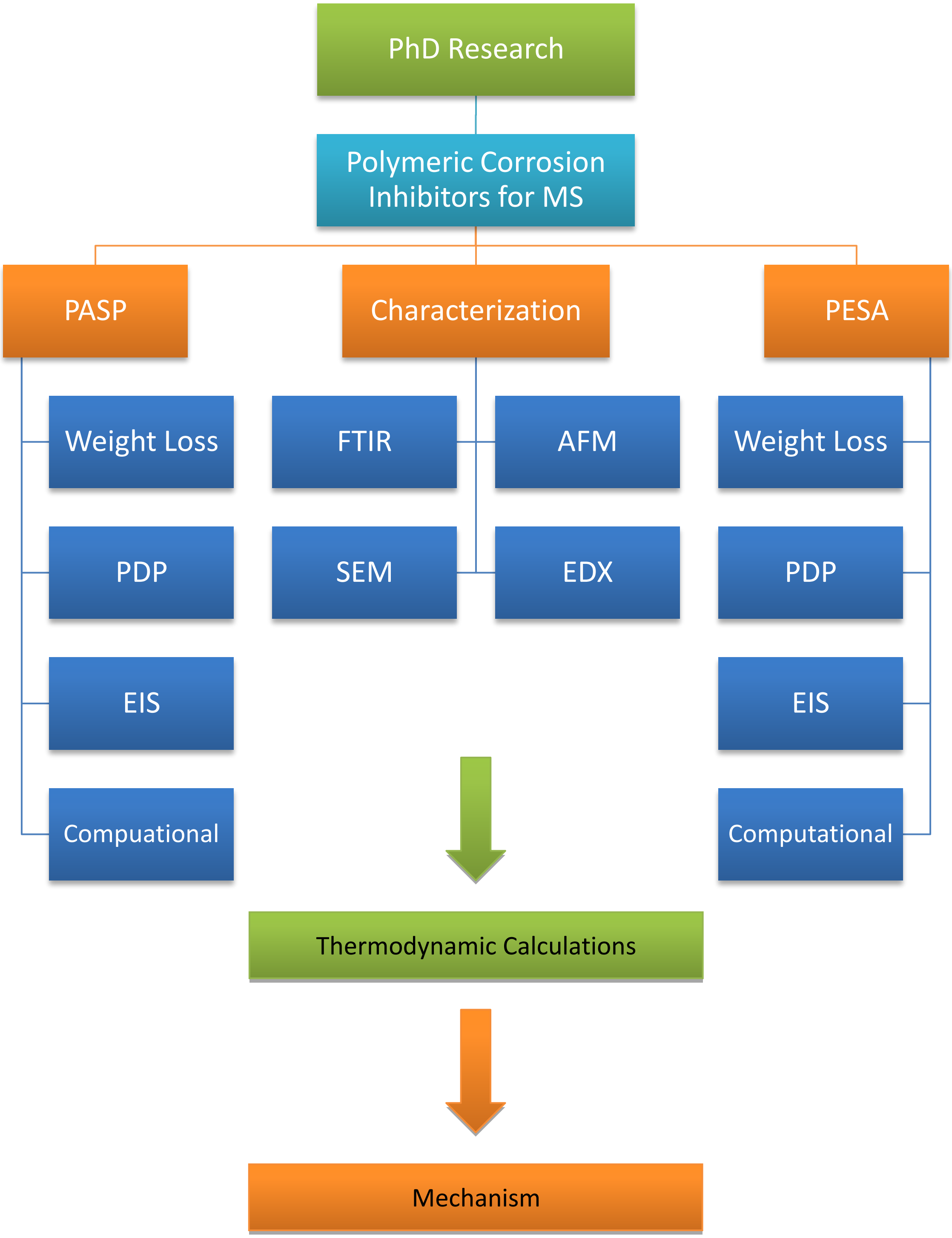
PhD Research
Polymeric Corrosion Inhibitors for MS
PASP
Characterization
PESA
Weight Loss
FTIR
AFM
Weight Loss
PDP
SEM
EDX
PDP
EIS
EIS
Compuational
Computational
Thermodynamic Calculations
Mechanism

1.7 The Overview

The main goal of this study is to study the corrosion inhibition efficiency of two environmentally friendly polymers called PASP and PESA and understand their inhibition mechanism using electrochemical analytical methods.

Chapter 2 gives overview literature review of a wide range of studies have investigated the corrosion inhibition properties of PASP and PESA in order to gain insights into their preliminary performance. This review will include also the reasons why we have selected these polymers and their chemical synthesis and current applications in the field of water treatments. Also, a basic background is given for each technique used in this study including the electrochemical analytical techniques, characterization methods, and computational calculations.

Chapter 3 focuses on the experimental details of the designed work and the design of three-electrodes cell used for the electrochemical experiments. In addition, this chapter gives the chemical details of the used polymers and testing solutions. The characterization techniques used to confirm the inhibition mechanism of the polymers have been investigated. This chapter also gives the instrument setup details of the electrochemical measurements. This chapter presents the basic setup of computational calculations and Monte Carlo simulation.

Chapter 4 presents the results and the discussion of the performance of these two polymers on mild steel using basic weight loss and different electrochemical techniques including Tafel and

EIS. The thermodynamic calculation and figures will be discussed and presented in plots in order to get the basic thermodynamic parameters. Chapter 4 also shows the output findings of DFT computational results for PASP and PESA and their Monte Carlo simulation on mild steel corrosion inhibition. Finally, the suggested mechanism will be presented and discussed of the inhibitive performance of PASP and PESA in the absence and presence of zinc ions. Chapter 5 concludes the experimental part and present the conclusions obtained in this study

CHAPTER 2

LITERATURE REVIEW

2.1 Polyaspartic Acid (PASP)

Polyaspartic acid (PASP) is a promising non-toxic and highly biodegradable anionic polypeptide used widely in different industries such as biomedical applications, paper processing, paint, and water treatments [26]. Figure 4 shows the chemical structure of PASP and its repeating units. PASP could be synthesized using many methods. The main methods are through the hydrolysis of polysuccinimide (PSA) or through the thermal polymerization of L-aspartic acid in the presence or absence of a catalyst. Figure 5 shows the synthesis reaction of PASP using thermal polymerization of L-aspartic acid in the absence of a catalyst and forming α-PASP and β-PASP moieties.

The commercial production of PASP by the thermal polymerization of L-aspartic acid has resulted in excellent yield and is environmental attractive because it uses only amino acid as a reactant and has no solvent use. This synthesis is extremely cost-effective to be scaled up for mass production without forming any environmental pollution. Additionally it meets biodegradability and non-toxicity regulations of polymers [27] [28] [29] [30] [31] [32].

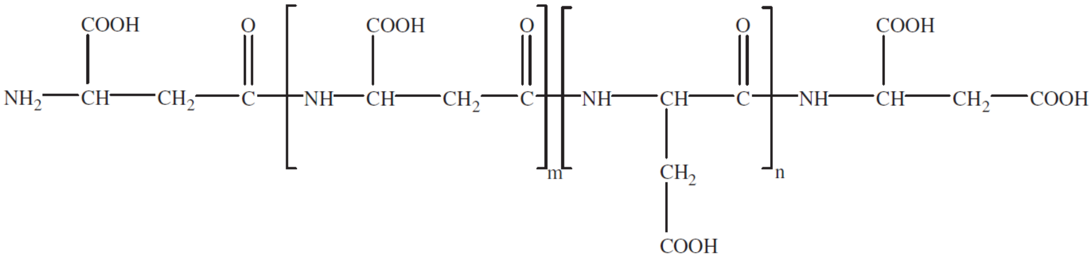

Figure 4: chemical structure of PASP and its repeating units

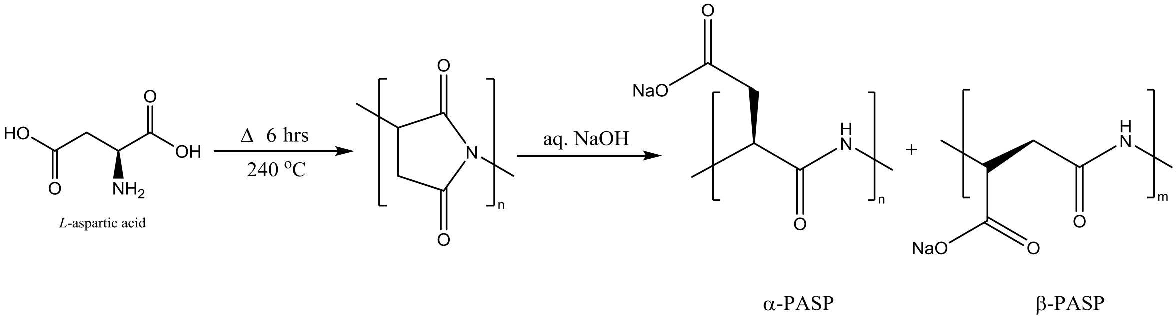

Figure 5: Synthesis reaction of PASP using thermal polymerization of L-aspartic acid

2.1.1 PASP as Scale Inhibitor

PASP as a known eco-friendly (green) scale inhibitor has raised remarkable interest because it has no toxicity and excellent biodegradability. In addition, PASP structure contains carboxylic and amide groups having good chelating and dispersibility functionality [33]. It is found in laboratory conditions that PASP biodegradability prepared from poly(succinimide) by thermal condensation has reached 70% within 30 days [34]. Martinod et al. used in their work chronoamperometry at room temperature in order to study the behavior of PASP on scaling inhibition in brines reproducing the composition of North Sea, where the Ca^{+2} concentration was 14,225 mg/L [35]. The results revealed that under such conditions, 4 mg/L of PASP had shown a significant reduction of produced weight of calcium carbonate scales. Furthermore, microscopic micrographs presented that PASP had modified the crystal morphology and led to vaterite formation. In a more recent study under similar experimental conditions, the chemical interaction between PASP and stainless steel (SS) interface of a working electrode was studied through coupling the electrochemical generation of $CaCO_3$ with microscopic observations. The results revealed that at low dosage of PASP, it has reduced the surface coverage of deposits on the substrate. Furthermore, PASP remarkably decreased the growth rate of CaCO3 crystals through blocking the active sites of crystal growth [36]. In another study, PASP exhibited very good scale inhibition performance reaching 95% for $CaCP_3$ and 90% for $cCaSO_4$ by applying a dosage of 5 ppm of PASP in a synthetic brackish water [37].

Recently, a study was conducted using static tests to evaluate the efficiency of PASP polymer in a diluted mineral water (Ca^{+2} 253 mg/L concentration) at 80 °C. Under these conditions, the inhibition efficiency of scale using PASP reached 80% for a dosage of 12 mg/L. Furthermore, Rapid Controlled Precipitation (RCP) test was conducted at 30 °C and revealed that a dosage of 0.3 mg/L of PASP was perfect to stop efficiently the precipitation of calcium carbonate. SEM and XRD tests presented some modifications were observed in the crystalline morphology after PASP addition, thus retarding the formation of precipitates [38]. Figure 6 shows the crystalline structure of $CaCO_3$ in the presence and absence of PASP.

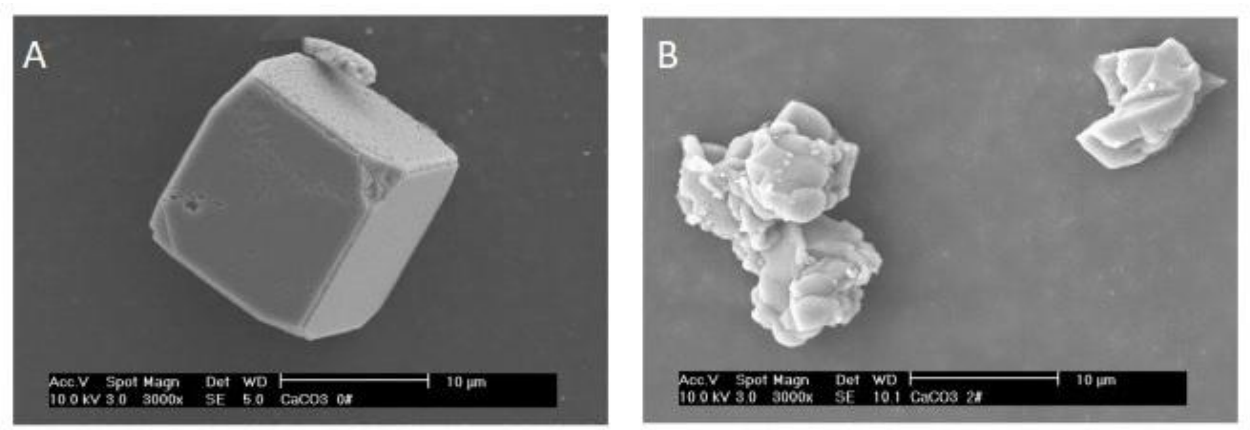

Figure 6: SEM images of CaCO3 crystals in the (A) absence of PASP (B) presence of PASP [38]

Nevertheless, the comprehensive inhibition performance of scales using PASP was not prominent when used for seawater and other stressed conditions, which limits its use in some applications [39]. Thus, to improve PASP inhibitive performance, studies on modified PASP have been carried out. Numerous efforts have been made to introduce new functional groups on the side chain of polyaspartic acid, such as hydroxyl group, carboxylic group, sulfonic group, and phosphonyl [40]. For inistance, Xu and his coworkers produced polyaspartic acid–melamine grafted copolymer through ring opening of polysuccinimide (PSI) with melamine [41]. Senthilmurugan et al. had synthesized maleic acid copolymers between acrylic acid (MA–AA) and ortho toluidine (MA–OT) and this copolymer had presented its efficient $CaCO_3$ scale inhibition [42]. However, even though such studies has improved the inhibition of scales using PASP, there are some problems associated including that those monomers are not easily biodegradable or their degradation products are poisonous, which doesn't support definition of green inhibitor.

2.1.2 PASP as Corrosion Inhibitor

Many researchers have evaluated PASP in the corrosion inhibition properties of steel or copper metals under different media. Additionally, PASP was studied and patented for its corrosion inhibition properties in sweet carbon dioxide environment and corrosion at the strong acidic condition and brine solution with no dissolved oxygen [43]. It is found in several types of research that the effective concentration of the inhibitor can be between 10 ppm to 5000 ppm which depends on several factors such as the media and temperature. It was observed that PASP with a molecular weight 5000 has corrosion efficiency 40% at room temperature. However, the inhibition efficiency has increased with the temperature raised to 50 ^{o}C.

To improve the performance of PASP, several studies on the modified PASP were conducted. The concept of this modification is introducing new functional groups on the PASP side chain such as hydroxyl, sulfonic, carboxylic, and phosphonyl groups [40]. PASP could be connected with some amino thiol or disulfide compounds as in structure of Figure 7 to improve its inhibition characteristics, where Rs correspond to various hydrocarbyl groups; and Z could be a hydrogen bond of a thiol compound or a covalent bond produces a disulfide molecule [44].

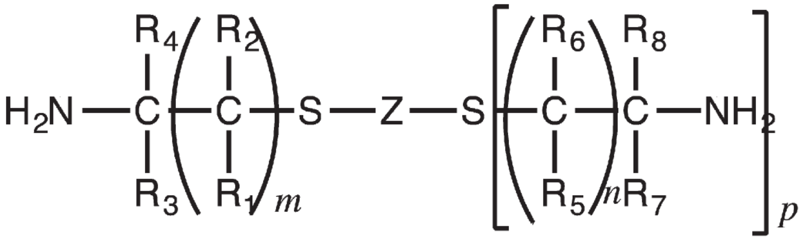

Figure 7: Corrosion inhibitor of Polyaspartate-based having thiol and disulfide functionalities

Table 3 shows a list of literature review and studies were conducted on PASP or its derivatives and the basic results found. The absent part in the previous researches is the mechanistic behavior of PASP in carbon or mild steels under variant mediums which will help researchers to understand the mechanism and would be able to improve it. For instance, an addition of iodide (I^-

) ion had improved the efficiency noticeably in acidic conditions, while no proof if a similar improved efficiency can be done under corrosive seawater media. No previous quantum or computational simulation studies were conducted on PASP in order to identify its adsorption points. Furthermore, it could be noticeable from this literature review that PASP is quite new polymeric material has potential promising applications in water treatment as it possesses multifunctional properties in corrosion and scale inhibition in addition to its dispersion function. Therefore, we have done extensive study to evaluate PASP corrosion inhibitive mechanism with computation

Table 3: Shows a literature review and list of studies conducted on PASP or its derivatives with main outputs.

Metal	Inhibitor	Media	Findings	Year	Ref.
Carbon steel	PASP	0.5 M H_2SO_4	• The efficiency is 80.33% at 6 g/L inhibitor concentration at 10 ^oC. • PASP showed Freundlich isotherm behavior. • Decreases anodic currents	2011	[29]
Mild steel	PASP + I^-	0.5 M H_2SO_4	• The efficiency is 87.9% achieved at 2 g/L PASP concentration at 30 ^oC. • The efficiency increased to 96.3% at 2 g/L PASP concentration + 1 mM KI at 30 ^oC. • Decreases cathodic currents	2013	[45]
Carbon steel	PASP/5-aminoorotic acid (AOA)	Synthetic solution	• PASP/5-AOA showed excellent inhibition properties for $CaCO_3$ and $Ca_3(PO_4)_2$ • The efficiency of PASP/5-AOA was ~ 100% against $CaCO_3$ of 1 mg/L dosage. • The efficiency of corrosion inhibition was ~ 60% at 12 mg/L dosage.	2013	[46]
Copper	PASP-imidazole	3% aminosulfonic acid	• Corrosion inhibition efficiency was 89.8% for 1 g/L PASP at 30 ^oC. • Corrosion inhibition efficiency was 95.4% for 1 g/L PASP/IM for 1:1 ratio.	2013	[47]
WE43 magnesium alloy	PASP	3.5% NaCl	• PASP has good corrosion inhibition performance for WE43 Mg alloy using electrochemical techniques. • Corrosion inhibition efficiency was 94.2% at 400 ppm concentration of PASP.	2015	[48]
Carbon steel	PASP-SEA-ASP	Seawater	• Corrosion inhibition efficiency was 49% at 100 ppm concentration.	2015	[49]
Carbon steel	Glycine-PASP	Seawater	• Corrosion inhibition efficiency was 83.8% at 250 ppm concentration.	2016	[50]
Carbon steel	PASP/2 amino-2 methyl-1 propanol	Synthetic solution	• The efficiency ~ 100% for PASP/AMP against $CaCO_3$, $CaSO_4$, and $Ca_3(PO_4)_2$ got achieved at dosages of 1, 4, and 14 mg L^{-1}, respectively. • Inhibition efficiency of corrosion for CS is ~ 28% at 24 mg/L dosage.	2017	[51]
Carbon steel	Valine-PASP	Seawater	• Corrosion inhibition efficiency for Val-PASP was 86.94% at 250 ppm dose. • scale inhibition efficiency reaches 92.3% at 125 ppm dose.	2017	[52]

2.2 Polyepoxysuccinic Acid (PESA)

Polyepoxysuccinic acid (PESA) is one of the new promising polymers has a wide range of potential applications due to its unique features. PESA has promising properties on scale inhibition, high biodegradability, dispersion, and broad application prospect [53]. PESA is a non-phosphorus, eco-friendly, and nitrogen free polymer developed first by the Betz laboratory and Proctor & Gamble Co in the US. in the early nineteens of 20th century. Different studies showed its unique scale inhibition performance and feature $CaCO_3$ and $Ca_3(PO_4)_2$ [54]. Furthermore, PESA was tested and implemented in reverse osmosis desalination plants. Nowadays, PESA has gained the interest of researchers in eco-friendly inhibitors [55].

2.2.1 Properties of PESA

PESA has been proven to have large molecular, good water-soluble, non-toxic, and biodegradable features, and its chemical backbone is shown in Figure 8. PESA polymer is synthesized by dissolving maleic anhydride in deionized water under heating conditions and dripping of NaOH solution forming sodium maleate. Then sodium tungstate and hydrogen peroxide are added and keeping the temperature at 70°C till getting epoxysuccinic acid. Finally, NaOH particles are charged as initiator with 1-hour heating at 70°C till obtaining the polymerized PESA, which is a light yellow viscous liquid. Figure 9 shows the chemical reaction synthesis of PESA [54][56].

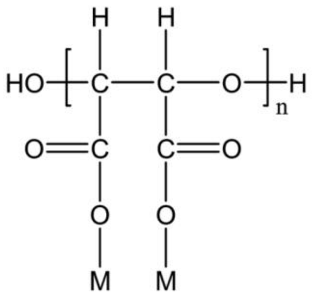

Notes: n=2-10, M: Na^+, H^+, K^+ or NH_4^+

Figure 8: Chemical structure of PESA

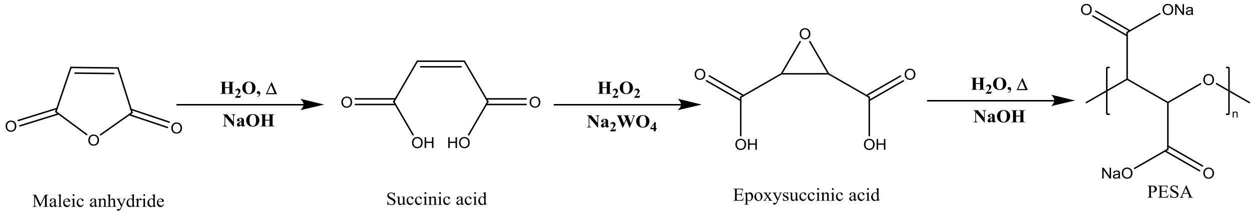

Figure 9: Chemical reaction synthesis of PESA

2.2.2 PESA as Scale Inhibitor and Water Treatments

PESA is considered a new polymeric material with few studies showing its performance in water treatment and desalination applications. In 2009, PESA was studied in cadmium and heavy metals extraction from sewage sludge in China with good extraction efficiency depending on solution pH value. The efficiency of extraction has reached > 70% for a pH range between 1 to 7. The maximum extraction efficiency resulted from this study was around 78% [57]. Similarly, PESA was studied for chromium removal from sewage sludge and showed better extraction efficiency than the one using *S, S*-ethylenediaminedisuccinic acid (EDDS) and ethylenediaminetetraacetic acid (EDTA) under similar experimental conditions. The efficiency of extraction was reached approximately 58% when pH value was 4.0 and a ratio of PESA to total heavy metals of 10:1, and was kept achieved above 40% within a pH range between 1 to 7 at a high ratio of PESA to total heavy metals of 10:1 [58].

An important study in 2009 evaluated the performance of PESA as a scale inhibitor in reverse osmosis desalination plant in static and dynamic methods. PESA presented strong scale inhibition in the static study with different types of scales such as $CaCO_3$, $CaSO_4$, $BaSO_4$ and $SrSO_4$ with an average inhibition efficiency 90% at a dosage 10 mg/l. Figure 10 shows the inhibition efficiencies of PESA for studied scales [55].

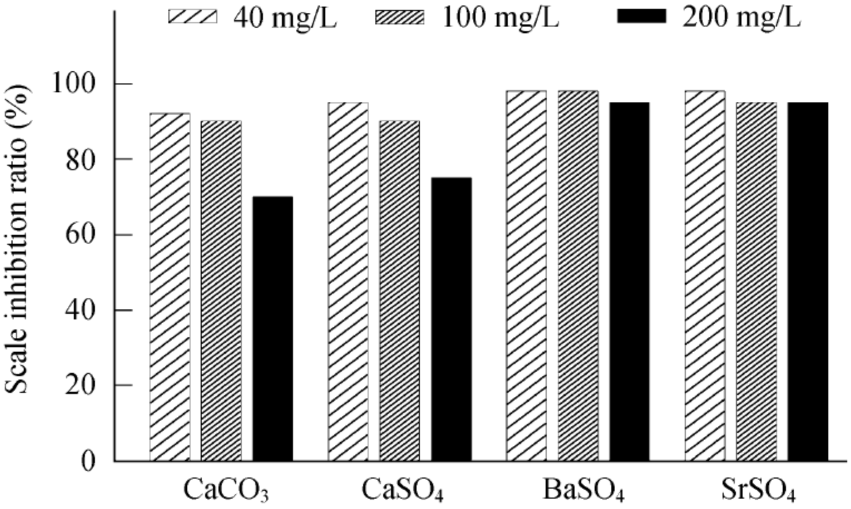

Figure 10: The inhibition efficiencies of PESA for different types of scales [55]

A study in 2011 evaluated the scale inhibition and dispersion of PESA was produced. It showed that PESA possesses excellent scale inhibition properties for $CaCO_3$ and $Ca_3(PO_4)_2$ and outstanding dispersion functionality for ferric oxide. The examined water consists of 500-1200 mg/L hardness, 1000 mg/L alkalinity, and 31.2 mg/L dosage of PESA, the results showed a scale inhibition ratio reaching up to 85%. While when the dosage of PESA is 20.8 mg/l, inhibition ratio on $Ca_3(PO_4)_2$ reached 38.9%, and at the optimum dosage 9.1 mg/l of PESA, the stability ratio was > 96%. This study revealed that PESA is an effective and versatile inhibitor could be used in desalination plants. Figure 11 shows the effect of PESA concentration on the inhibition efficiency for $CaCO_3$ and $Ca_3(PO_4)_2$ [54].

In 2012, a final study was conducted to evaluate PESA and PASP on their scale inhibition properties for different scales by static and rapid precipitation controlled methods. Briefly, the results showed that the inhibition efficiency of PESA was superior to that of PASP for $CaCO_3$, and the concentration of PESA needed to attain the same efficiency was lower than that of PASP. Figure 12 shows SEM images of $CaCO_3$ scale in the absence and presence of PESA.

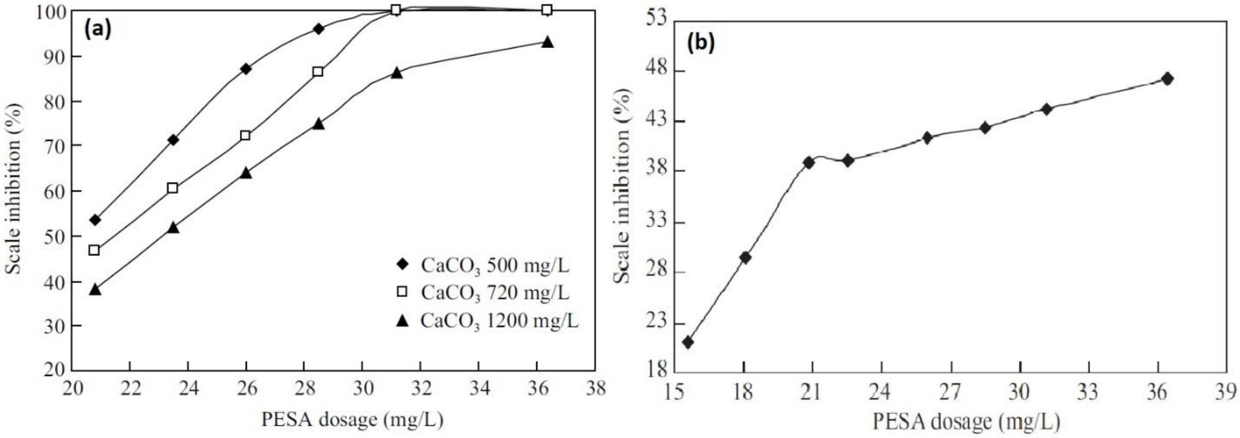

Figure 11: Effect of PESA concentration on the inhibition efficiency for (a) $CaCO_3$ (b) $Ca_3(PO_4)_2$

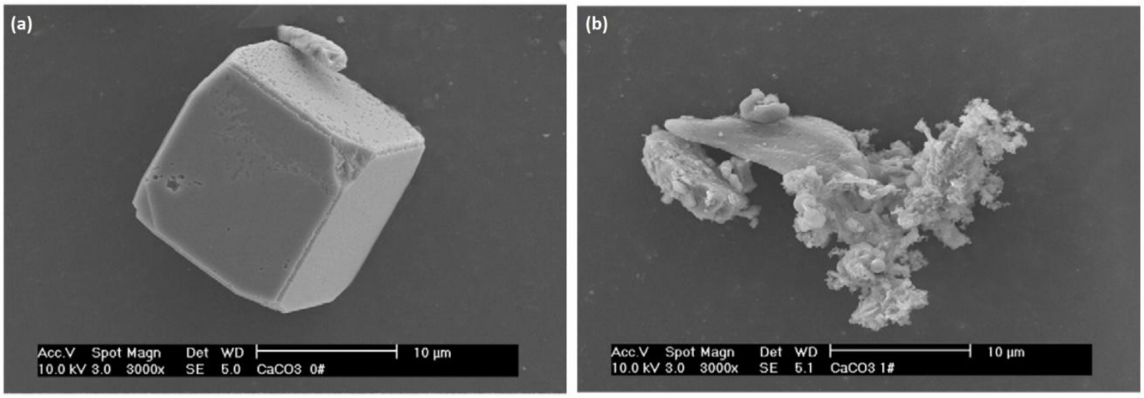

Figure 12: SEM images of CaCO3 scale in the (a) absence (b) presence of PESA

In a recent study in 2017, PESA was tested as draw solution for the forward osmosis (FO) desalination process. The effects of membrane orientation, temperature and flow rate on FO performance are studied using PESA as a draw solute. the overall performance of PESA demonstrates that it is a promising draw solute [59]. Finally, a unique study was performed for the molecular dynamics simulation for the interaction of PESA as scale inhibitor with calcite ($CaCO_3$) crystal surfaces providing a scientific explanation of the molecular interactions between scale inhibitors and scales on molecular levels [60].

2.2.3 PESA as Corrosion inhibitor

As a new polymer, PESA was not studied in terms of corrosion inhibition for metals before. The only title found in the literature review is a preliminary study shows that PESA possesses good corrosion inhibition study for carbon steel under specific conditions. However, this paper doesn’t include advanced electrochemical testing techniques and only giving basic information. A recent study in 2015 performed tests on a mixture of 5 different inhibitors: polyepoxysuccinic acid (PESA), polyaspartic acid (PASP), polyamino polyether methylene phosphonate (PAPEMP), sodium gluconate (Glu) and Zn^{+2} ions. The mixture of these inhibitors PASP, PESA, PAPEMP, Glu, and Zn2+ is considered as eco-friendly inhibitor and noticed to exhibit a mixed-type inhibition behavior. This mixture has efficiently inhibited the corrosion on CS (carbon steel) at relatively low concentrations under remarkably corrosive soft water media. The study evaluated the inhibition of PESA alone for potable soft water alone using concentrations from 50 to 200 mg/l of PESA and getting efficiencies of 22% and 74%, respectively. This study revealed that PESA could be a versatile corrosion inhibitor under various environments [20]. Unfortunately, this study didn’t explain the mechanism or give more insights into PESA performance as corrosion inhibitor using electrochemical techniques. Furthermore, no other studies found in literature evaluated PESA as corrosion inhibitor under any other conditions for the best of our knowledge and till the date of writing this thesis.

Therefore, we have selected to study PESA polymer as eco-friendly corrosion inhibitor under various conditions.

2.3 Computational Techniques

As an important part to develop corrosion inhibition mechanisms and the correlation between organic or polymeric inhibitors with the metal surface, a wide range of computational quantum chemical calculations and simulations were developed. The utilization of computer modeling methods to corrosion processes requires an understanding of the physical principles of corrosion and mathematics which control the corrosion process. These calculations are able in most of the cases to justify the experimental results and give molecular-level insights on the adsorption bonding points and energy between the inhibitor and metal surface [61].

2.3.1 Quantum Calculations

Vosta and co-worker had introduced the quantum chemistry in the investigation of corrosion inhibition in correlation with electrochemical chemistry in order to establish a relationship between corrosion inhibition and molecular structure [62]. Later in nineteens, the researchers utilized these techniques in understanding the interaction between corrosion inhibitor and metal surface [63][64]. Many quantum chemistry methods have been used in this application. It is found that the reactivity of an inhibitor is linked closely to its frontier molecular orbitals (MO) such as HOMO (highest occupied molecular orbital) and LUMO (lowest unoccupied molecular orbital) and some other parameters [65]. Density functional theory (DFT) is becoming an attractive method because it gives accurate and basic important values for small and huge complex molecules at low cost. Thus, DFT is considered a mainstay in correlating some empirical results in corrosion science with quantum chemical mechanics. However, a number of chemical quantum concepts have been built within DFT framework [66]. Finally, in this thesis, we used DFT calculations in order to gain deeper insights at molecular levels of the inhibitive mechanism of PASP and PESA with MS. Figure 13 shows the potential electron transfer between an azole inhibitor and an iron surface while CB represents conduction band and VB represents valence band. Figure 14 shows electrostatic potential (ESP) and the frontier molecule orbital density distributions of three triazole compounds in gas phase [67].

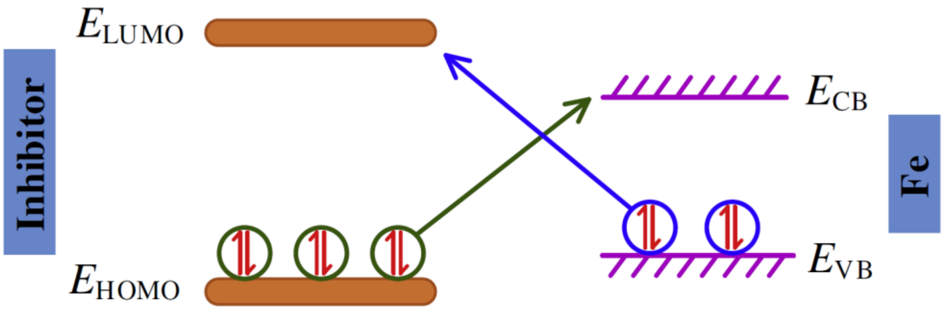

Figure 13: The potential electron transfer between an azole inhibitor and an iron surface [67]

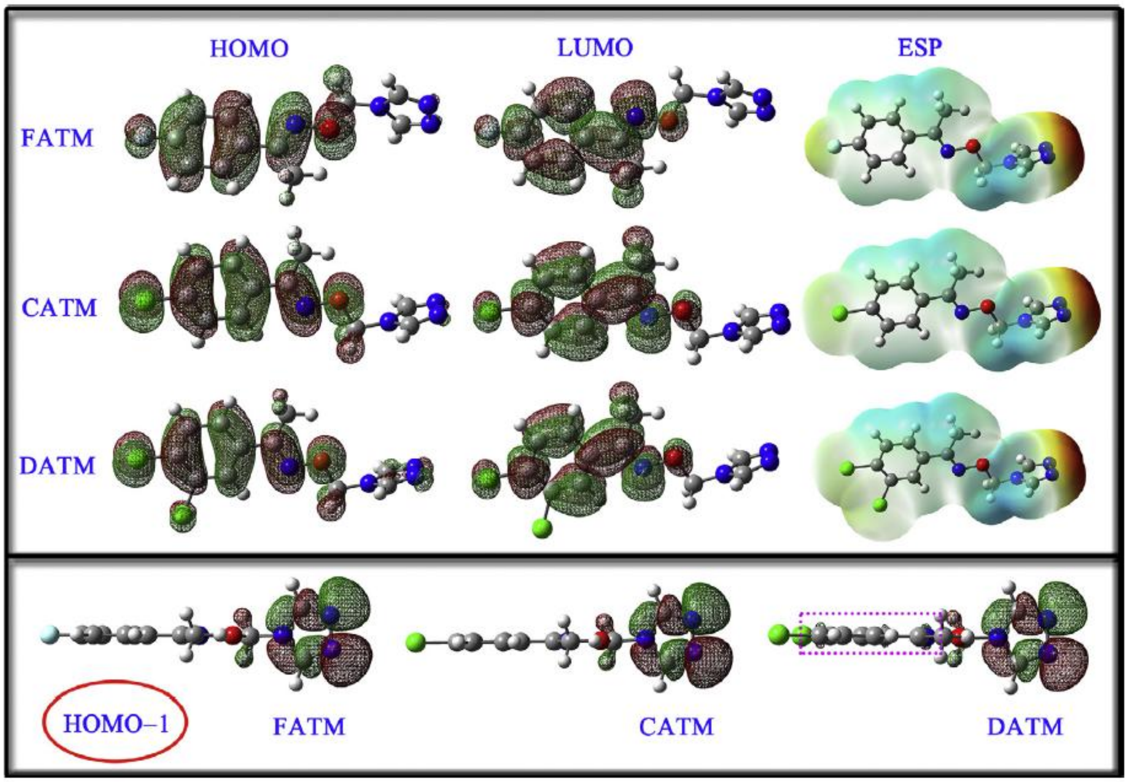

Figure 14: Electrostatic potential (ESP) and the frontier molecule orbital density distributions of three triazole compounds in gas phase [67]

2.3.2 Monte Carlo Simulation

In addition to quantum calculations for corrosion inhibitors researches, an interest was raised to focus on modeling the interaction between corrosion inhibitor and metal surface including the calculation of interaction energies. This new approach offered advantages of gaining important physical insights about the mechanisms of corrosion inhibitors. Therefore, Metropolis Monte Carlo simulation method was employed in studying the adsorption configurations of inhibitors on the metal surface and to provide the preferential adsorption sites on both materials [68]. In this research, we used Monte Carlo simulation in evaluating the adsorption configuration of PASP and PESA on the mild steel surface. Then, we will compare these theoretical findings with empirical results. The resulted figure is giving you an adsorption energy range. Figure 15 shows the overall energy, average overall energy, Vander Waals energy, electrostatic attraction energy, and intermolecular energy for the DATM/Iron surface [67].

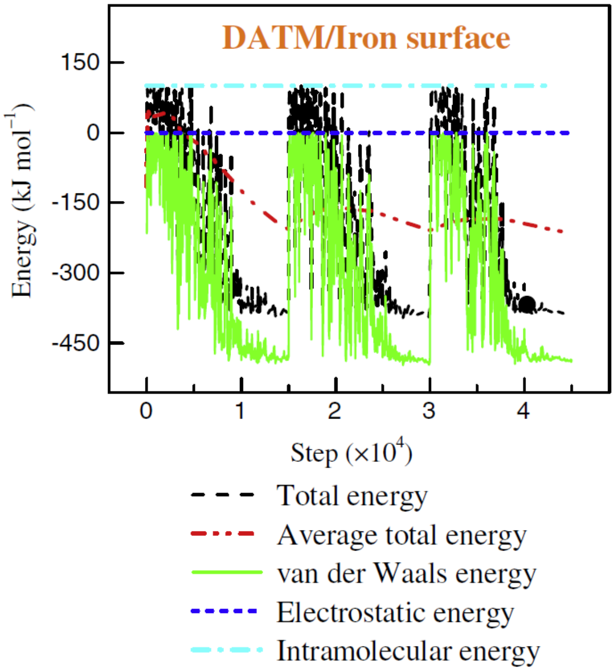

Figure 15: Total energy distribution for DATM/Iron system [67]

2.4 Weight Loss Measurements

This gravimetrical method starts with previously weighed metal specimens that are taken off from the testing solution or the environment at after various contact times, and the final loss in weight will be calculated due to metallic corrosion (per unit area of the sample). Weight loss experiments should be performed in the presence and absence of elevated concentrations of an inhibitor at elevated temperatures or contact times [69]. The corrosion rate (C_R), inhibition efficiency (η%), and surface coverage (θ) could be determined using the following equations.

$$CR\ (mm/year) = \frac{8.76 \times 10^4 \times W}{D \times A \times t} \tag{1}$$

$$\theta = \frac{CR_0 - CR_i}{CR_0} \tag{2}$$

$$\eta\ (\%) = \frac{CR_0 - CR_i}{CR_0} \times 100 \tag{3}$$

where, W = weight loss (g), A = area of specimen (cm^2), D = mild steel density (g cm^3), and t = exposure time (h), CR_i and CR_0 are corrosion rates in presence and absence of inhibitors, respectively. In this study, we have conducted weight loss measurements at different polymer concentrations and temperatures. Figure 16 shows the weight loss versus time of aluminum alloy immersed in 0.5 M HCl.

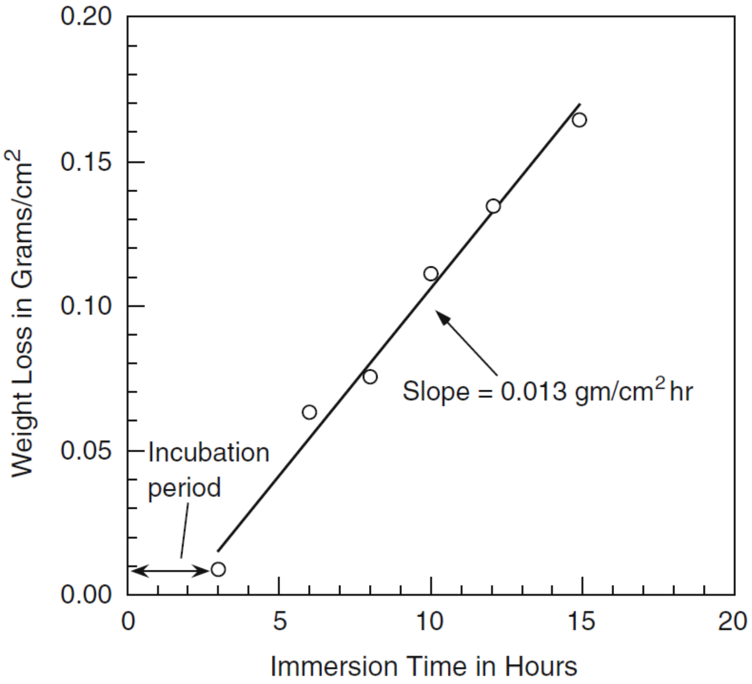

Figure 16: Weight loss vs. time for Al alloy 7075 in 0.5 M HCl [70]

2.5 Electrochemical Measurements

Corrosion process of metals occurs via electrochemical reactions at the interface between the metal and an electrolyte solution. For example, a thin film of moisture on a metal surface forms the electrolyte for atmospheric corrosion. Wet concrete is the electrolyte for reinforcing rod corrosion in bridges. Thus, the electrolyte is playing a key role in corrosion process and have a remarkable impact on corrosion kinetics (rates). Corrosion normally occurs at a rate determined by the electrochemical reactions of anode and cathode. The first is the anodic reaction, in which a metal is oxidized, releasing electrons into the metal. The other is the cathodic reaction, in which a solution species (often O_2 or H^+) is reduced, with the electrons removed from the metal. This process called polarization and Figure 17 shows that. When these two reactions are in equilibrium, the flow of electrons from each reaction is balanced, and no net electron flow (electrical current) occurs. The two reactions can take place on one metal or on two dissimilar metals (or metal sites) that are electrically connected [71]. Figure 18 shows anodic and cathodic currents.

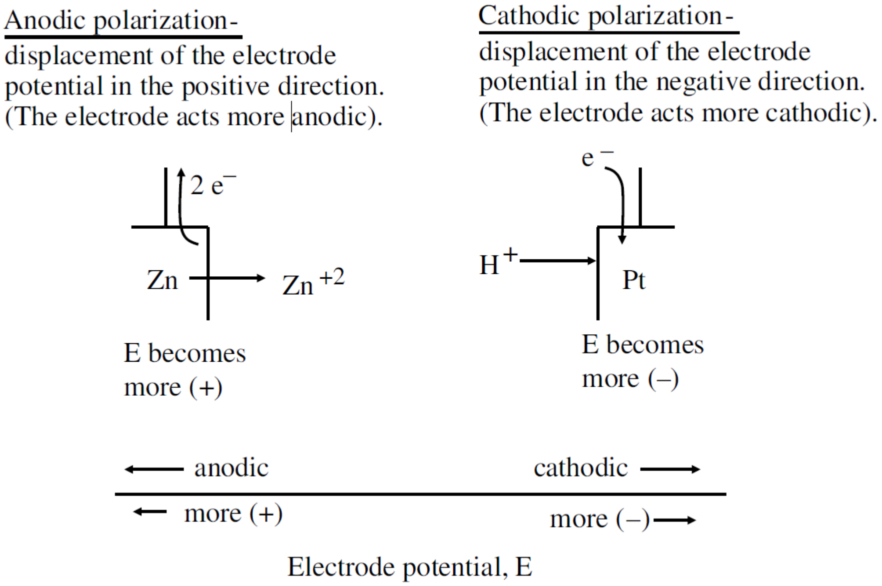

Figure 17: A representation of anodic and cathodic polarizations [71]

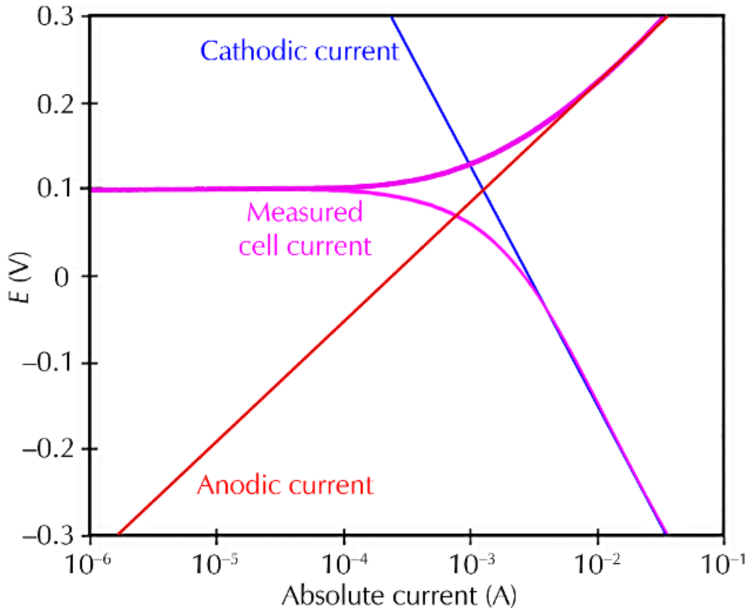

Figure 18: Corrosion process showing anodic and cathodic current components [72]

The equilibrium potential assumed by the metal in the absence of electrical connections to the metal is called the Open Circuit Potential (Eoc. In most electrochemical corrosion experiments, the first step is the measurement of E_{ocp}. The terms E_{ocp} and Corrosion Potential (E_{corr}) are usually interchangeable, but E_{ocp} is preferred.

2.5.1 Open Circuit Potential

Open circuit potential (E_{ocp}) is an indicative factor in corrosion inhibition mechanisms that is identified as the corrosion potential in the absence of net electrical current flowing through the metal surface. When corrosion reaction reaches equilibrium, E_{ocp} reaches a steady-state and it becomes equal to the corrosion potential (E_{corr}). The evolution of potential versus time constitutes a methodology for monitoring interface changes between a metal and its environment [73]. Figure 18 shows E_{ocp} for mild steel in 0.5 M H_2SO_4 in the absence and presence of different concentration of an inhibitor [74].

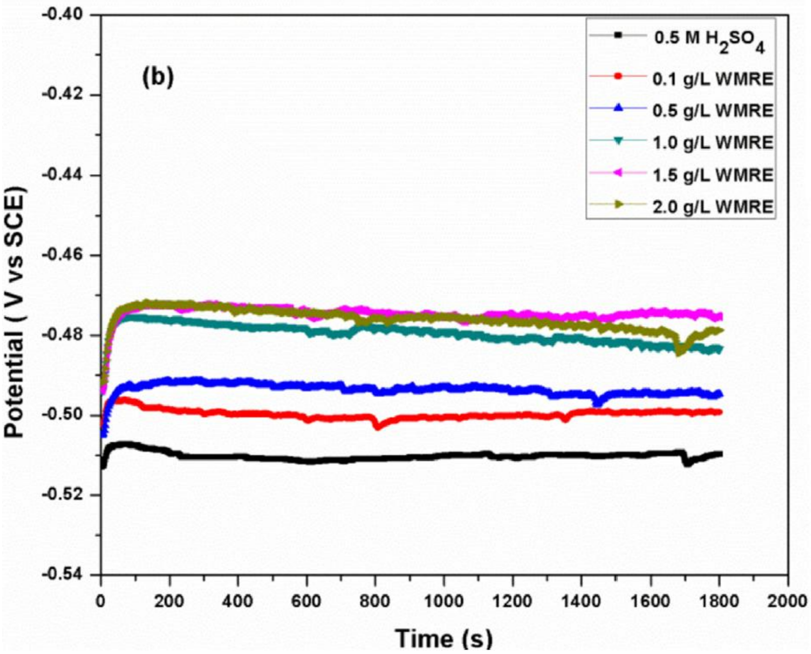

Figure 19: Eocp for mild steel in 0.5 M H2SO4 in the absence and presence of different concentration of an inhibitor [74]

2.5.2 Polarization Resistance

Polarization resistance (R_p) or potentiodynamic polarization (PD) resistance is a technique could be utilized to calculate metal's resistance that is under evaluation against corrosion. Any electrode can be polarized when its potential is moved away by force from its original value at open circuit potential (E_{ocp}) or corrosion potential. The polarization of an electrode causes current to flow due to electrochemical reactions it induces at the electrode surface. The polarization resistance (R_p) is defined by the following equation:

$$R_p = \left(\frac{\Delta E}{\Delta i}\right)_{\Delta E \to 0} \tag{4}$$

Where ΔE is the variation of applied potential around the corrosion potential and Δi is the resulting polarization current [75]. Polarization resistance behaves as a resistor and can be calculated by taking the inverse of the slope of the current potential curve at open circuit or corrosion potential. During the polarization of an electrode, the magnitude of the current is controlled by reaction kinetics and diffusion of reactants both towards and away from the electrode. The relationship between current density and potential of anodic and cathodic electrode reactions under charge transfer control is given by the Butler-Volmer equation:

$$i = i_{corr}\left(e^{2.303\frac{\eta}{\beta_a}} - e^{2.303\frac{\eta}{\beta_c}}\right) \tag{5}$$

$$\eta = E - E_{corr} \tag{6}$$

Where E is the applied potential and i the measured current density. The overpotential (η) is defined as the difference between applied potential and the corrosion potential E_{corr}. This E_{corr} is the open circuit potential of a corroding metal. The corrosion current, i_{corr}, and the Tafel constants β_a, and β_c can be measured from the experimental data. For large anodic overpotentials ($\eta/\beta_a >> 1$) the Butler-Volmer equation simplifies to the Tafel equation for the anodic reaction:

$$\eta = \log(i_{corr}) + \beta_a . \log(i) \tag{7}$$

Analogously, for large cathodic overpotentials ($\eta/\beta_c << -1$) the Tafel equation for the cathodic reaction is given by:

$$\eta = \log(i_{corr}) - \beta_c . \log|i| \tag{8}$$

For small η, i.e. for potentials close to corrosion potential, the above equation can be reduced to:

$$i_{corr} = 2.303 \frac{\beta_a \beta_c}{\beta_a + \beta_c} \left(\frac{1}{R_p}\right) \tag{9}$$

Or, when the expression is rearranged:

$$R_p = 2.303 \frac{\beta_a \beta_c}{\beta_a + \beta_c} \left(\frac{1}{i_{corr}}\right) \tag{10}$$

The Tafel equations predict a straight line for the variation of the logarithm of current density with potential. Therefore, currents are often shown in semilogarithmic plots known as Tafel plots. This type of analysis is referred to as Tafel Slope Analysis. All these electrochemical parameters such as corrosion potential (E_{corr}), corrosion current density (i_{corr}), inhibition efficiency (E_i%), anodic and cathodic Tafel slopes (β_a and β_c) will be calculated from corresponding curves and will be given in tables. The values of E_i% will be calculated using the following equation [76]. Figure 20 shows

$$E_i(\%) = \left(\frac{i^o_{corr} - i_{corr}}{i^o_{corr}}\right) \times 100 \tag{11}$$

Figure 20 shows an example of polarization carves (Tafel Plots) of mild steel in 0.5 M sulfuric acid in the absence and presence of a corrosion inhibitor WMRE (watermelon rind extract) [74].

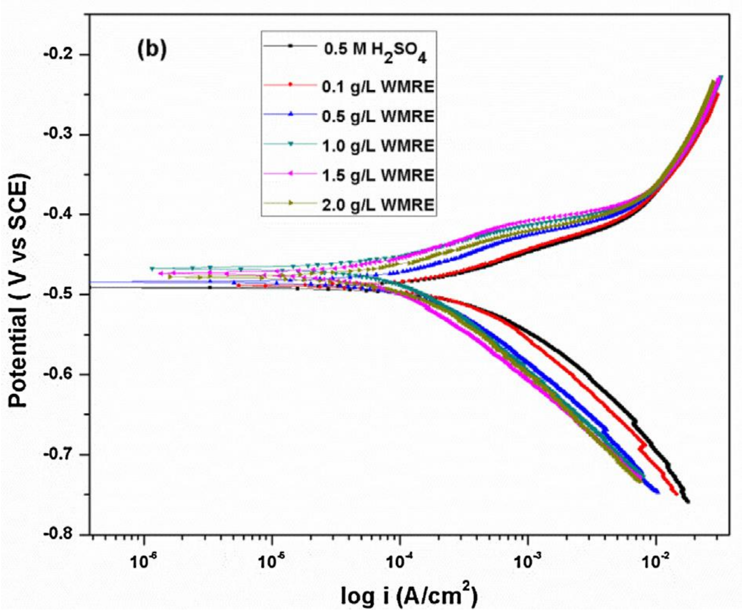

Figure 20: Tafel plots of mild steel in 0.5 M H_2SO_4 in the absence and presence of WMRE corrosion inhibitor [74]

Finally, potentiodynamic polarization method is one of the most widely used electrochemical methods for measuring corrosion rate of metals. However, the measurement modifies the surface condition of the corrosion system. So usually this technique is only performed at the termination of the exposure.

2.5.3 Electrochemical Impedance Spectroscopy

Electrochemical Impedance Spectroscopy (EIS) is an accurate, powerful, new nondestructive method used to study corrosion processes of a wide range of materials including corrosion inhibitors and coatings in different liquid environments. EIS can give insights on surface properties, reaction kinetics and inhibition mechanistic information obtained after building an equivalent cell and performing the calculations. During the EIS experiments, alternating current (AC) is applied with alternating perturbation to the system being investigated. The perturbation is characterized by the potential or the current in a sine wave at a certain frequency or a germination of some different frequency sine waves [77][78]. Through dividing the alternating potential, $\vec{V}$, by the alternating current, $\vec{I}$, the impedance function (a vector parameter) Z is:

$$Z = \frac{\vec{V}}{\vec{I}} \tag{12}$$

In general, the impedance parameter consists of a real part (resistive) and imaginary part (capacitive or inductive). For an electrochemical interface of a corroding system, i.e., a metal in an electrolyte, the real part of the impedance is usually associated with the electrical resistance of the electrolyte, charge transfer resistance of corrosion reactions and ohmic resistance of the surface film, while the imaginary part is associated with capacitance of the electrochemical double layer at the interface and adsorption/desorption at the metal surface, which is also influenced by the surface film.

Different corrosion systems (e.g., charge transfer control, diffusion control or a mixture type) may show different features in the EIS spectra. Through analyzing the EIS data (Nyquist plot, Bode plot), the corrosion mechanism of the system can be identified. In practice, EIS data are often interpreted in terms of electrical equivalent circuits that can be used to describe the electrical features of the electrochemical interfaces [76]. Electrochemical impedance is usually measured by applying an AC potential to an electrochemical cell and then measuring the current through the cell. Assume that we apply a sinusoidal potential excitation. The response to this potential is an AC current signal. This current signal can be analyzed as a sum of sinusoidal functions (a Fourier series).

Electrochemical impedance is normally measured using a small excitation signal. This is done so that the cell's response is pseudo-linear. In a linear (or pseudo-linear) system, the current response to a sinusoidal potential will be a sinusoid at the same frequency but shifted in phase (see Figure 21) [79].

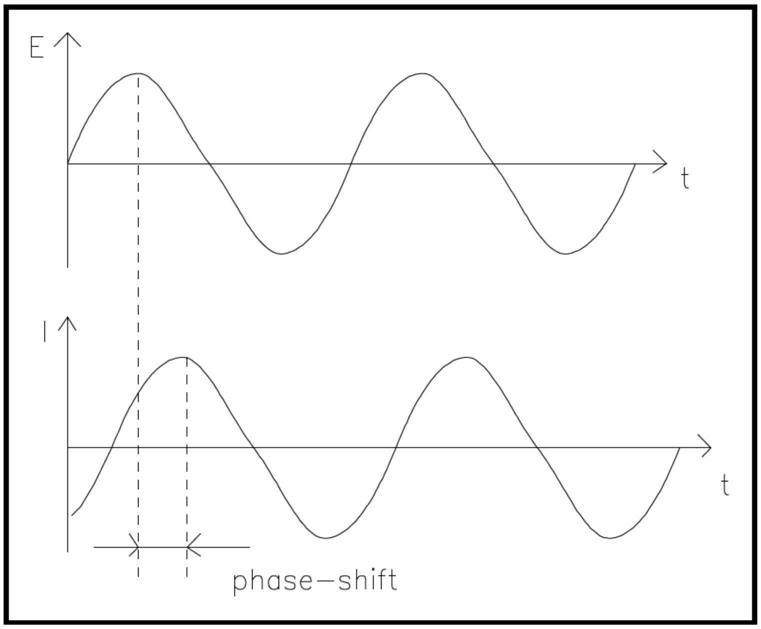

Figure 21: Sinusoidal Current Response in a Linear system [79]

The excitation signal, expressed as a function of time, has the form

$$E_t = E_0 \sin(\omega t) \tag{13}$$

where Et is the potential at time t, E_0 is the amplitude of the signal and ω is the radial frequency. The relationship between radial frequency ω (radians/second) and frequency f (hertz) is:

$$\omega = 2\pi f \tag{14}$$

In a linear system, the response signal, I_t , is shifted in phase (ϕ) and has a different amplitude, I_0.

$$I_t = I_0 \sin(\omega t + \phi) \tag{15}$$

An expression analogous to Ohm's Law allows us to calculate the impedance of the system as:

$$Z = \frac{E_t}{I_t} = \frac{E_0 \sin(\omega t)}{I_0 \sin(\omega t + \phi)} = Z_0 \frac{\sin(\omega t)}{\sin(\omega t + \phi)} \tag{16}$$

The impedance is therefore expressed in terms of a magnitude, Z_0 , and a phase shift, ϕ. it is possible to express the impedance as a complex function. The potential and the current can be described as:

$$E_t = E_0 \exp(j\omega t) \tag{17}$$

$$I_t = I_0 \exp(j\omega t - \phi) \tag{18}$$

The impedance is then represented as a complex number:

$$Z(\omega) = \frac{E}{I} = Z_0 \exp(j\phi) = Z_0(cos\phi + jsin\phi) \tag{19}$$

The expression for $Z(\omega)$ is composed of a real and an imaginary part. If the real part is plotted on the X-axis and the imaginary part is plotted on the Y-axis of a chart, we get a "Nyquist Plot". Figure 22 shows an example Nyquist Plot with Impedance vector. Notice that in this plot the Y-axis is negative and that each point on the Nyquist Plot is the impedance at one frequency. This figure has been annotated to show that low frequency data are on the right side of the plot and higher frequencies are on the left. On the Nyquist Plot the impedance can be represented as a vector (arrow) of length |Z|. The angle between this vector and the X-axis, commonly called the “phase angle”, is φ (=arg Z). Nyquist Plots have one major shortcoming. When you look at any data point on the plot, you cannot tell what frequency was used to record that point [79].

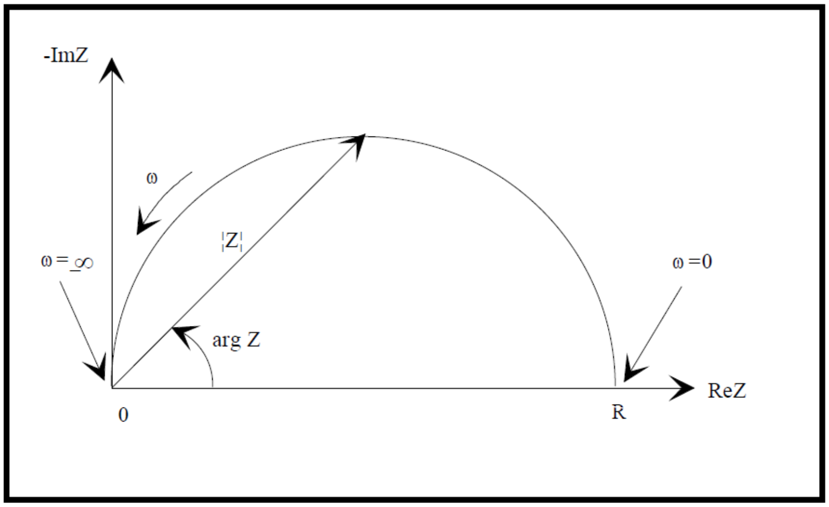

Figure 22: Nyquist Plot with Impedance Vector [79]

The above Nyquist Plot results from the electrical circuit of Figure 23. The semicircle is characteristic of a single "time constant". Electrochemical impedance plots often contain several semicircles. Often only a portion of a semicircle is seen.

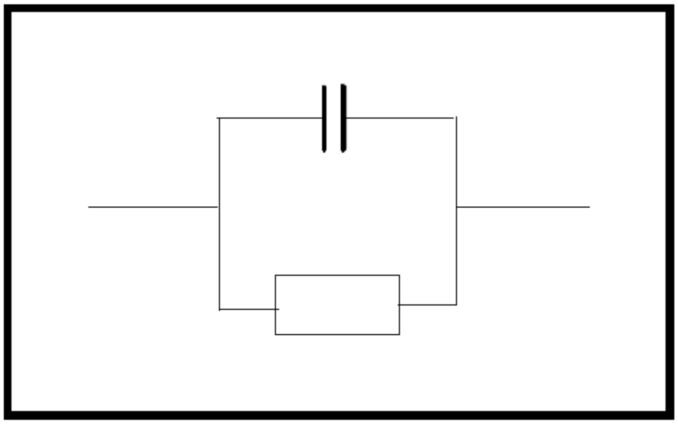

Figure 23: Simple Equivalent Circuit with One Time constant

Another popular presentation method is the Bode Plot. The impedance is plotted with log frequency on the X-axis and both the absolute values of the impedance (|Z|=Z0) and the phase shift on the Y-axis. The Bode Plot for the above electric circuit is shown in Figure 24. Unlike the Nyquist Plot, the Bode Plot does show frequency information.

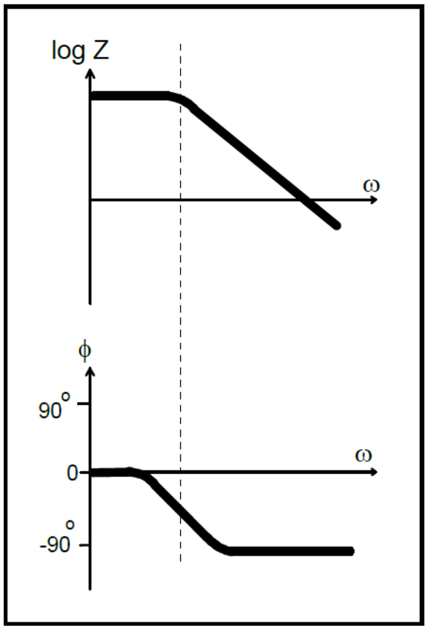

Figure 24: Bode Plot with One Time Constant [79]

The corrosion current and rate will be calculated from charge transfer resistance (R_{CT}) values obtained from EIS measurements and the inhibition efficiency (η%) is calculated using the following equation:

$$\eta\ (\%) = \frac{R^{o}_{CT} - R_{CT(inh)}}{R^{o}_{CT}} \times 100 \tag{20}$$

where, R^{o}_{CT} and $R_{CT(inh)}$ are the values of charge transfer resistance in the absence and presence of inhibitor, respectively.

Double layer capacitance (C_{dl}) values were calculated from charge transfer resistance and CPE parameters (Y_0 and n) using Equation (8):

$$C_{dl} = (Y_0 {R_{ct}}^{1-n})^{1/n} \tag{21}$$

Where Y_0 is CPE constant and n is CPE exponent lies between 0 and 1.

2.6 Surface Analytical Techniques

Several surface characterization and analytical techniques were used in this research study in order to gain information about the metal-solution interface reactions taking place during the corrosion process. Each technique gives some partial information about the mechanism and after merging all findings, we can build an understanding of the mechanism. The main purpose of all the below techniques is to be able to elucidate the inhibition mechanism of PESA and PASP polymers on mild steel in aerated 3% NaCl solution. The techniques are described below.

2.6.1 Fourier Transform Infrared Spectroscopy

Fourier Transform Infrared Spectroscopy (FTIR) is the main techniques used to obtain vibrational spectra of the organic materials. When IR light passes through a sample, molecules absorb specific frequencies that match the vibrational frequency of bonds and change the dipole moment of the molecules. Details about the molecular structure and functional groups of the sample can be revealed by analyzing the spectrum of absorbed frequencies. In an IR spectrum, the units for the *X*-axis are normally wavenumbers representing the absorbance frequency. The application of a Fourier transform (FT) spectrometer allows a rapid collection of IR spectra with a larger signal-noise ratio, higher resolution and higher wavelength accuracy [5].

Attenuated total reflectance Fourier transform infrared spectroscopy (ATR-FTIR) measurements were performed in this study as well equipped with a linearized MCT detector. This technique is more helpful than normal FTIR measurement because it can give information about the absorbed organic inhibitor or polymer on the metal surface without destructing the sample. It is very effective when the inhibitor is the adsorption type which builds a thin protective layer on the metal surface.

Figure 25 shows a schematic drawing of (A) transmission-mode microscopy and (B) ATR-mode microscopy for chemical imaging of breast tissue biopsies [80]. Figure 26 shows an example of FTIR spectrum of NAC (structure embedded) in 15% HCl before and after the immersion of X80 steel [81].

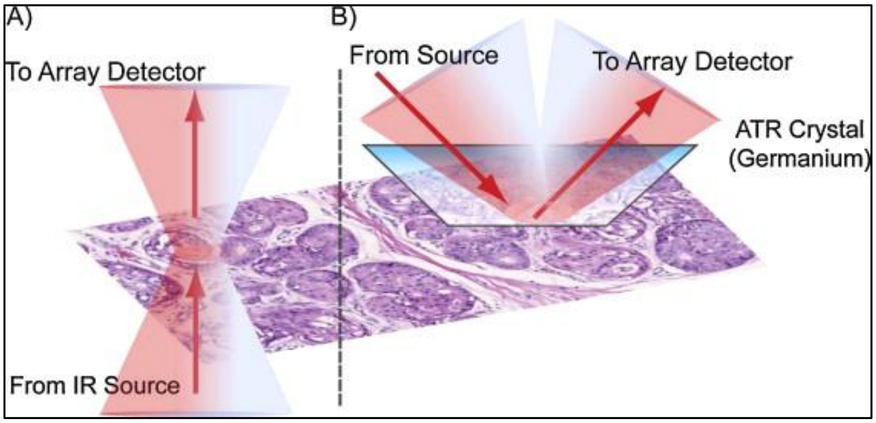

Figure 25: a schematic drawing of (A) transmission-mode microscopy and (B) ATR-mode microscopy

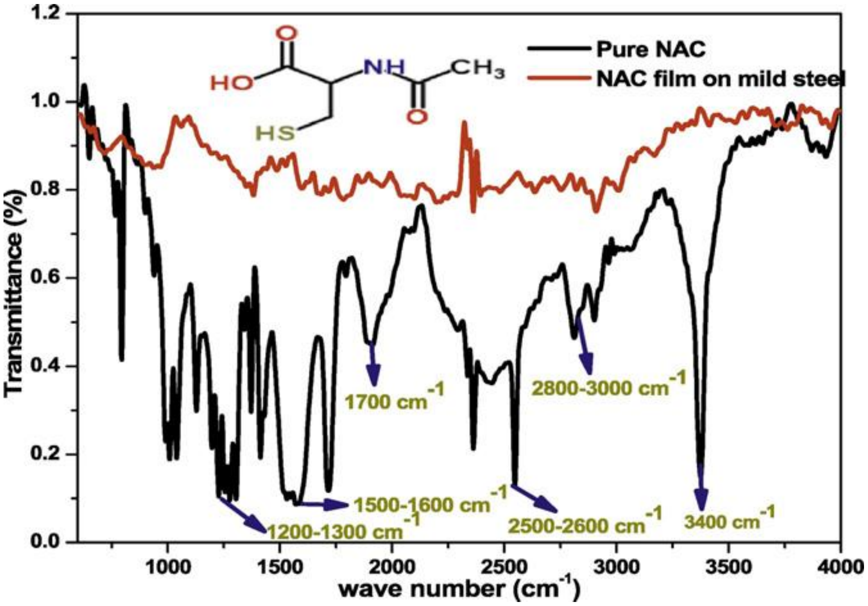

Figure 26: An example of FTIR spectrum of NAC (structure embedded) in 15% HCl before and after the immersion of X80 steel

2.6.2 Atomic Force Microscopy

Atomic force microscopy (AFM) is a type of scanning probe microscopy (SPM) that allows high-resolution imaging of surfaces in a variety of environments. The AFM scans the sample surface using a cantilever with a sharp tip in the order of nanometers. During the scanning, the cantilever will be bent or deflected by the forces between the tip and the scanned surface. The deflection of a scanning cantilever is recorded by a detector and is used to generate the topographic image of the scanned surface. The AFM cantilever deflection is mostly caused by Van der Waals interaction between the tip and sample surface. Depending on the tip-sample distance the Van der Waals interaction can be a repulsive force or an attractive force, based on which the AFM can be operated in contact mode or non-contact (tapping) mode.

In the contact mode, the cantilever is held a few angstroms from the sample surface, and the force between the tip and the surface is kept constant during scanning by maintaining a constant deflection. Whereas in the tapping mode, the cantilever is held in the order of tens to hundreds of angstroms from the sample surface, and the cantilever is excited to oscillate at or close to its resonance frequency. The changes in the oscillation amplitude, phase, and frequency during the scanning are used to extract rheological information about the surface. Moreover, AFM imaging by tapping mode yields both a topographic image and a phase image. The phase image is influenced by variations in surface composition, adhesion, friction, viscoelasticity, etc. Phase images obtained simultaneously with topographic images give additional information about microstructure [5][82].

In this study, *ex-situ* AFM measurements were performed. Data were collected and analyzed with the WSxM software. The starting surfaces were measured in air with the same setup for comparison. Figure 27 shows a detailed schematic representation of (a) AFM components, (b) Tip-sample interaction for quantitative nanomechanics studies, (c) Scattering scanning near-field optical microscopy (s-SNOM) for nanospectroscopy in chemical identification, and (d) AFM-based scanning electrochemical microscopy (SECM) where the insulated AFM serves as a nanoelectrode probe [83][84]. Figure 28 shows an example of AFM micrographs of mild steel surface (a) before immersion (b) after immersion without inhibitor (c) after immersion with 150 ppm MPTS (d) after immersion with 150 ppm CPTS at 303 K [9].

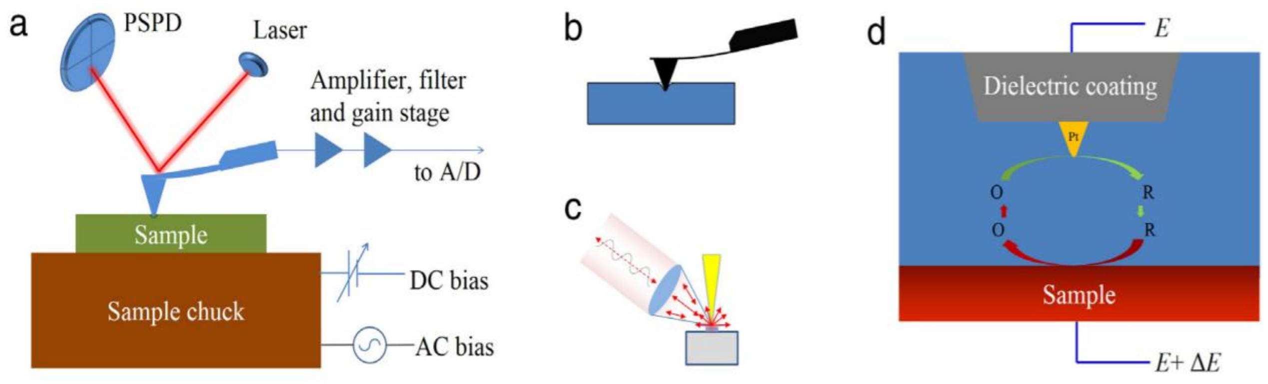

Figure 27: a detailed schematic representation of AFM components [83]

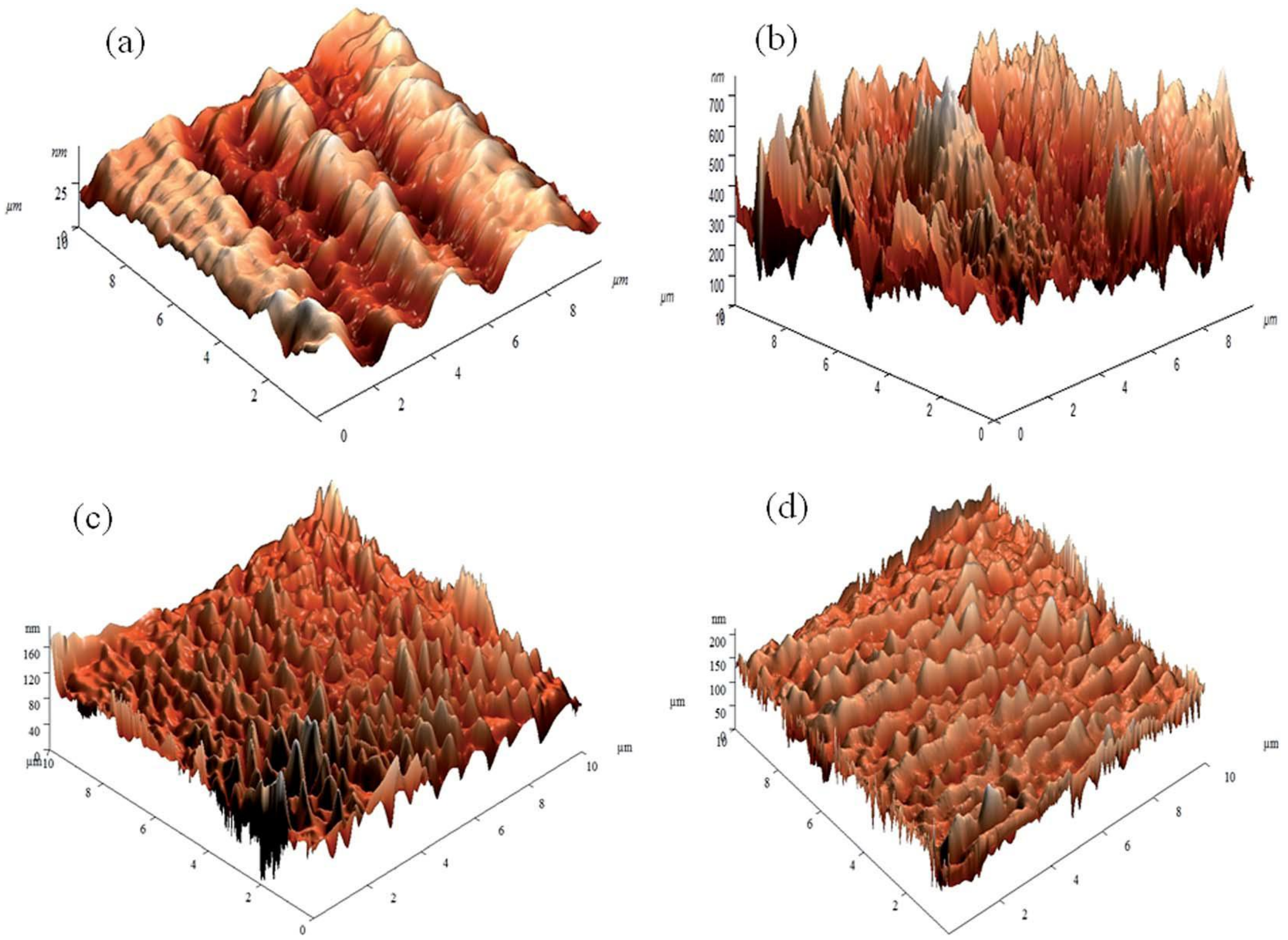

Figure 28: An example of AFM micrographs of mild steel surface at various environments [9]

2.6.3 Scanning Electron Microscopy

A **scanning electron microscope** (**SEM**) is a technique of electron microscopes that generates images of a specimen by allowing the electron to scan the sample surface with a concentrated beam of electrons. The electrons in the incident beam interact with atoms existing in the sample, and then generating different signals contain detailed data about the sample's morphology and topography and composition in some cases. This electron beam has a specific scan pattern, and it has position is combined with detected signals in order to produce the final image. SEM can reach a resolution more than 1 nanometer (nm). Samples can be tested under high vacuum in conventional SEM, or under low vacuum or wet conditions in some pressure or environmental models, and even at different range of temperatures with some specific instruments [85].

The most commonly used model of SEM is the detection of a secondary beam of electrons emitted from the atoms excited by the incident electron beam. The secondary electrons have a number can be emitted depending on specimen topography and other factors. By scanning the sample and combining the secondary electrons emitted using a special type of detector, an image will appear displaying the morphology or topography of the surface. SEM samples have to be prepared in conceding to withstand the internal vacuum conditions in SEM chamber and high energy of incident beam of electrons with a size to be fitted on the specimen stage. Specimens should be mounted properly to a specimen holder using a special type conductive tape. SEM technoqie is used widely in corrosion researches due to its packability to give excellent surface morphology before and after the corrosion. Nonconductive specimens collect charge when scanned by the electron beam, and especially in secondary electron imaging mode, this causes scanning faults and other image artifacts. For conventional imaging in the SEM, specimens must be electrically conductive, at least at the surface, and electrically grounded to prevent the accumulation of electrostatic charge [86].

Non-conducting materials are usually coated with an ultrathin coating of electrically conducting material, deposited on the sample either by low-vacuum sputter coating or by high-vacuum evaporation. Conductive materials in current use for specimen coating include gold, gold/palladium alloy, platinum, and graphite. Figure 29 shows an example of SEM micrographs after corrosion product removal of the surfaces of mild steel samples immersed for 24 h in (a) 0.01 M NaCl at pH 8 (b) 0.01 M NaCl and 4 mM 2-MeHImn 4-OHCin at pH 8 [87].

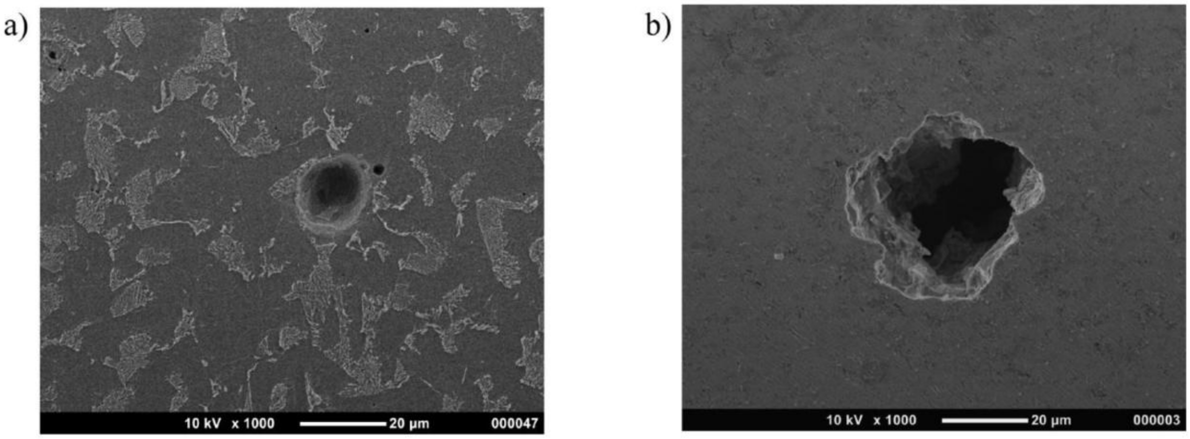

Figure 29: SEM images of mild steel samples immersed for 24 h in (a) 0.01 M NaCl (b) 0.01 M NaCl and inhibitor [87]

In this study, SEM micrographs have been taken in order to evaluate mild steel surface morphology without the inhibitors and after inhibitors addition. This tool also helps to evaluate the depth of pitting corrosion could be caused by chloride (Cl^-) ions on the mild steel surface. The effect of inhibitor’s dose can be observed as well using SEM micrographs. The SEM system is mostly equipped with EDS (Energy Dispersive Spectroscopy) detector which will be explained in the coming section.

2.6.4 Energy Dispersive Spectroscopy

Energy dispersive X-ray spectroscopy (EDS) is a well-known analytical chemistry technique used to conduct elemental chemical analysis of a sample. It depends on the interaction between a specific source of X-ray excitation and a sample for testing. It has high characterization ability are because of the fundamental principle that each element in the periodic table has a unique atomic structure which have a unique set of emitting peaks on the electromagnetic emission spectrum similarly to the principle of spectroscopy [88].

To stimulate the emission of characteristic X-rays from a specimen, a high-energy beam of charged particles such as electrons or protons or a beam of X-rays is focused on the sample being studied. At rest, an atom within the sample contains ground state electrons in discrete energy levels or electron shells bound to the nucleus. The incident beam may excite an electron in an inner shell, ejecting it from the shell while creating an electron-hole where the electron was. An electron from an outer, higher-energy shell then fills the hole, and the difference in energy between the higher-energy shell and the lower energy shell may be released in the form of an X-ray. The number and energy of the X-rays emitted from a specimen can be measured by an energy-dispersive spectrometer. As the energies of the X-rays are characteristic of the difference in energy between the two shells and of the atomic structure of the emitting element, EDS allows the elemental composition of the specimen to be measured [88]. Figure 30 shows the EDS spectra for the Q235 carbon steel after 88 h of immersion in 1 M HCl solution for (a) polished Q235 carbon steel, (b) blank 1 M HCl solution [89].

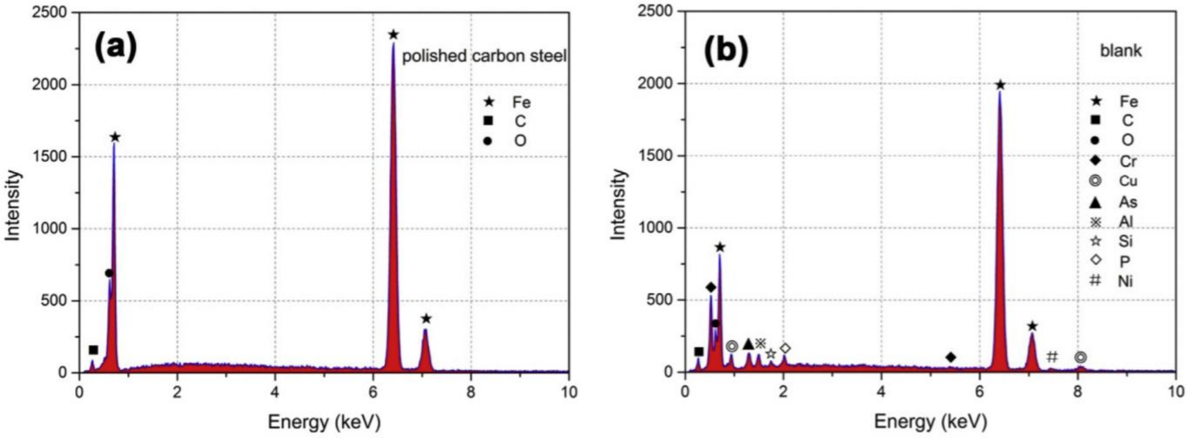

Figure 30: EDS spectra for carbon steel after 88 h of immersion in 1 M HCl solution for (a) polished sample, (b) blank 1 M HCl solution [89].

2.7 Corrosion Rate Calculations

Electrochemical methods provide an alternative to traditional methods used to determine the rate of corrosion. Direct and quantitative determination of corrosion rates can be determined by simple electrochemical measurements using PDP, PR, and EIS or from the traditional method using weight loss measurements. The simplest way of measuring the corrosion rate of a metal is to expose the sample to the test medium (e.g. sea water) and measure the loss of weight of the material as a function of time. Although these tests are simple, there is no simple way to extrapolate the results to predict the lifetime of the system under investigation.

The corrosion rate depends on the kinetics of both anodic (oxidation) and cathodic (reduction) reactions. According to Faraday's law, there is a linear relationship between the metal dissolution rate or corrosion rate CR, and the corrosion current i_{corr}:

$$CR = \frac{M}{nF\rho}\, i_{corr} \tag{22}$$

where M is the atomic weight of the metal, ρ is the density, n is the charge number which indicates the number of electrons exchanged in the dissolution reaction and F is the Faraday constant, (96.485 C/mol). The ratio M/n is also sometime referred to as equivalent weight. So, the above equation gives the corrosion rate based on weight loss method. The detailed procedure of corrosion rate calculations using weight loss method is explained in the standard ASTM D2688-11 [90]. However, the corrosion rates of electrochemical methods were explained in earlier sections [75]. Figure 31 shows the change in corrosion rates of P/M low alloy steels at various concentrations of inhibitors for as sintered specimens [91]. Two units generally are used in corrosion rates measurements which are mpy (mils per year) and mmy (mili-meter per year). Table 4 shows a simple way to convert data between the most common corrosion units in usage, i.e. corrosioncurrent (mA cm^{-2}), mass loss (g m^{-2} day^{-1}) and penetration rates (mm y^{-1} or mpy) for all metals or for steel.

Units	mA cm^{-2}	mm year^{-1}	mpy	g m^{-2} day^{-1}
mA cm^{-2}	1	3.28 M/nd	129 M/nd	8.95 M/n
mm year^{-1}	0.306 nd/M	1	39.4	2.74 d
mpy	0.00777 nd/M	0.0254	1	0.0694 d
g m^{-2} day^{-1}	0.112 n/M	0.365 /d	14.4 /d	1

Table 4: Corrosion rates conversion table

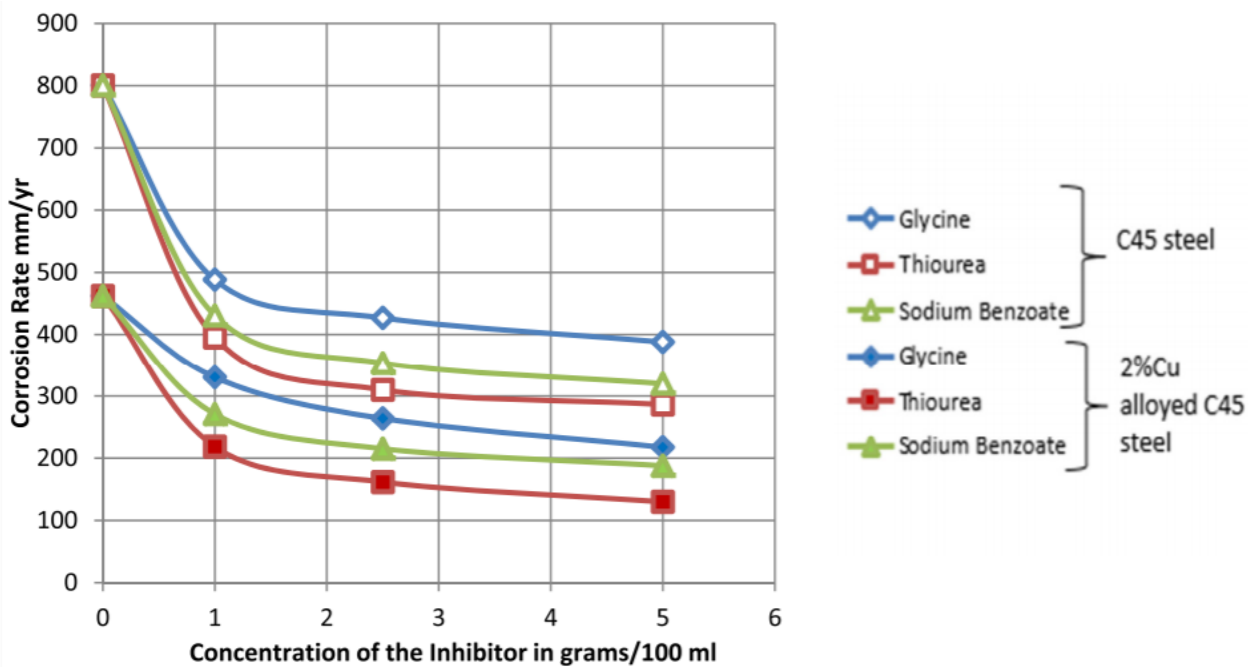

Figure 31: Corrosion rates of P/M low alloy steels at various concentrations of inhibitors [91]

2.8 Thermodynamic Calculations

Thermodynamic parameters are important elements in understanding corrosion reaction thermodynamics. The apparent activation energy (E_a) for metal dissolution in contact with a corrosive environment can be calculated using the below Arrhenius equation forms:

$$\log CR = \frac{-E_a}{2.303\, RT} + \log A \tag{23}$$

$$i_{corr} = A \exp\left(\frac{-E_a}{RT}\right) \tag{24}$$

where R is the molar gas constant (8.314 J K^{-1} mol^{-1}), T is the absolute temperature (K) and A is the Arrhenius pre-exponential factor. A plot can be fitted of log CR against 1/T for the corrosion rate for the studied metal in the presence and absence of corrosion inhibitor at different concentrations of the inhibitor. Figure 32 shows Arrhenius plot of log CR versus 1000/T for mild steel corrosion in 15% HCl solution using MPTS inhibitor [9]. Figure 33 shows alternative Arrhenius plot for mild steel in 1 M HCl in the absence and presence of different concentrations of NO_2AM inhibitor [92]. From Fig. 32, the activation energy can be calculated using the expression $E_a = -(slope) \times 2.303\, R$. So, if the calculated E_a values of the inhibited solutions were higher than that for the uninhibited solution and continued to increase on increasing the inhibitor's concentration, that would reflect good inhibition performance by increasing the energy barrier of corrosion reaction [93]. The enthalpy for unimolecular reaction can be calculated using the equation:

$$E_a - \Delta H^* = RT \tag{25}$$

For unimolecular reactions, $Ea > \Delta H^*$ by a value which approximately equal to RT.

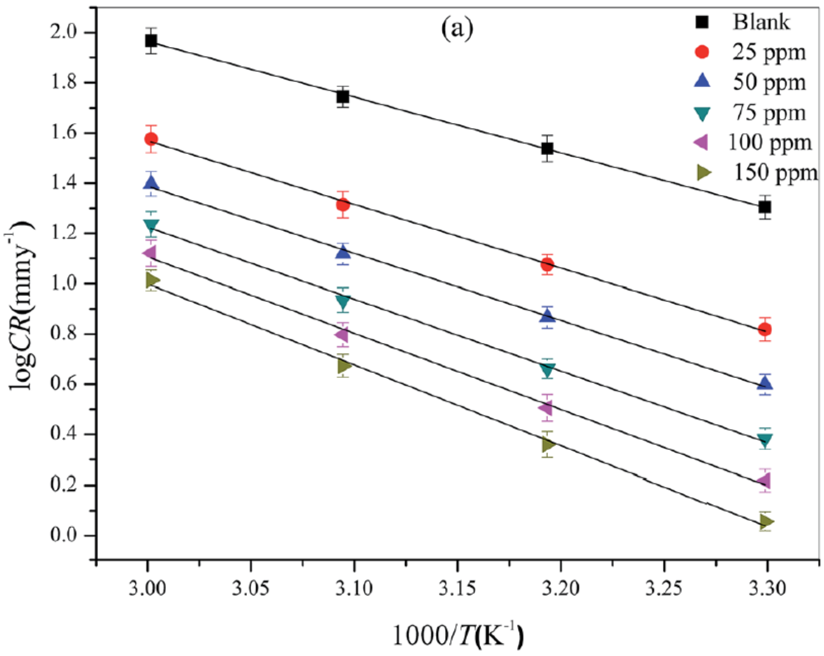

Figure 32: Arrhenius plot for mild steel corrosion in 15% HCl solution using MPTS inhibitor [9]

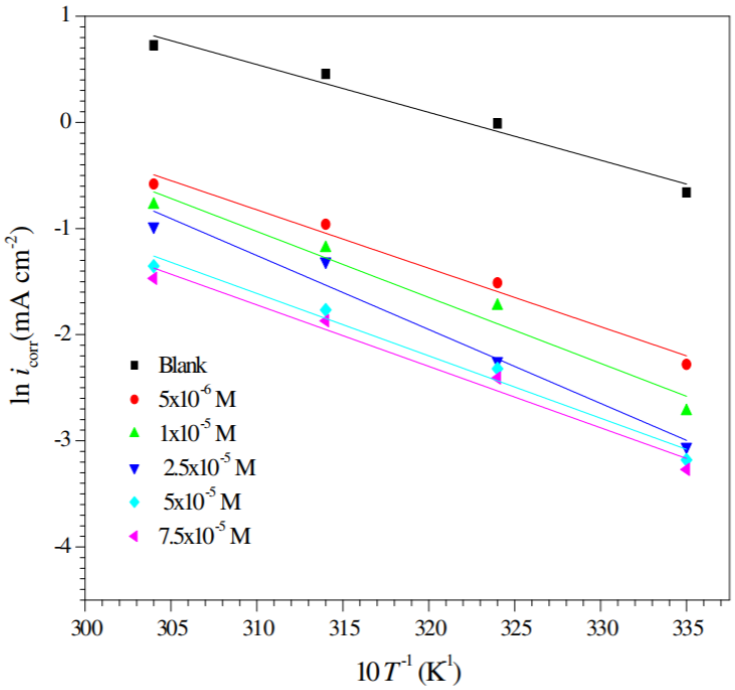

Figure 33: Arrhenius plot for mild steel in 1 M HCl in the absence and presence of NO_2AM inhibitor

The values of standard enthalpy of activation (ΔH*) and standard entropy of activation (ΔS*) for the formation of the activation complex in the transition state can be calculated by using the transition state equation as below:

$$\log\frac{CR}{T} = -\frac{\Delta H^*}{2.303\ RT} + [\log\frac{R}{Nh} + \frac{\Delta S^*}{2.303\ R}] \qquad (26)$$

Where, h is Plank’s constant and N is the Avogadro number, respectively. Plotting log (CR/T) versus 1/T gives straight lines of a slope [- $\Delta H^*/2.303R$] and an intercept [log(R/Nh) + ($\Delta S^*/2.303R$)], from which ΔH^* and ΔS^* can be calculated. The negative ΔS^* values can indicate that the formation of the activated complex in the rate determining step represents an association rather than a dissociation step, meaning that a decrease in disorder takes place during the course of the transition from reactants to activated complex [94]. Figure 34 shows the transition state plot of log CR/T versus 1000/T for mild steel in 15% HCl solution at different concentrations of MPTS inhibitor [9].

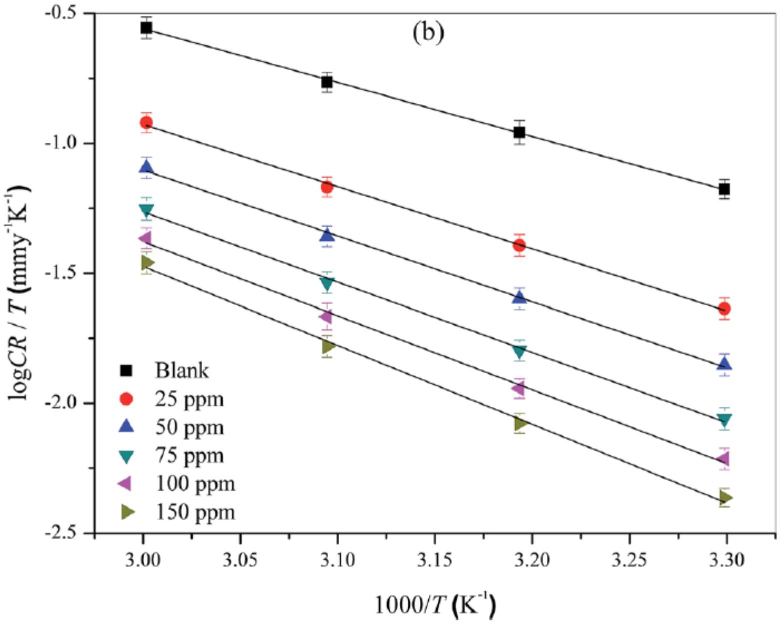

Figure 34: The transition state plot of log CR/T versus 1000/T for mild steel in 15% HCl using MPTS inhibitor [9]

2.9 Polymeric Inhibitors Mechanism

Reviewing the inhibitive mechanisms of polymeric inhibitors is going to help us in understanding the mechanism of the studied polymers PASP and PESA. Therefore, the below table shows some studied polymers and their suggested mechanism by the researchers.

Inhibitor	Mechanism	Ref.
Polyurethane: PNVP-PU and PDMAEMA-PU	Anodic inhibition mechanism with MS by forming Polymer-Fe complexes which lead to surface passivation by adsorption process. It involved physisorption and chemisorption. 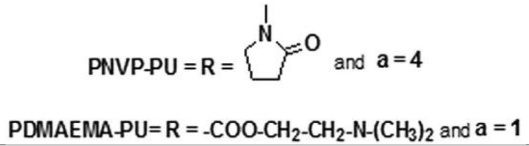	[95]
Polyvinylamide derivatives	The adsorption mechanism of the inhibitor, which corresponds to the displacement of water molecules and other ions adsorbed on the metal surface and the subsequent decrease in electrical capacity and increase in Rct. the inhibitor affects both parts of Tafel plots. Thus, they can be considered a mixed-type (cathodic and anodic) inhibitors. 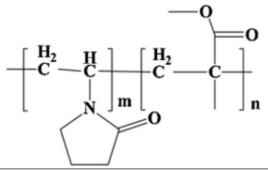	[96]
Polyethylene glycol (PEG)	The mechanism is suggested to be anodic mechanism by through the adsorption of PEG on MS surface from the heteroatoms (O). This is forming a protective film on steel surface and minimize corrosion. 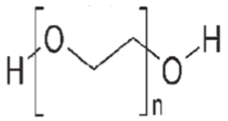	[97]
Poly(vinyl pyrrolidone) (PVP)	The mechanism is suggested to be anodic mechanism by through the adsorption of PVP on MS surface from the heteroatoms (N & O). This is forming a protective film on steel surface and minimize corrosion. 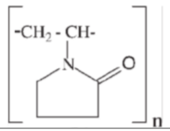	[97]
Plant leaves extract (PLE) and zinc	The formed complexes of (hystamine-Zn-hystamine, serotonin-Zn-serotonin, and quercetin-Zn-quercetin) are working as anodic and cathodic inhibitors. The chelation between Zn and organic inhibitors forming films of PLE-Zn which is depositing on metal surface and acting through anodic and cathodic inhibition mechanism.	[98]

CHAPTER 3

Experimental Section

3.1 Chemicals

All experiments were carried out in 3% NaCl solution prepared using NaCl analytical grade powder purchased from SIGMA-ALDRICH (USA) with purity ≥ 99%. The used water for preparing the standard solutions, testing and cleaning is distilled water with a conductivity < 2 μS/cm. The polymers used in all experiments were procured from Shandong Taihe Water Treatment Technologies Company. The chemical & physical properties of PASP and PESA are detailed in Table 5 for PASP and in Table 6 for PESA. Zinc standard solution was purchased from SIGMA-ALDRICH (USA) of 1000 mg/l Zn in an acidic solution. The dosage range of the inhibitors employed was 0.1 to 2.0 g/L. Figure 35 shows the prepared inhibitors solutions for corrosion tests.

Weight Loss	OCP	Tafel	EIS
0.1, 0.5, 1.0, 1.5, 2.0 g/l PASP or PESA	0.1, 0.5, 1.0, 1.5, 2.0 g/l PASP or PESA	0.1, 0.5, 1.0, 1.5, 2.0 g/l PASP or PESA	0.1, 0.5, 1.0, 1.5, 2.0 g/l PASP or PESA
0.01 g/L Zn with PASP	0.01 g/l Zn with PASP	0.01 g/l Zn with PASP	0.01 g/l Zn with PASP
0.002 g/L Zn with PESA	0.002 g/L Zn with PESA	0.002 g/l Zn with PESA	0.002 g/l Zn with PESA

Figure 35: the prepared inhibitors solutions for corrosion tests

Item	Units	Results
Chemical name	-	Sodium of Polyaspartic Acid (PASP)
Chemical structure	-	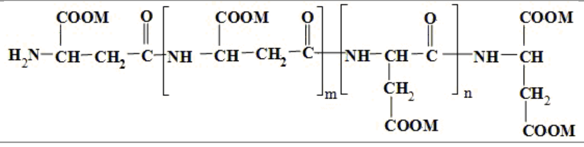
Molecular weight	-	500 - 1000
CAS number	-	181828-06-8
Appearance	-	Yellow to amber liquid
Solid content	%	40 ± 0.5
Density (20℃)	g/cm^3	1.254
pH(1% water solution)	-	9.20

Table 5: Chemical and physical properties of PASP

Item	Units	Results
Chemical name	-	Sodium of Polyepoxysuccinic Acid (PESA)
Chemical structure	-	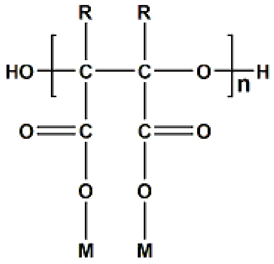 ; M = Na
Molecular weight	-	500 - 1000
CAS number	-	51274-37-4
Appearance	-	Pale yellow transparent liquid
Solid content	%	40 ± 0.5
Density (20℃)	g/cm^3	1.334
pH(1% water solution)	-	11.51

Table 6: Chemical and physical properties of PESA

3.2 Mild Steel Electrode

Through the whole study, we used a fixed grade of mild steel of a grade UNS G10180 (C1018) where its chemical composition is detailed in Table 6. It is important to highlight that prior to all measurements, the specimens were polished using silicon carbide papers of 400, 600, 800, 1000 and 1200 grade to obtain a mirror-like surface. Then, the MS specimen was degreased ultrasonically with acetone, washed with deionized water and then dried in a desiccator prior to use in electrochemical measurements. The dimensions of MS electrode or coupons were prepared as below depending on the usage.

3.2.1 Weight loss measurements

Mild steel C1018 specimens (1/2" × 3" × 1/16") of a surface area 3.24 in^2 were used for these experiments. Steel specimens were immersed in 400 ml 3% NaCl solution containing different concentrations of inhibitors at elevated temperatures for 168 hours (7 days) in open air conditions. Figure 36 shows weight loss MS coupons.

Figure 36: Mild steel coupons used for weight loss tests

3.2.2 Electrochemical measurements

The three-electrode cell is a jacketed type GAMRY EuroCell mounted on hotplate magnetic mixer with temperate controlling equipment as shown in Figure 37. GAMRY Jacketed EuroCell is a single compartment system having a counter electrode of graphite, reference electrode of saturated calomel electrode (SCE) and the working electrode of MS C1018 cylindrical mild steel specimen with an exposed surface area of 5.23 cm^2 as shown in Figure 38. All these electrodes were purchased from GAMRY company in order to be compatible with GAMRY cells.

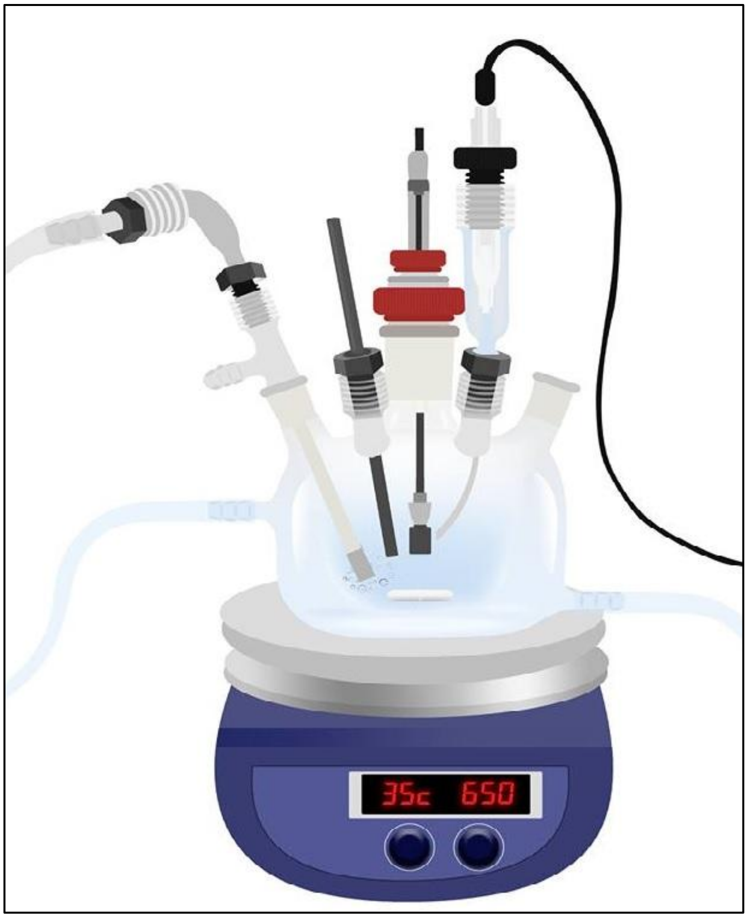

Figure 37: GAMRY EuroCell mounted on hotplate magnetic mixer with temperate controlling

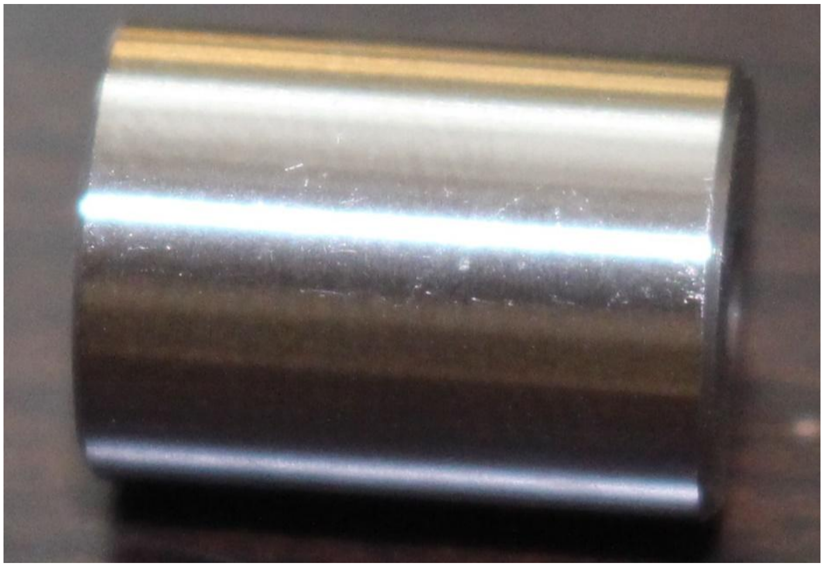

Figure 38: Gamry cylindrical MS C1018 coupon

3.3 Weight loss procedure

The below procedure was applied which is a summary of ASTM D 2688-05:

1- Coupons should be stored in well-sealed envelopes before and after exposure and to be handled with tissue paper or gloves.

2- The initial weight of the coupon with its number will be recorded (W_i)

3- Prepare the mixer to have a controlled temperature (25 - 45 ^oC) with an error of ± 1 ^oC.

4- Prepare the testing solution in the absence and presence of corrosion inhibitors and in 500 ml beakers.

5- Insert the coupons to be in the middle of testing solutions using Teflon tape if required.

6- Keep the coupons under very slow mixing speed (30 – 50 rpm) for 7 days (168 hrs) using multiple magnetic stirrers with water bath as in Figure 39.

7- Remove the coupon after passing the exposure time and dry them using tissue paper and distilled water. Keep the coupons in a desiccator for 8 hrs. till you get full dryness.

8- Weigh the coupons using analytical balance and consider this as a final weight (W_f).

9- Calculate the corrosion rate using the below equation:

$$CR\ (mm/year) = \frac{8.76 \times 10^4 \times W}{D \times A \times t} \tag{27}$$

where, W = weight loss ($W_f - W_i$, g), A = area of specimen (5.23 cm^2), D = mild steel density (7.85 $g.cm^{-3}$), and t = exposure time (168 h). The surface coverage and inhibition efficiency are calculated as per the below equations considering CR_i and CR_0 are corrosion rates in presence and absence of inhibitors, respectively.

$$\theta = \frac{CR_0 - CR_i}{CR_0} \tag{28}$$

$$\eta\,(\%) = \frac{CR_0 - CR_i}{CR_0} \times 100 \tag{29}$$

Figure 39: Multiple magnetic stirrers with controlled-temperature water bath

3.4 Electrochemical Measurements

All electrochemical measurements were carried out at constant temperatures in a three-electrode electrochemical cell at fixed mixing rate using magnetic stirrer. The three-electrode cell is a jacketed type GAMRY EuroCell mounted on hotplate magnetic mixer with temperate controlling equipment as shown in Figure 36. GAMRY Jacketed EuroCell is a single compartment system having a counter electrode of graphite, reference electrode of saturated calomel electrode (SCE) and the working electrode of MS C1018 cylindrical mild steel specimen. The experiments were performed using Gamry potentiostat (PCI 4 and Reference +600) integrated with Gamry framework system with EIS300, DC105, and E-Chem Analyst software for EIS, PDP measurements, and data fitting respectively. Potentiostat calibration was performed before starting the experiments. Tafel curves were obtained from the Potentiodynamic polarization measurements at scan rate 1 mV s^{-1} for a potential range of - 250 to 250 mV vs. SCE at the open circuit potential (E_{corr}). The linear anodic segments of cathodic and anodic curves of Tafel plot were extrapolated to obtain corrosion current densities (i_{corr}) and corrosion rates (CR). The inhibition efficiency percentage (η%) is calculated using the following equation:

$$\eta\,(\%) = \frac{i^0_{corr} - i_{corr}}{i^0_{corr}} \times 100 \qquad (30)$$

where, i^0_{corr} and i_{corr} are the values of corrosion current density in the absence and presence of inhibitor, respectively.

Electrochemical Impedance scans were performed at a sinusoidal excitation AC voltage of +10 mV (rms) and the response was determined in the frequency range of 100 kHz–10mHz with 10 points per decade. The resulting data were fitted to an equivalent circuit using E-Chem software. The corrosion current and rate were calculated from charge transfer resistance (R_{CT}) values obtained from EIS measurements and the inhibition efficiency (η%) was calculated using the following equation:

$$\eta\,(\%) = \frac{R^o_{CT} - R_{CT(inh)}}{R^o_{CT}} \times 100$$

(31)

where, R_{CT}^{o} and $R_{CT(inh)}$are the values of charge transfer resistance in the absence and presence of inhibitor, respectively.

3.5 Surface Characterization

Surface analysis of mild steel specimen of the adsorbed film was performed by different techniques. FTIR tests were performed for the polymers (PASP and PESA) and for the formed film on mild steel surface using Thermo Omnic FTIR spectrophotometer. Scanning electron microscopy of TESCAN LYRA 3 was used to get surface micrographs. The SEM system is equipped with energy dispersive x-ray detector by Oxford Co. was used to get the surface analysis and understand the composition of the adsorbed film. The AFM images for the uninhibited and inhibited MS specimens were obtained using Agilent 5100 SPM system in tapping mode of a rate 1-3 lines per second. It is designed to evaluate the formed film and inhibition mechanism of PASP or PESA inhibitors.

3.6 Computational Study

Quantum chemical calculations were carried out to provide atomic-level information into the activity of PASP/PESA as corrosion inhibitor using AMI method in the VAMP module using the BIOVIA-Materials Studio 8.0 software. The AM1 semi-empirical quantum chemical calculation theory was adopted because of the huge size of the polymers studied. PASP/PESA conformers were optimized to a global minimum in the gas phase. Thereafter, electronic parameters such as HOMO and LUMO orbitals, which indicate reactivity sites of PASP/PESA, were obtained.

Metropolis Monte Carlo simulations using simulated annealing procedure were further carried out to quantify the adsorption of PSAP/PESA alone and PSAP-Zn/PESA-Zn mixtures on the steel surface. The calculation was carried out using the Adsorptor locator module using the BIOVIA-Materials Studio 8.0 software licensed to KFUPM. The simulation box consisted of 5-layers of iron atoms cleaved along the (110) plane. A supercell of (13 × 13) was created and vacuum layer of 50 nm height was fabricated. Equilibrium adsorption configurations and the adsorption energies for the interaction of the systems on Fe (110) surface were obtained. More details on the Methodology of Monte Carlo simulations are available elsewhere.

CHAPTER 4

Results & Discussions

4.1 PASP Inhibitor Results

In this section, the results and findings of tests and characterizations were done on PASP inhibitor will be presented and discussed.

4.2.1 Weight loss results

Weight loss results for MS in 3% NaCl solution were obtained in mpy (milli-inch per year) after 168 hours (7 days) immersion in open-air solutions in the absence and presence of different concentrations of PASP and then Zn ions at different temperatures (298-308 K) as listed in Table 7. After immersion time elapsed, the coupons were cleaned using tissue paper and washed with deionized water followed by acetone and then dried in a desiccator at ambient temperature. Inspection of the data in table 7 reveals that inhibition efficiency increases with increasing the concentration of PASP until 2 g/L. The addition of 0.01 g/L Zn^{+2} improved the efficiency significantly. On the other hand, increase in temperature led to a decrease in the efficiency of PASP and no remarkable effect was noticed after zinc ion addition. Such behavior can be explained on the basis that PASP adsorbed on MS surface and the increase in temperature caused desorption of a portion of adsorbed molecules and led to a decrease in the efficiency [9][99]. Figures 40 and 41 shows the corrosion rate and inhibition efficiency using PASP inhibitor only and with 0.01 g/l Zn ion, respectively.

Temp.		**298 K**				**303 K**				**308 K**			
Conc. (g/l)		**CR (mpy)**	**CR (mmy)**	**θ**	**η%**	**CR (mpy)**	**CR (mmy)**	**θ**	**η%**	**CR (mpy)**	**CR (mmy)**	**θ**	**η%**
Blank		**19.9**	**0.5055**	**-**	**-**	**27.4**	**0.6960**	**-**	**-**	**36.8**	**0.9347**	**-**	**-**
PASP	**Zn**												
0.1	**-**	12.6	0.3200	0.37	**37**	18.2	0.4623	0.33	**33**	25.4	0.6452	0.31	**31**
0.5	**-**	11.0	0.2794	0.45	**45**	16.2	0.4114	0.41	**41**	22.1	0.5613	0.40	**40**
1.0	**-**	10.2	0.2591	0.49	**49**	15.1	0.3835	0.45	**45**	20.8	0.5283	0.43	**43**
1.5	**-**	9.3	0.2362	0.53	**53**	13.4	0.3404	0.51	**51**	18.9	0.4801	0.49	**49**
2.0	**-**	7.8	0.1981	0.61	**61**	11.5	0.2921	0.58	**58**	16.1	0.4089	0.56	**56**
0.1	**0.01**	3.4	0.0864	0.83	**83**	5.6	0.1422	0.80	**80**	7.60	0.1930	0.79	**79**
0.5	**0.01**	0.51	0.0129	0.97	**97**	0.93	0.0236	0.97	**97**	1.20	0.0305	0.97	**97**
1.0	**0.01**	0.04	0.0010	1.00	**100**	0.08	0.0020	1.00	**100**	0.10	0.0025	1.00	**100**
1.5	**0.01**	0.01	0.0002	1.00	**100**	0.01	0.0002	1.00	**100**	0.02	0.0004	1.00	**100**
2.0	**0.01**	0.00	0.0001	1.00	**100**	0.01	0.0001	1.00	**100**	0.01	0.0002	1.00	**100**

Table 7: Weight loss results at different inhibitors concentrations and temperatures

Table 7 shows that PASP alone has moderate inhibition at high concentration. It was found that the efficiency at 2 g/L is 61% at 298 K, while it reached almost 100 % when 0.01 g/l Zn^{+2} were added to PASP at the same temperature. The inhibition efficiency of PASP and Zn was concluded to be more efficient than PASP alone at all temperatures and dosages. This may suggest that PASP has moderate adsorption on metal surface under the anodic mechanism, while Zn ions work as a cathodic inhibitor and synergize PASP mechanism to achieve high-efficiency results.

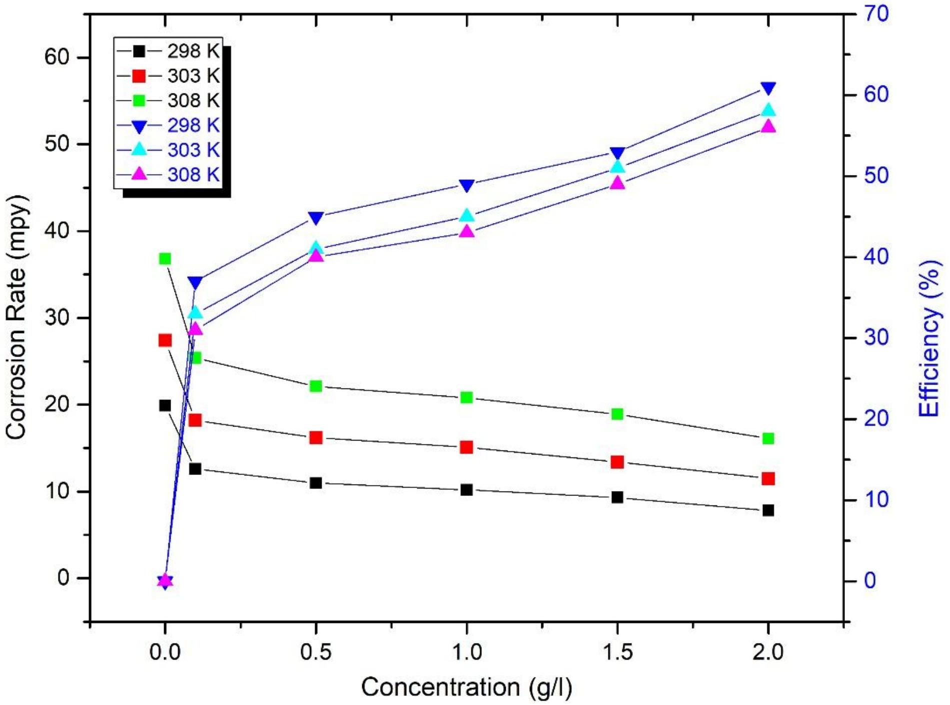

Figure 40: Corrosion rates and efficiency of MS using PASP inhibitor at different concentrations

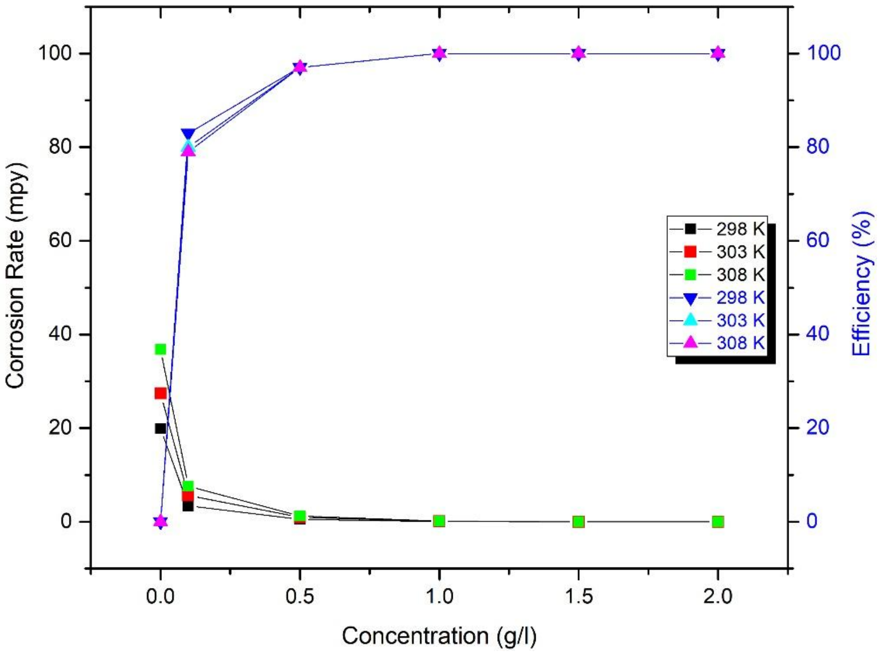

Figure 41: Corrosion rates and efficiency of MS using PASP inhibitor at different concentrations + 0.01 g/l Zn

4.2.2 Thermodynamic parameters

The activation energy (Ea) for MS dissolution in 3% NaCl was calculated by using the following Arrhenius equation:

$$\log CR = \frac{-E_a}{2.303\ RT} + \log A \tag{32}$$

Where R (8.314 J K^{-1} mol^{-1}) is the ideal gas constant, A is Arrhenius pre-exponential factor, and T is Kelvin temperature. Figure 42 (a, b) presents a plot of log CR versus 1/T in absence and presence of both cases of PASP only and with 0.01 g/l Zn^{+2}. As shown in these figures, the activation energy (E_a) was calculated from the slope as summarized in Table 8. It is noticeable that activation energy values for the inhibited solutions are higher than the ones of the uninhibited solutions, and continue to increase as inhibitor concentration increases especially in the presence of zinc ions [93].

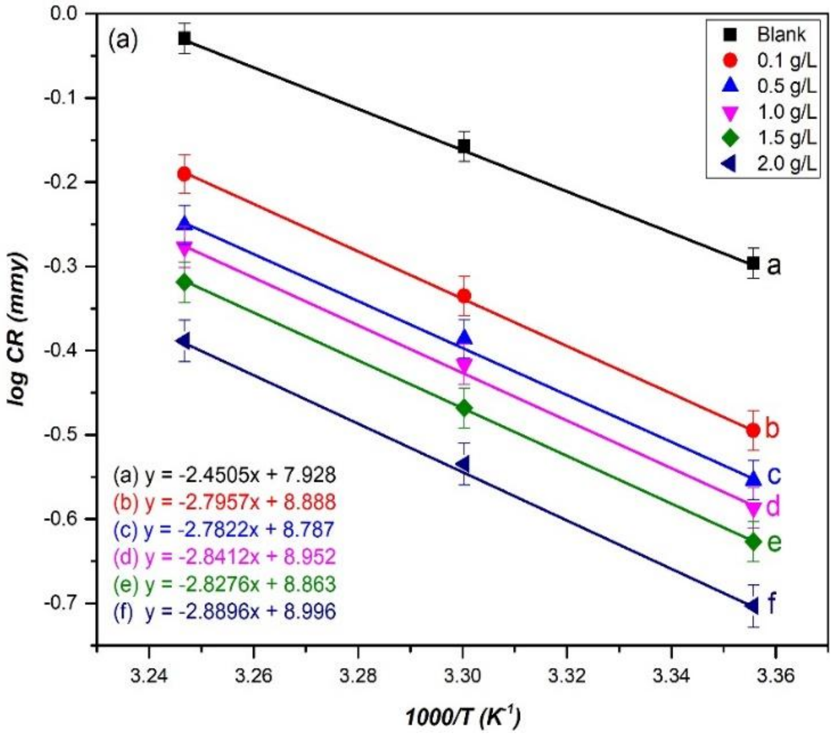
(a)
Blank
0.1 g/L
0.5 g/L
1.0 g/L
1.5 g/L
2.0 g/L
a
b
c
d
e
f
(a) y = -2.4505x + 7.928
(b) y = -2.7957x + 8.888
(c) y = -2.7822x + 8.787
(d) y = -2.8412x + 8.952
(e) y = -2.8276x + 8.863
(f) y = -2.8896x + 8.996
log CR (mmy)
1000/T (K^{-1})
0.0
-0.1
-0.2
-0.3
-0.4
-0.5
-0.6
-0.7
3.24
3.26
3.28
3.30
3.32
3.34
3.36

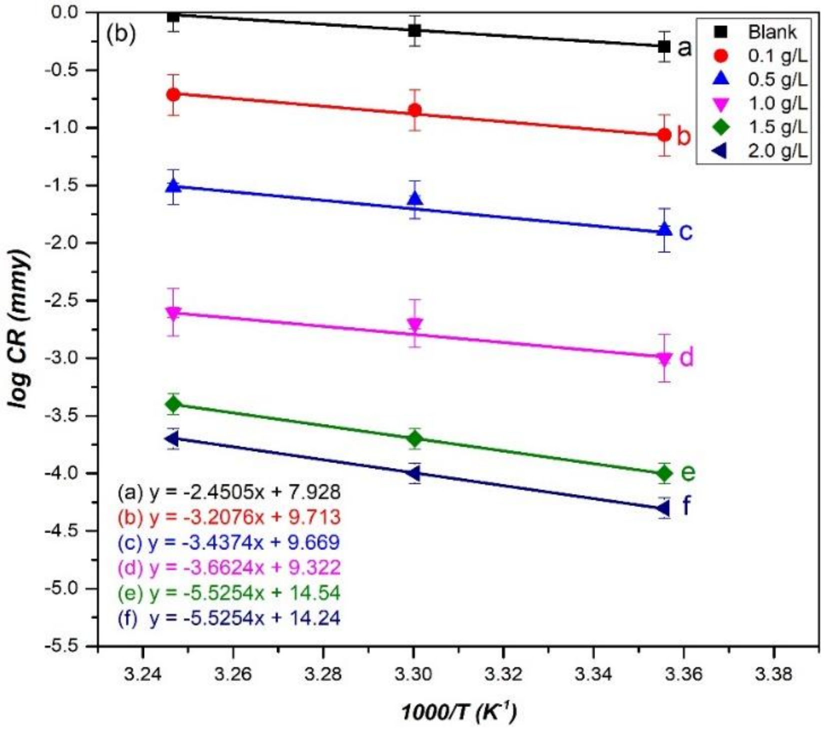

Figure 42: Arrhenius plots of log CR vs. 1000/T for MS corrosion in 3% NaCl solution (a) PASP (b) PASP + 0.01 g/L Zn

The thermodynamic parameters including the standard enthalpy of activation (ΔH^*) and the standard entropy of activation (ΔS^*) for the formation of an activated complex in the transition state were calculated using the following equation:

$$\log\frac{CR}{T} = -\frac{\Delta H^*}{2.303\,RT} + [\log\frac{R}{Nh} + \frac{\Delta S^*}{2.303\,R}] \tag{33}$$

Where, h is Plank's constant and N is the Avogadro number, respectively. Plotting log (CR/T) versus 1/T gives straight lines of a slope [- $\Delta H^*/2.303R$] and an intercept [log(R/Nh) + ($\Delta S^*/2.303R$)] as in Figure 43 (a and b), from which ΔH^* and ΔS^* were calculated as listed in Table 8. As tabulated in Table 8, for the both sets $E_a > \Delta H^*$ by a value which almost equal to RT. Thus, metal surface corrodes in 3% NaCl solutions in the absence and presence of inhibitors by what is called unimolecular reaction. The gradual increase of ΔS^* values for all cases indicates a decrease in disorder takes place during the course of the transition from reactants to the activated complex which reflects a decrease in the formation of activated complex and a decrease of overall corrosion reaction rate [100].

Inhibitors (g/l)		**E_a (kJ mol^{-1})**	**ΔH^* (kJ mol^{-1})**	**ΔS^* (J mol^{-1} K^{-1})**
Blank		46.91402	44.39488	-101.603
PASP	**Zn**	-	-	-
0.1	**-**	53.52067	51.00153	-83.2158
0.5	**-**	53.62669	50.72461	-82.6701
1.0	**-**	54.37632	51.85718	-82.025
1.5	**-**	54.71148	51.61793	-79.8773
2.0	**-**	55.31115	52.79202	-67.2277
0.1	**0.01**	61.34096	58.89718	-67.3753
0.5	**0.01**	65.67587	63.2972	-68.2655
1.0	**0.01**	69.93403	67.60664	-74.904
1.5	**0.01**	86.65896	84.13063	-57.3327
2.0	**0.01**	86.65896	84.24742	-51.6077

Table 8: Activation thermodynamic parameters for MS in 3% NaCl in the absence and presence of inhibitors

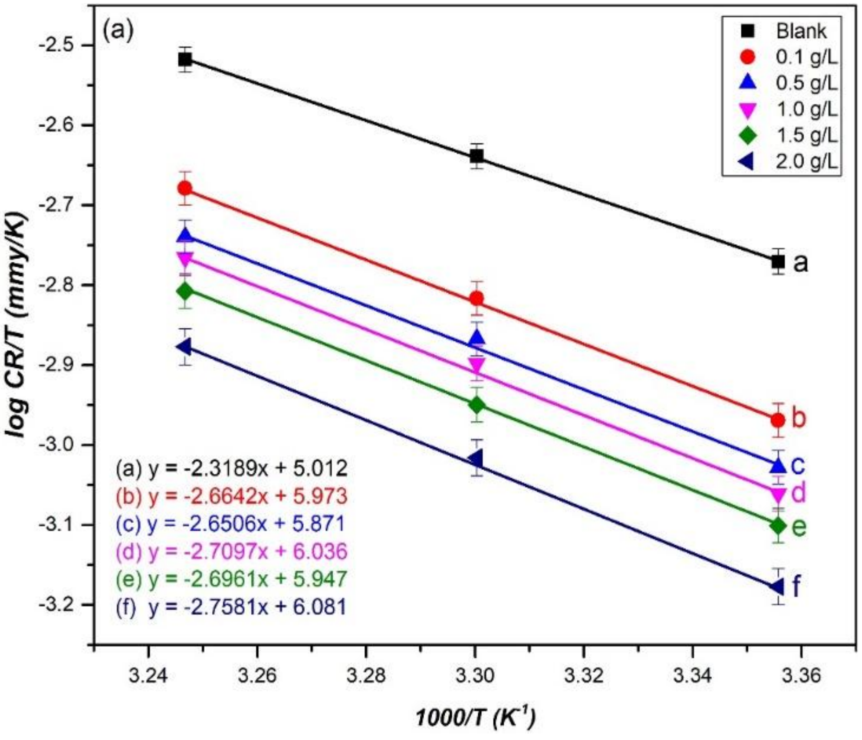
(a)
Blank
0.1 g/L
0.5 g/L
1.0 g/L
1.5 g/L
2.0 g/L
a
b
c
d
e
f
(a) y = -2.3189x + 5.012
(b) y = -2.6642x + 5.973
(c) y = -2.6506x + 5.871
(d) y = -2.7097x + 6.036
(e) y = -2.6961x + 5.947
(f) y = -2.7581x + 6.081
log CR/T (mmy/K)
-2.5
-2.6
-2.7
-2.8
-2.9
-3.0
-3.1
-3.2
1000/T (K-1)
3.24
3.26
3.28
3.30
3.32
3.34
3.36

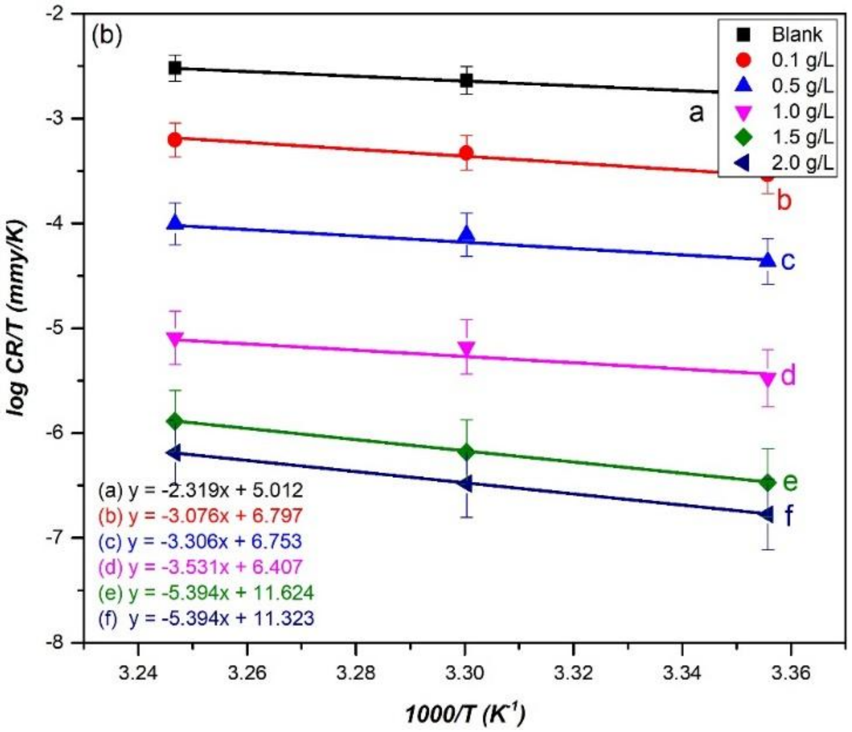

Figure 43: Transition state plots for MS in 3% NaCl solutions at different concentrations (a) PASP (b) PASP + 0.01 g/L Zn

4.2.3 Open circuit potential measurements

Open circuit potential (E_{ocp}) is an indicative factor in corrosion inhibition mechanism that is identified as the corrosion potential in the absence of net electrical current flowing through the metal surface. When corrosion reaction reaches equilibrium, E_{ocp} reaches a steady-state and it becomes equal to the corrosion potential (E_{corr}). The evolution of potential versus time constitutes a methodology for monitoring interface changes between a metal and its environment [73][101]. The E_{ocp} curves of MS working electrode in aerated 3% NaCl solutions in the presence and absence of PASP synergistic inhibitors are shown as shown in Figure 44 (a and b). These figures represent the variation of the E_{ocp} under the experimental conditions as a function of time in presence of PASP alone and then with Zn ions as a synergistic cathodic inhibitor. It could be observed from figure 44 that at steady-state, E_{ocp} was achieved after approximately 4500 seconds of immersion in the presence of PASP, while a steady state of E_{ocp} value was not achieved even after 6500 seconds of immersion in the absence of PASP which can be attributed to the porous nature of corrosion product layer. It is observable that - after reaching equilibrium - the potential is shifting toward negative values, which can be attributed to corrosion reactions on metal surface under this strong corrosive environment. In the presence of PASP, the E_{ocp} value at the steady state shifted to less negative values and reached steady-state conditions due to the adsorption of PASP on metal surface after the inhibition time which significantly reduces the porosity of the corrosion layer. It is also noted that the positive shift of corrosion potential was found to be concentration potential. Similar observations have been seen in figure 44 as the addition of Zn ions enhanced the inhibition efficiency and exhibited a synergistic effect on PASP under these test conditions.

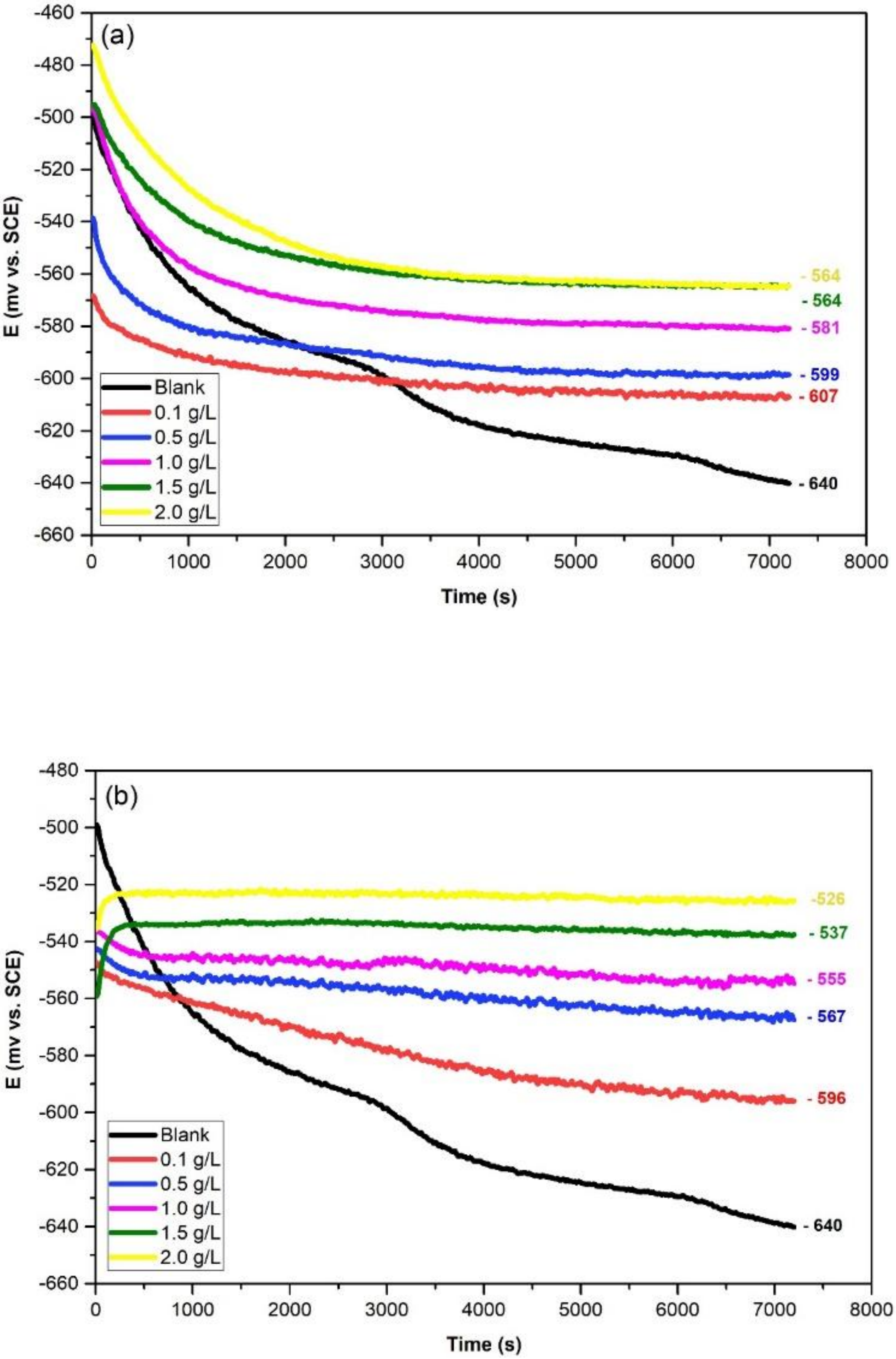

Figure 44: Open circuit potential for MS using (a) PASP inhibitor (b) PASP inhibitor + 0.01 g/L Zn

4.2.4 Polarization measurements

Potentiodynamic polarization scans of PASP and its mixtures for mild steel in 3% NaCl solution were conducted at 35 °C (308 K) in presence and absence of inhibitors was undertaken in order to understand PASP inhibition mechanism whether it is anodic, cathodic or mixed-type organic inhibitor as shown in Figures 45 and 46. The electrochemical parameters including corrosion potential (E_{corr}), corrosion current density (i_{corr}), anodic Tafel slope (β_a), cathodic Tafel slope (β_c), corrosion rate (C_{rate}) and inhibition efficiency (η) values are listed in Table 9. This technique utilizes data obtained from cathodic and anodic polarization measurements by extrapolating the linear Tafel segments in a large domain of potential to the corresponding corrosion potential to obtain the corrosion currents. The calculation of inhibition efficiency (η%) was done from the polarization measurements and listed as well.

To understand the mechanistic behavior of PASP, it is good to highlight the corrosion mechanism of mild steel in nearly neutral aerated aqueous medium such as NaCl solution [73]. The reactions are as follows:

$$Fe \rightarrow Fe^{2+} + 2e^- \tag{34}$$

$$Fe^{2+} + Cl^- \rightarrow FeCl_2 \tag{35}$$

$$FeCl_2 + 2H_2O \rightarrow Fe(OH)_2 + 2H^+ + 2Cl^- \tag{36}$$

$$Fe^{2+} \overset{O_2}{\rightarrow} Fe^{3+} + 1e^- \tag{37}$$

The corresponding reduction reaction at cathodic sites is:

$$O_2 + 2H_2O + 4e^- \rightarrow 4OH^- \quad (38)$$

The products of the two anodic and cathodic reactions form $Fe(OH)_2$ which precipitates gradually on the metal surface and reacts with dissolved oxygen giving a complex corrosion product layer that consists of several iron oxides and hydroxides which includes: FeO, FeOOH, and Fe_2O_3.

Tafel polarization curves, illustrated in Fig 45, show that the adsorption of PASP on the MS surface causes a moderate decrease in current density (i_{corr}) which conforms with results of OCP measurements. The addition of PASP to NaCl solution shifts corrosion potentials to a more positive direction. It can be observed that PASP suppresses the anodic reaction significantly while it has a limited effect on the cathodic reaction. The area of Tafel cathodic branch that appears from -600 to -1000 mV versus SCE can be attributed to neutral solutions to oxygen reduction reaction under diffusion control.

Various approaches have been reported to determine corrosion currents of processes controlled only by convective diffusion at a relatively low rotation speed (up to 1000 rpm), the corrosion rate can be considered equal to the limiting diffusion current [73][102]. In this case, the cathodic reaction is independent of PAPS concentration. Therefore, the cathodic branch cannot be extracted to get i_{corr} [103]. Because PASP alone is anodic inhibitor since the anodic current exhibits a plateau, its extrapolation allows calculating inhibition efficiency but not accurately. Thus, i_{corr} was determined from the Tafel curves by extrapolation of both anodic and cathodic branches. In addition, electrochemical impedance spectroscopy was pursued findings that are more accurate.

Zinc is a well-known cathodic inhibitor synchronize in corrosion inhibition of mild steel with anodic adsorption inhibitors [104]. In Figure 46, the inhibition efficiency has increased dramatically with the addition of 0.01 g/l Zn^{+2} with PASP. It is clear, that the inhibitive effect increases as PASP concentration increases in the presence of Zn. In additions, it is shown in polarization curves that both anodic and cathodic branches were changed through the inhibition of anodic and cathodic corrosion reactions. At dosages more than 0.1 g/L of PASP, the inhibition efficiency reached to an excellent level and corrosion rates became very slow lower than 1 mpy.

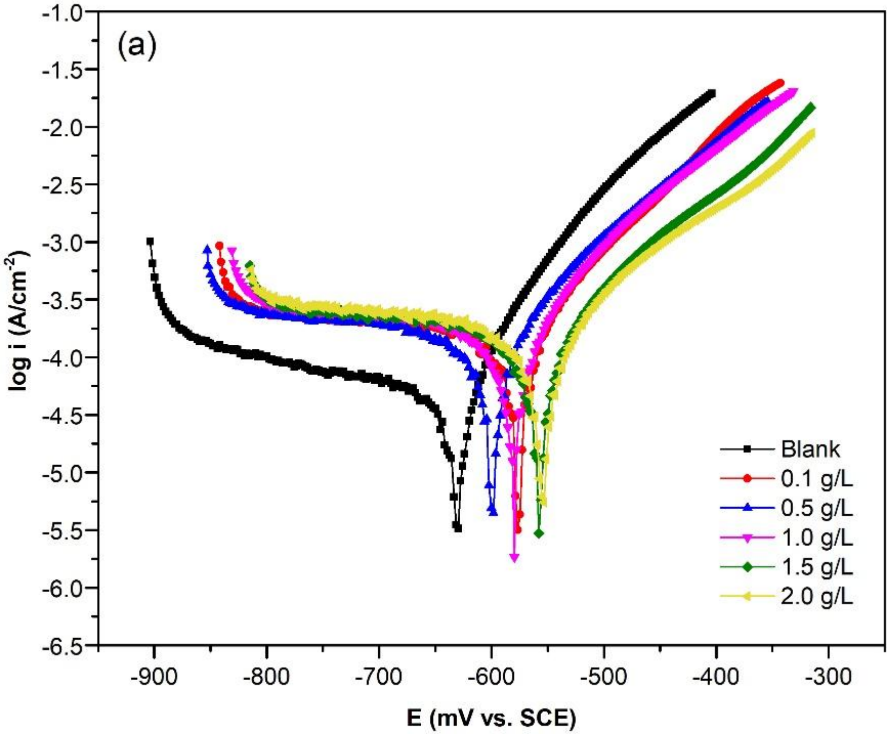

Figure 45: Tafel plots of using PASP inhibitor at different concentrations

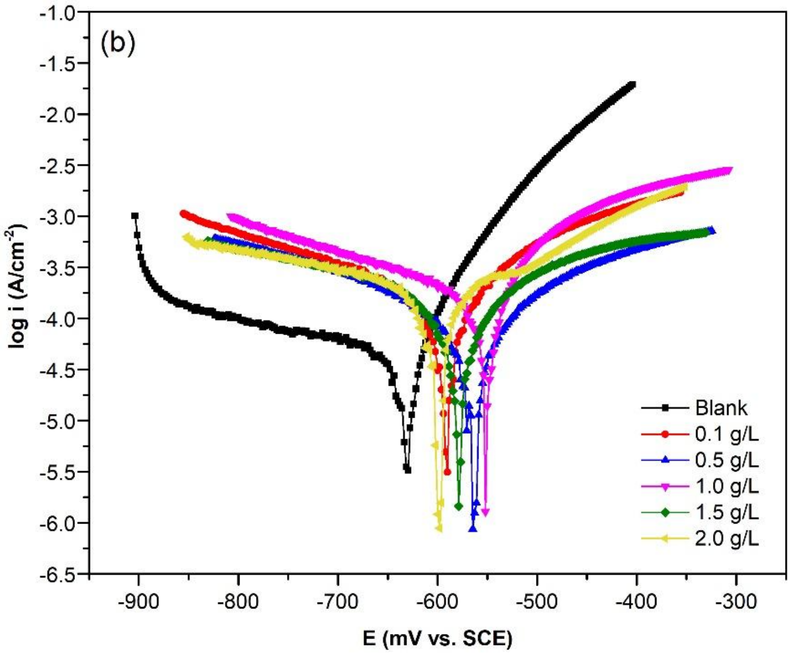

Figure 46: Tafel plots of using PASP + 0.01 g/L Zn at different concentrations

Inhibitor	E_{corr} (mV/SCE)	i_{corr} (mA/cm^2)	β_a (mV/dec)	β_c (mV/dec)	C_{rate} (mpy)	η (%)	θ
Blank - 3% NaCl	**-629**	**0.0132**	**68**	**533**	**47.50**	**-**	**-**
0.1 g/L PASP	**-580**	**0.0671**	**56**	**109**	**30.64**	**35**	**0.35**
0.5 g/L PASP	**-598**	**0.0629**	**58**	**87**	**28.76**	**39**	**0.39**
1.0 g/L PASP	**-580**	**0.0562**	**51**	**80**	**25.34**	**46**	**0.46**
1.5 g/L PASP	**-557**	**0.0495**	**43**	**72**	**22.63**	**52**	**0.52**
2.0 g/L PASP	**-553**	**0.0385**	**38**	**49**	**17.60**	**63**	**0.63**
0.1 g/L PASP + 0.01 g/L Zn	**-590**	**0.0156**	**17**	**27**	**7.15**	**85**	**0.85**
0.5 g/L PASP + 0.01 g/L Zn	**-565**	**0.0016**	**11**	**11**	**0.71**	**98**	**0.98**
1.0 g/L PASP + 0.01 g/L Zn	**-564**	**0.0011**	**10**	**11**	**0.52**	**99**	**0.99**
1.5 g/L PASP + 0.01 g/L Zn	**-564**	**0.0009**	**10**	**11**	**0.31**	**> 99**	**≈ 100**

2.0 g/L PASP + 0.01 g/L Zn	**-564**	**0.0008**	**10**	**10**	**0.25**	**> 99**	**≈ 100**

Table 9: Potentiodynamic polarization results using Tafel plots

4.2.5 EIS measurements

EIS technique is used to assess the mild steel corrosion inhibition efficiency of PASP in aerated 3.5% NaCl solution. Potentiostatic Electrochemical Impedance scans were conducted to provide insights on the process kinetics and the effect the adsorption of PASP on the metal surface has the double layer thickness and charge transfer process at the inhibitor-metal interface. Potentiostatic EIS data presented Bode and Nyquist diagrams for PASP and PASP-Zn mixtures in Figures 47 and 48 respectively and corresponding results are illustrated in Table 10. EIS phase angle data are presented in Figure 49.

The appearance of capacitive semicircles as observed in all Nyquist spectra for both inhibited and the uninhibited specimen is believed to be due to charge transfer resistance and double layer capacitance. Typically, impedance spectra in the form of the depressed semicircle in the complex plane with center under the real axis are believed to be the behavior of solid electrodes. The appearance of inductive semicircles in Nyquist plot when no inhibitor is added can be attributed to the molecular diffusion of oxygen through a porous layer built up by corrosion which is the reaction limiting step [105].

The equivalent circuit by which the EIS plots were analyzed is presented in Figure 50 where, R_s is the solution resistance, R_{ct} is the charge transfer resistance, C_{dl} is the electrochemical double layer capacitance, R_f is the combined resistance of adsorbed inhibitor layer and the protective corrosion product layer (the protective layer) and C_f is the protective layer capacitance.

At low frequencies (ω → 0) the equivalent circuit is reduced to combination Rs, Rf and Rct, while at high frequencies (ω → ∞) the equivalent circuit is reduced to Rs which represents the intersect of Nyquist plot with real impedance axis near its origin.

By comparing the Nyquist plot of an uninhibited solution with plots for inhibited solutions it is observed that uninhibited solution plot exhibits a complex combination of low-frequency inductive loop and high-frequency capacitive loops with two major time constants. When PASP is added to the solution, the effect of the inductive loop is reduced and at high concentrations, only one capacitive loop remains. It is also noticed that the polarization resistance significantly increases with increasing PASP concentration which is illustrated by the increase of the corresponding Nyquist semicircle plots. Bode plots exhibit increment in double layer impedance on both low frequency and high-frequency ranges by increasing PASP concentration which can be attributed to the reduction of the porosity of the corrosion product layer as well as increasing charge transfer resistance due to the reduction double layer capacitance as a result of PASP adsorption.

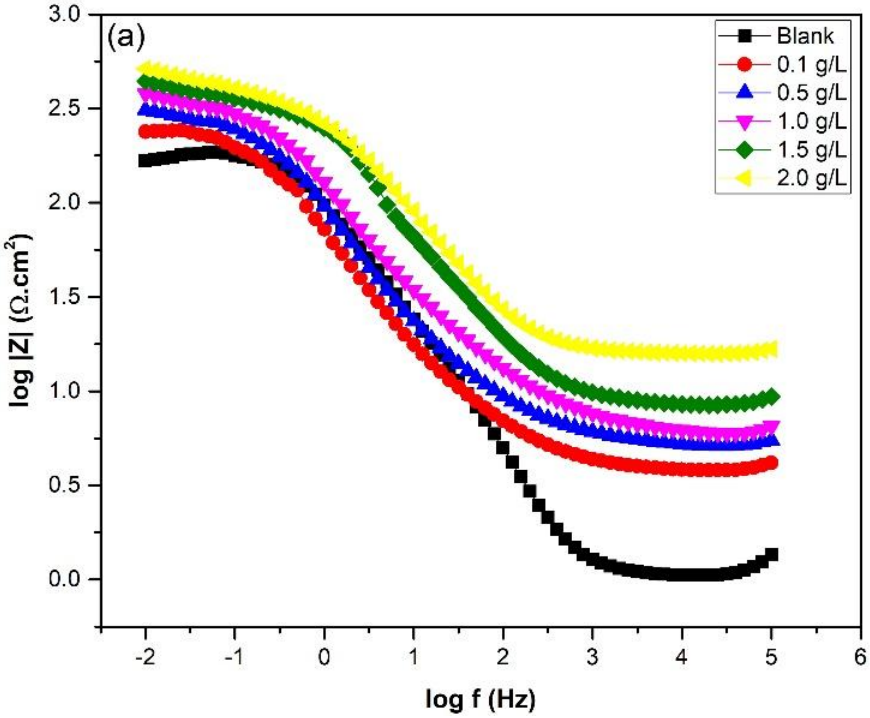
(a)
Blank
0.1 g/L
0.5 g/L
1.0 g/L
1.5 g/L
2.0 g/L
log |Z| (Ω.cm^2)
3.0
2.5
2.0
1.5
1.0
0.5
0.0
-2
-1
0
1
2
3
4
5
6
log f (Hz)

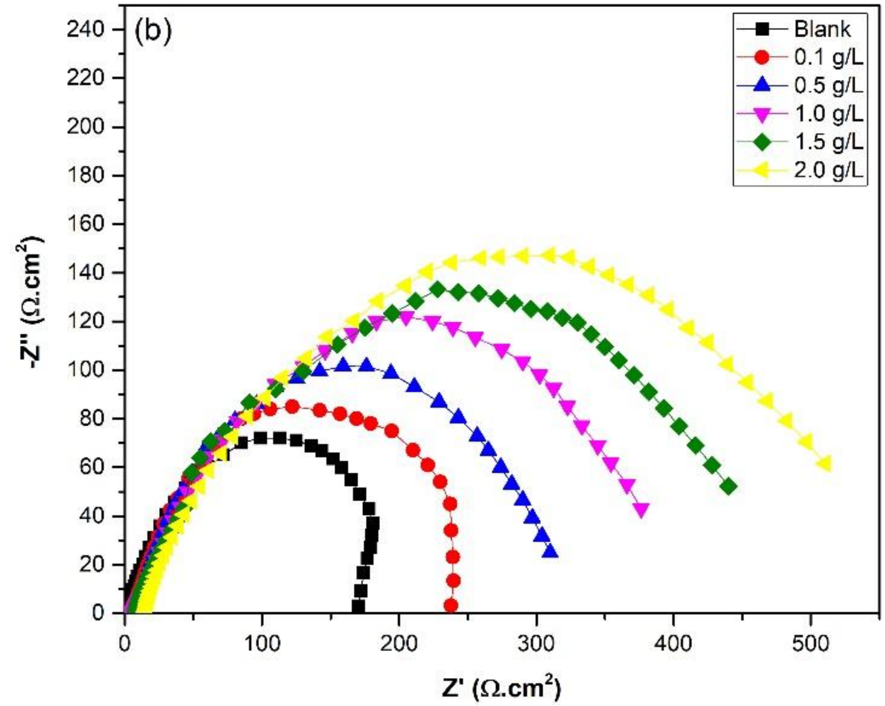

Figure 47: Plots for impedance spectra for mild steel in 3% NaCl in the presence and absence of PASP (a) Bode (b) Nyquist

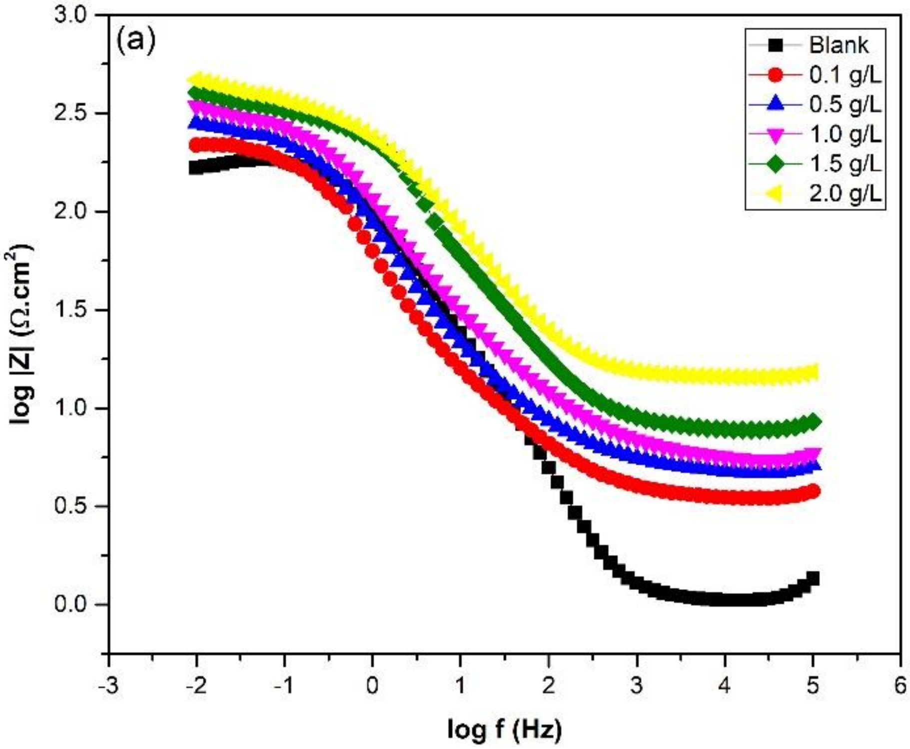

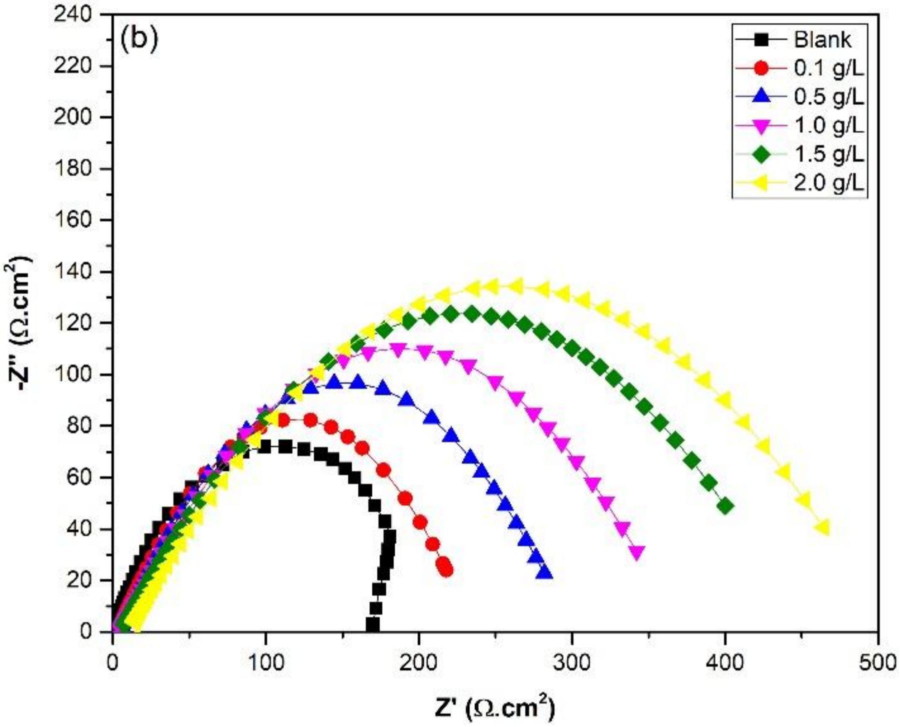

Figure 48: Plots for impedance spectra for mild steel in 3% NaCl in the presence and absence of PASP and 0.01 g/l Zn (a) Bode (b) Nyquist

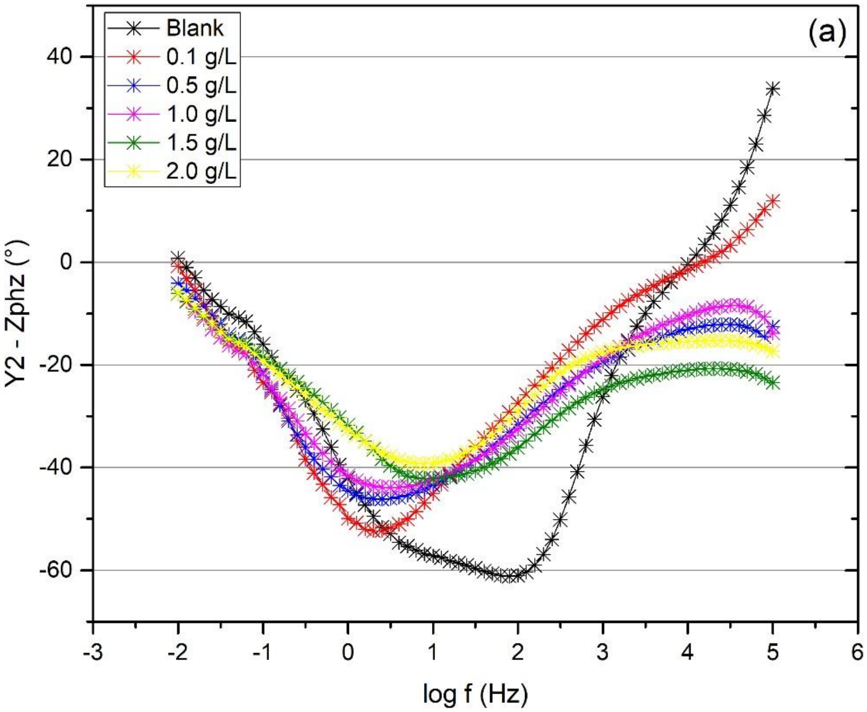

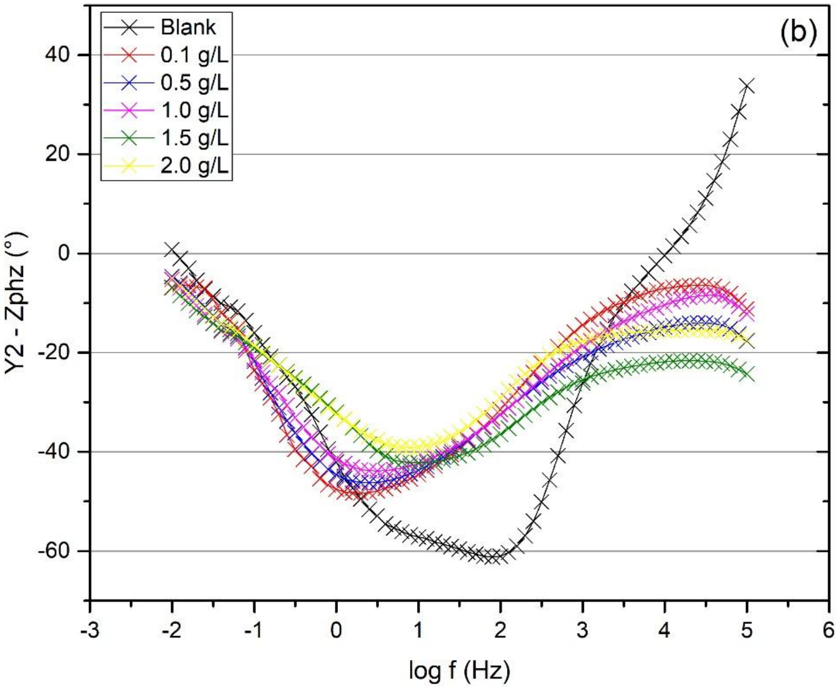

Figure 49: Phase angle of EIS for MS using (a) PASP inhibitor (b) PASP inhibitor + 0.01 g/L Zn

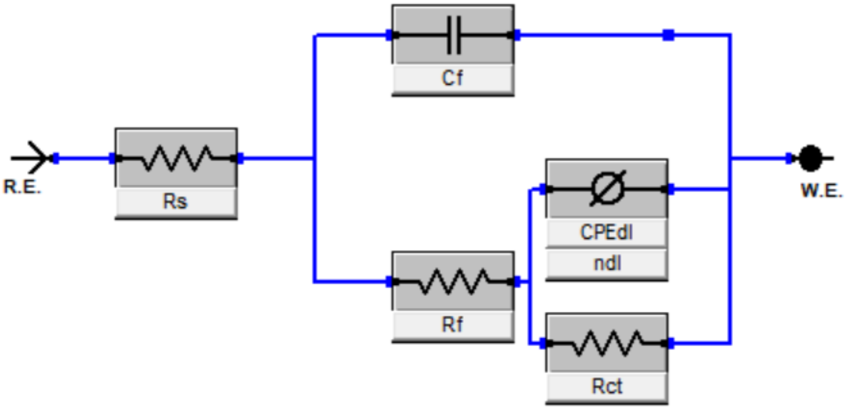

Figure 50: Equivalent circuit used to model impedance data of carbon steel in aerated 3% NaCl solution

Inhibitor	Rs (ohm)	R_{ct} (ohm)	R_f (ohm)	Cdl	Cf	CR (mpy)	η (%)
Blank - 3% NaCl	0.760	40.61	0.42	6.20×10^{-3}	1.53×10^{-3}	56.4	-

0.1 g/L PASP	0.710	48.70	0.71	14.7×10^{-3}	5.54 × 10-^{4}	28.9	48.8
0.5 g/L PASP	0.730	60.54	0.42	12.0×10^{-3}	3.43×10^{-4}	21.8	61.3
1.0 g/L PASP	0.750	76.22	0.42	10.6×10^{-3}	2.29×10^{-4}	15.5	72.5
1.5 g/L PASP	0.730	90.26	0.45	3.52×10^{-3}	1.31×10^{-4}	11.3	79.9
2.0 g/L PASP	0.740	106.30	0.45	3.20×10^{-3}	0.94×10^{-4}	7.6	86.4
0.1 g/L PASP + 0.01 g/L Zn	0.661	44.27	0.18	17.5×10^{-3}	10.0×10^{-4}	9.0	84.1
0.5 g/L PASP + 0.01 g/L Zn	0.656	60.26	0.26	16.5×10^{-3}	1.22×10^{-5}	3.5	93.9
1.0 g/L PASP + 0.01 g/L Zn	0.670	74.10	0.38	12.9×10^{-3}	2.76×10^{-6}	2.7	95.2
1.5 g/L PASP + 0.01 g/L Zn	0.661	77.63	0.72	3.74×10^{-3}	2.46×10^{-6}	2.6	95.5
2.0 g/L PASP + 0.01 g/L Zn	0.651	86.63	1.89	3.25×10^{-3}	4.72×10^{-7}	2.2	96.1

Table 10: Electrochemical parameters calculated from EIS measurements for mild steel in 3% NaCl in the presence and absence of different concentrations of inhibitors at 298 K.

4.2.6 Surface analysis results

4.2.6.1 Analysis of FTIR spectra

FTIR was utilized to characterize the polymer PASP. In addition, steel specimen was immersed in 2.0 g/L PASP solution for 24 hours and then thin surface layer was scratched and analyzed by FTIR in order to evaluate the presence of adsorbed polymer on the steel surface. Figure 51 revealed the adsorption peaks appear at 1153 cm^{-1} and 3421 cm^{-1} correspond to the antisymmetric stretch of C-O and O-H of the carboxylic group. The peak at 1397 cm^{-1} refers to the C-N symmetric stretching of the acylamide group. The peak at 1633 cm^{-1} is assigned to the bending of amine N-H bond.

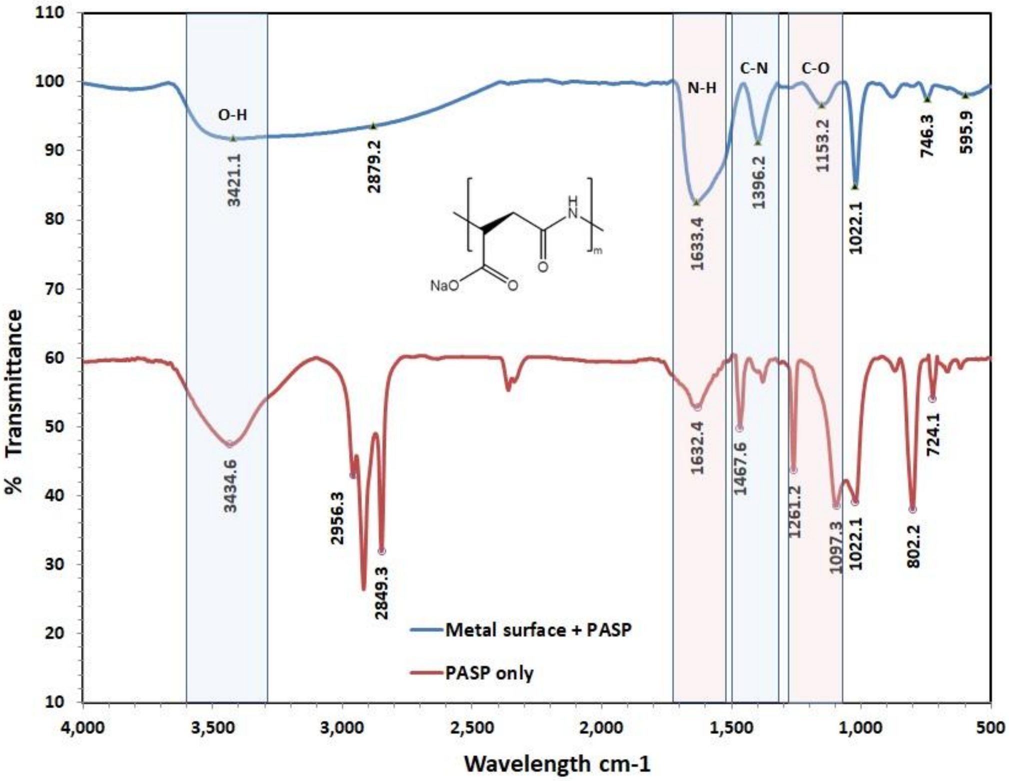

Figure 51: FTIR of PASP inhibitor and on MS surface at 2.0 g/L PASP

4.2.6.2 Scanning electron microscopy (SEM)

SEM micrographs of MS specimens before and after immersion in 3% NaCl solution as well as in the presence of 2.0 g/L PASP and 2.0 g/L PASP with 0.01 g/L Zn^{+2} are shown in Figure 52 (a-d). The morphology of the MS specimen before immersion (a) is very smooth and shows no corrosion, while MS specimen immersed in 3% NaCl solution is the absence of inhibitor (b) is very rough and the surface is severely corroded. However, the addition of 2.0 g/L PASP suppresses the corrosion rate and surface damage has been diminished considerably especially in the presence of 0.01 g/L Zn^{+2} with 2.0 g/L PASP as in figure 52 (c, d) comparing to blank specimen; suggesting formation of a protective inhibitor film on MS surface. It is also noticeable that this protective film is thicker in the presence of Zn ions because it works synergistically as a cathodic inhibitor.

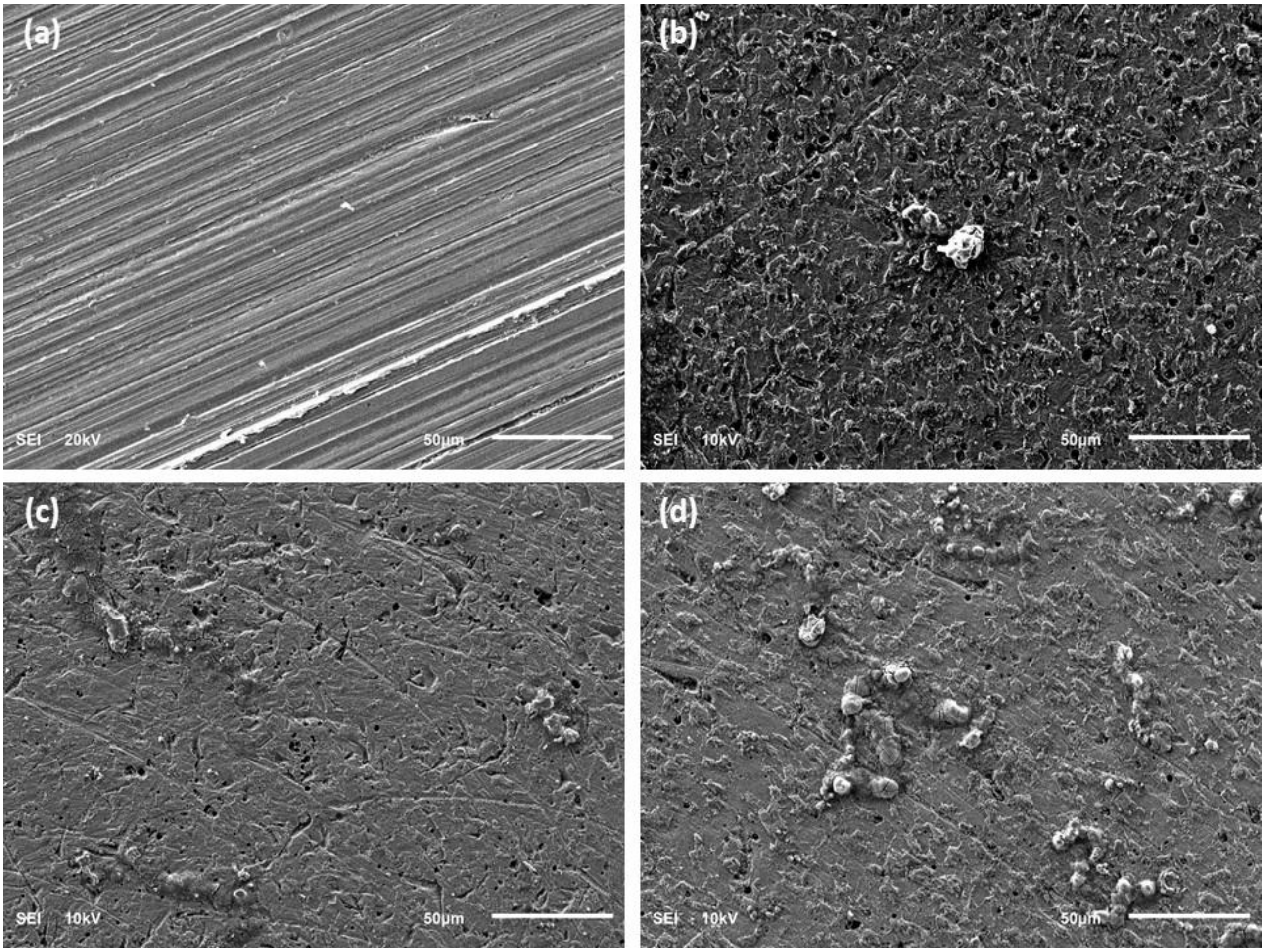

Figure 52: SEM micrographs of mild steel in 3% NaCl solution after 24 hrs immersion time at 298 K (a) polished before immersion, (b) after immersion without inhibitor, (c) after immersion with 2.0 g/L PASP (d) after immersion with 2.0 g/L PASP and 0.01 g/L Zn

4.2.6.3 Energy dispersive X-ray spectroscopy (EDS)

The EDS technique was employed in order to get the information about the composition of MS surface in the absence and presence of inhibitors in 3% NaCl solution. The results of EDS spectra are presented in Figure 53 (a-d). The spectra of uninhibited specimen contain the peaks corresponding to the elements present in MS, whereas inhibited MS contains the peaks corresponding to the elements present in the inhibitor molecules, indicating the adsorption of inhibitor molecules at the surface. It is noticeable that the percentage of atomic content of Fe for MS before immersion was 85.8% and after immersion reached 89.5% due to surface cleaning. However, after the addition of PASP only and PASP with Zn inhibitors, the percentage of atomic Fe has decreased to 70.8% and 64.6%, respectively. The suppressed percentage of Fe in the inhibited specimens is due to the formation of an inhibitive film on MS surface. This can be noticed as well with an increase atomic oxygen (O) representing the organic molecule and atomic zinc (Zn) in EDS spectra of the sample (d).

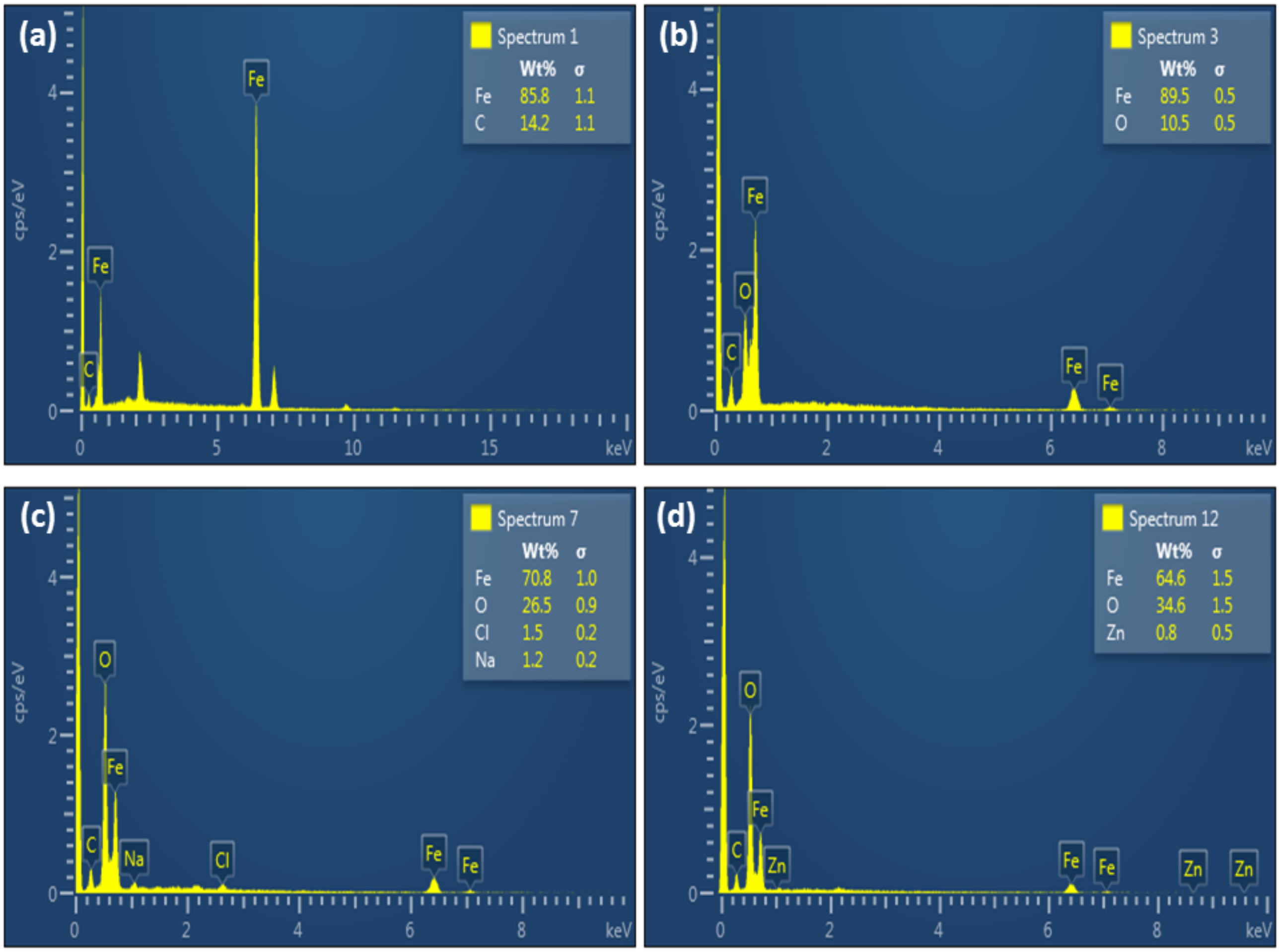

Figure 53: EDS spectra of MS specimens (a) polished before immersion, (b) after immersion without inhibitor, (c) after immersion with 2.0 g/L PASP, (d) after immersion with 2.0 g/L PASP and 0.01 g/L Zn.

4.2.6.4 Atomic force microscopy (AFM)

The three-dimensional AFM images of polished (before immersion), uninhibited and inhibited mild steel specimens are shown in Fig 54 (a-d). The immersion time was only 4 hours in order to minimize pits depth and be able to get AFM micrographs. The roughness of polished mild steel specimen is computable with SEM images as shown earlier. The roughness and thickness of the surface have changed noticeably which reflects the formation of amorphous filming layer on the metal surface. This layer was not covering the full surface area in the case of using 2.0 g/L PASP alone, while it has much better coverage when 0.01 g/L of Zn^{+2} was added. The mechanism of zinc and PASP as well is the formation of filming precipitation layer on the mild steel surface.

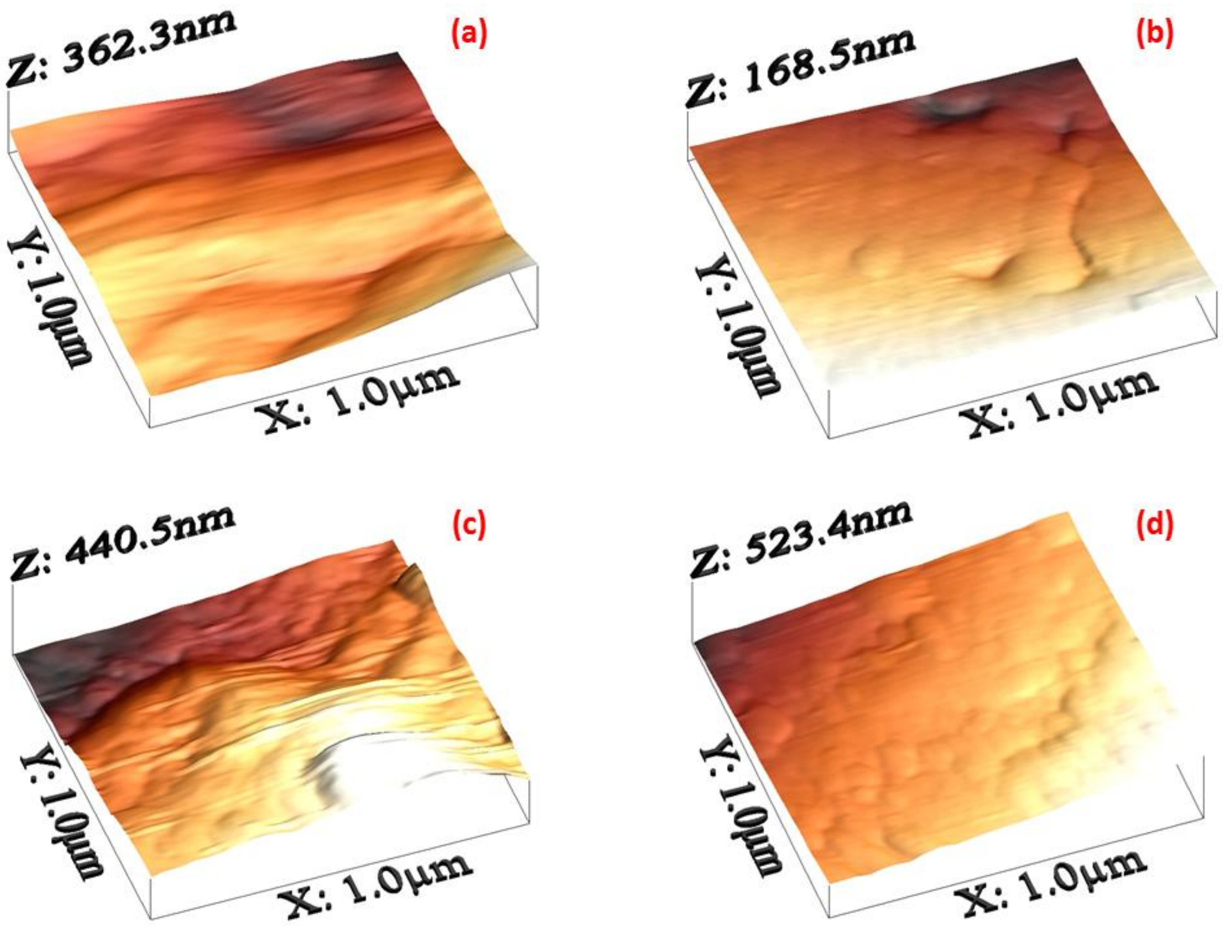

Figure 54: AFM micrographs of MS specimens (a) polished before immersion, (b) after immersion without inhibitor, (c) after immersion with 2.0 g/L PASP, (d) after immersion with 2.0 g/L PASP and 0.01 g/L Zn.

4.2.7 Computational study

4.2.7.1 Quantum chemical calculations

The results obtained from quantum chemical calculations demonstrate that the electronic characteristics of the PASP are important parameters for prediction its reactivity on the steel surface.

Generally, HOMO and LUMO orbitals show the regions of the molecule which can donate or accept an electron, respectively. A molecule with large HOMO orbital is easy to donate an electron to unoccupied *d*-orbital of the metal atom. The one that has large LUMO orbital is easy to accept an electron from a metal atom. The optimized structure, HOMO and LUMO diagrams of PASP molecule using AM1 model chemistry in the gas phase are illustrated in Figure 55. In the figure, it is observed that the HOMO orbital localizes at –COONa and the -C=O group attached to the NH_2 group in the polymer backbone. These are the regions donating an electron to unoccupied *d*-orbital of metal. On the other hand, LUMO localizes at the same region around the carboxylate group and the amide group on the polymer backbone. These regions can accept an electron from the metal surface. Thus, these analyses indicate that the carboxylate and the amide groups play an important role as active sites for the interaction of PASP with a steel surface.

Optimized Structure

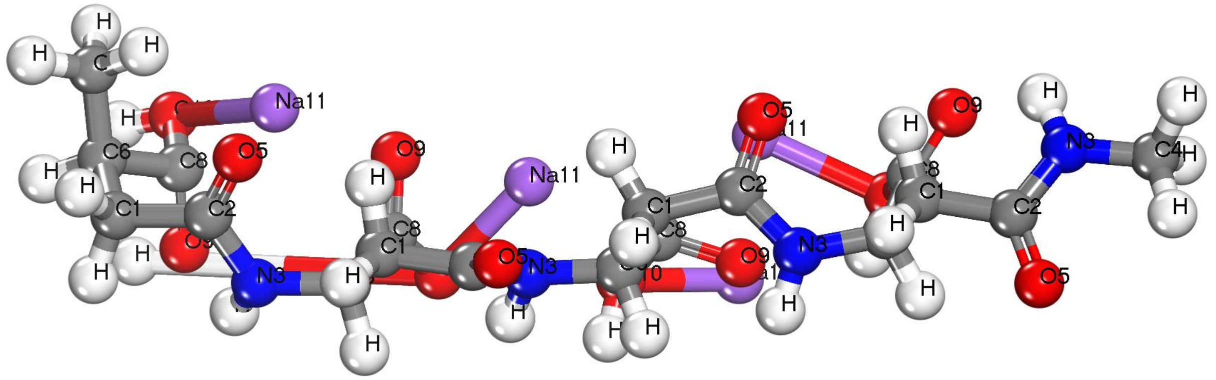

HOMO orbital

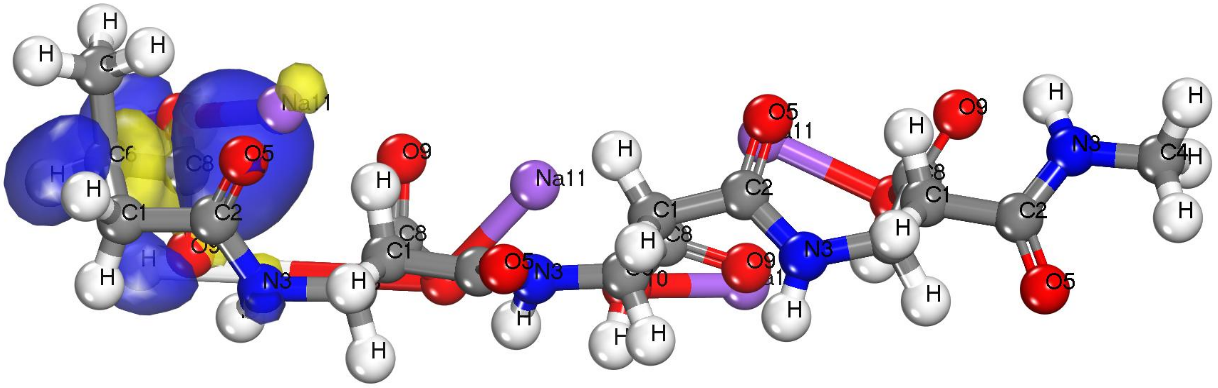

LUMO orbitals

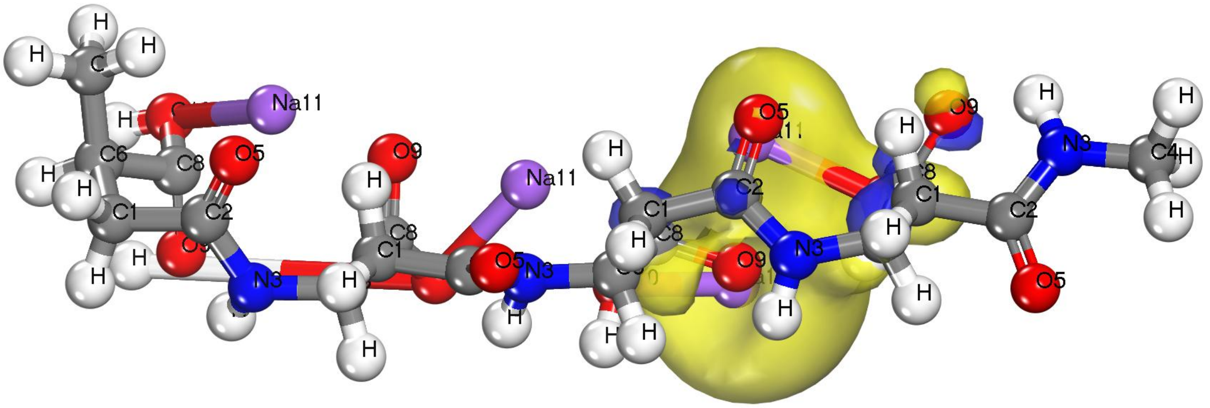

Figure 55: Optimized structure, HOMO and LUMO orbital distribution of PASP calculated using VAMP module at AM1 level of theory in Material Studio 8.0 software.

4.2.7.2 Monte Carlo simulations

Metropolis Monte Carlo simulations using simulated annealing procedure were further carried out to quantify the adsorption of PSAP alone and PSAP-Zn on the steel surface. Figure 56 shows (a) snapshot of the stable equilibrium configuration of PASP adsorption on Fe (110) surface and (b) adsorption energy profile for the Fe (110)/PASP interface. While Figure 57 show (a) snapshot of the stable equilibrium configuration of PASP-Zn^{2+} adsorption on Fe (110) surface and (b) adsorption energy profile for the Fe (110)/PASP-Zn^{2+} interface. As can be seen in Figure 56 (a), PASP is adsorbed in a parallel orientation to the metal surface using the carboxylate group and the hydrogen bonds present in the polymer chain. Similar structures were obtained with the PASP-Zn^{2+} system (Figure 57(a)). Figure 56 (b) shows the probability distribution curves for the adsorption energies of PASP on Fe (110) surface while Figure 57 (b) depicts probability distribution curves for the adsorption energies of PASP-Zn^{2} on Fe (110) surface. As observed in the two figures, it is evident that PASP-Zn^{2+} has higher negative adsorption energy when it interacts with steel surface than PASP alone due to the synergistic effect of Zn addition. It has been reported that the higher the negative adsorption energies, the stronger the interaction of inhibitor molecules with metal surfaces [106]. This result indicates that PASP-Zn^{2} is expected to inhibit steel corrosion in 3% NaCl solution than PASP alone. The theoretical results are in good agreement with the experiment.

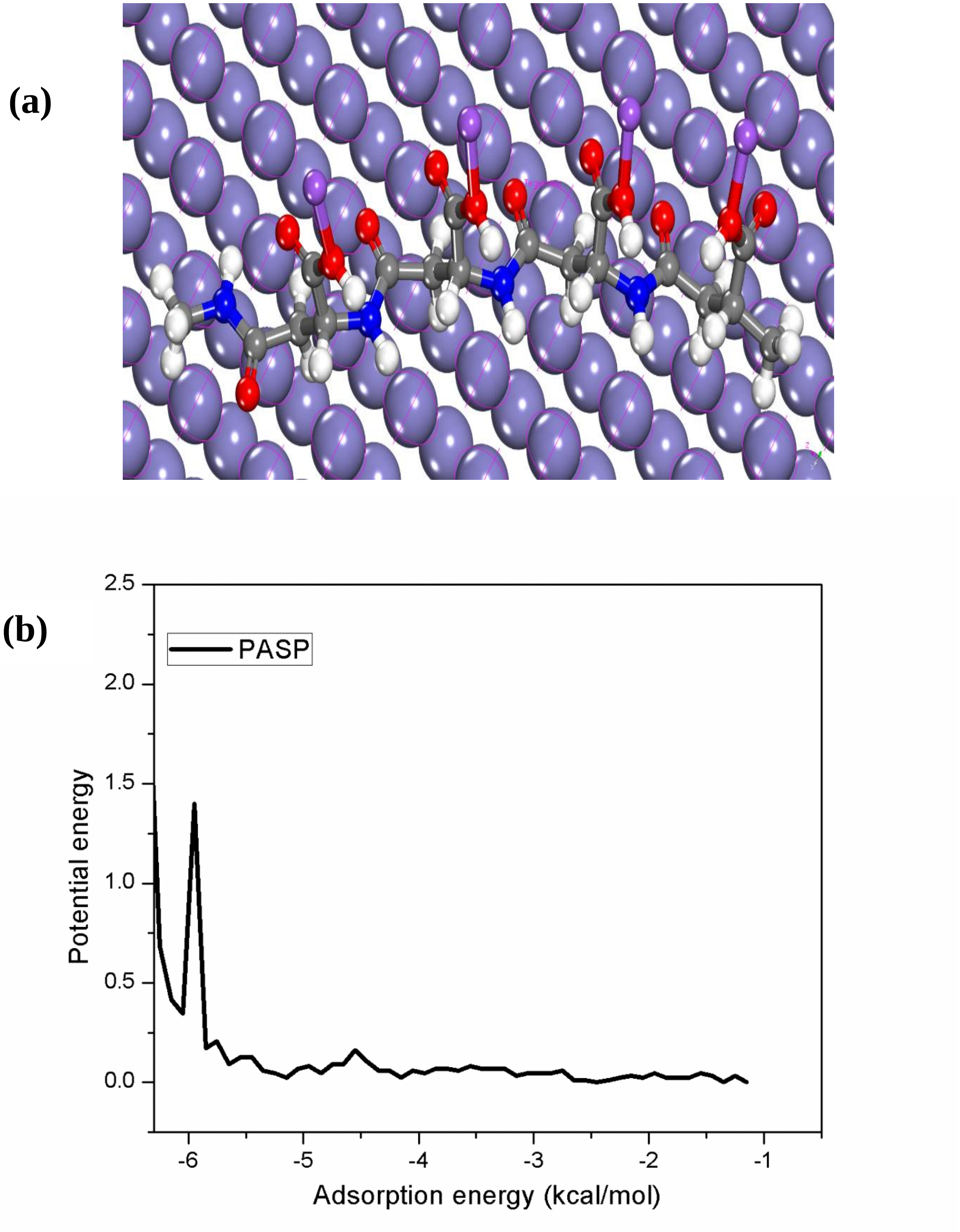

Figure 56: (a) Snapshot of the stable equilibrium configuration of PASP adsorption on Fe (110) surface and (b) Adsorption energy profile for the Fe (110)/PASP interface

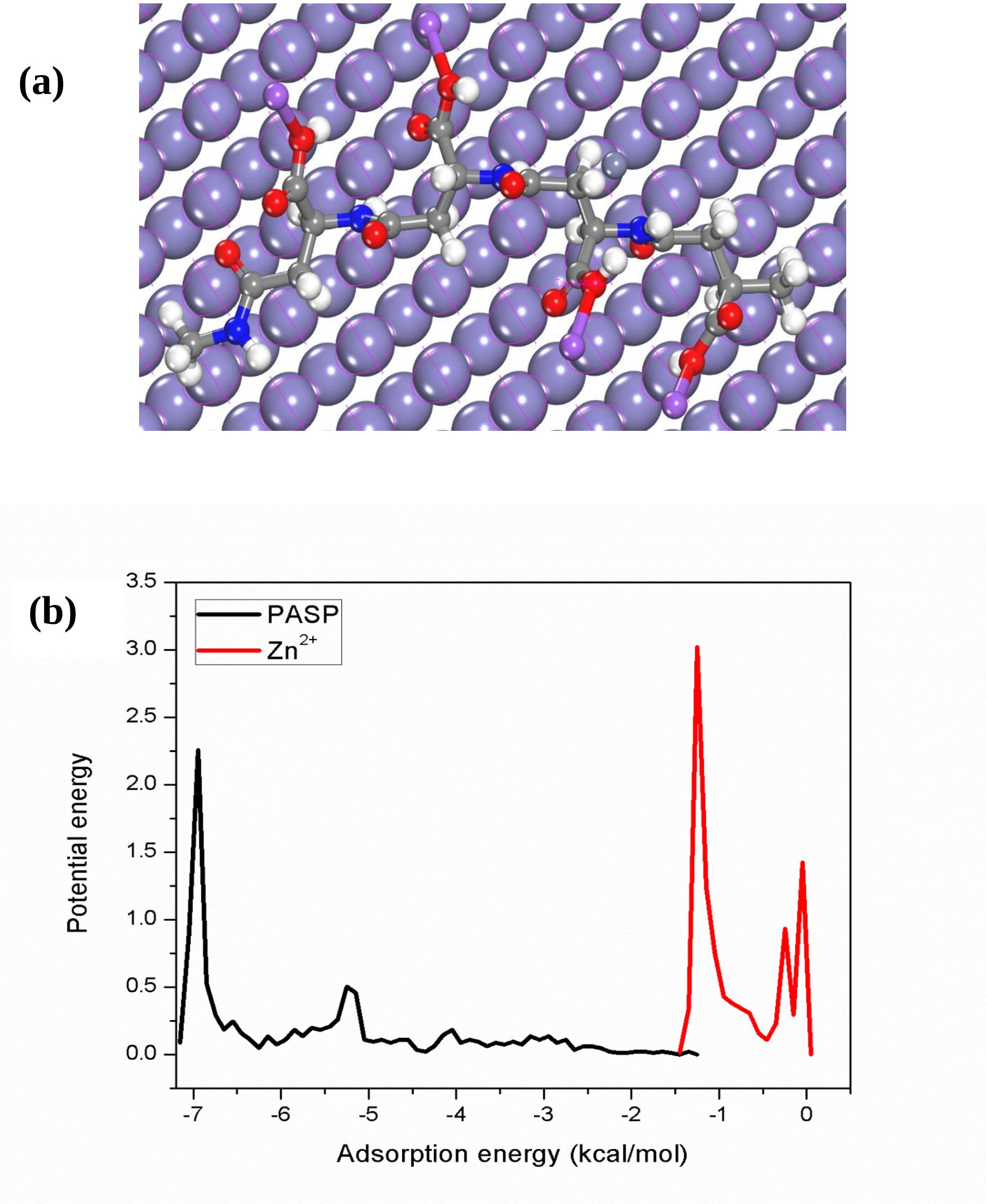

Figure 57: (a) Snapshot of the stable equilibrium configuration of PASP-Zn^{+2} adsorption on Fe (110) surface and (b) Adsorption energy profile for the Fe (110)/PASP-Zn^{+2} interface.

4.2.8 PASP mechanism

The inhibitive mechanism of PASP on mild steel in aerated 3% NaCl solution can be explained based on the above findings and adsorption results. The large electron-rich HOMO orbitals localized at -COONa and -C=O attached to NH_2 group and having lone pairs of electrons are getting adsorbed by donating electrons to d-orbitals of mild steel in a parallel position. Furthermore, LUMO orbitals localized around the above groups accept electrons from the metal surface. This model of adsorption of PASP on metal interface reduces the anodic reaction of the corrosion cell as observed in Tafel curves and thus PASP can be named as an anodic inhibitor. This adsorption layer was characterized and proofed using FTIR on the metal surface. However, PASP polymer is large which hinders a smooth parallel adsorption PASP on the metal-solution interface. The addition of Zn^{+2} at neutral pH has improved the inhibition efficiency noticeably by hindering the cathodic part of corrosion reaction, considering zinc ions has the ability to chelate with carboxylic groups in PASP molecule which is going to precipitate on mild steel surface and block the cathodic sites. PASP-Zn complexes are similar to other complexes generated between Zn (II) ions carboxylic groups [107] [108] [109]. So, PASP forms a PASP-Zn complex building a precipitation layer on mild steel surface and minimizing corrosion. This layer was characterized using SEM, AFM, and EDX and showed a thick layer of precipitates was formed after the addition of zinc ions. Therefore, zinc ions played a synergistic mechanism in mild steel inhibition at this stressed corrosive environment and formed a mixed-type of corrosion inhibition behavior in the corrosion cell. Figure 58 shows a schematic illustration of the suggested adsorption mechanism of PASP.

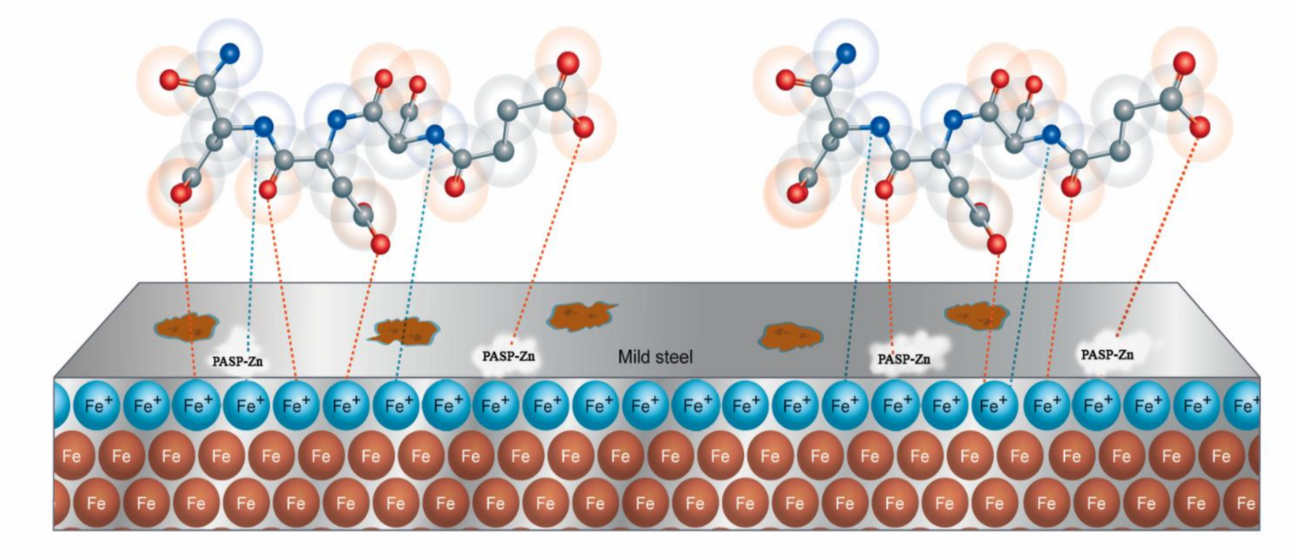

Figure 58: The schematic illustration of different modes of interactions on metal/solution interface in the presence of PASP and Zn inhibitors

4.2.9 PASP Conclusions

Based on the result obtained from this study, the following conclusions may be drawn:

(1) The synthesized PASP is a moderate corrosion inhibition of mild steel in 3% NaCl aerated solution and considered as anodic corrosion inhibitor since it is adsorbed on the metal surface.

(2) Zinc ions addition has shown remarkable improvement of mild steel corrosion inhibition and has good synergistic effect with PASP.

(3) Potentiodynamic polarization study confirms the results obtained from weight loss method and revealed the electrochemical inhibition behavior of PASP and Zn.

(4) The micrographs obtained from SEM and AFM confirmed that there is a good protection film on metal surface minimizing the corrosion rate of mild steel in 3% NaCl.

(5) Computational quantum chemistry studies showed a correlation with the experimental results and findings where PASP has efficient adsorption sites and could be adsorbed on the metal surface.

4.2 PESA Inhibitor Results

In this section, the results and findings of tests and characterizations were done on PESA inhibitor will be presented and discussed.

4.2.1 Weight loss results

Weight loss results for MS in 3% NaCl solution were obtained in mpy (milli-inch per year) after 72 hours (3 days) immersion in open-air solutions in the absence and presence of different concentrations of PESA and then Zn ions at different temperatures (298-318 K) as listed in Table 11. After immersion time elapsed, the coupons were cleaned using tissue paper and washed with deionized water followed by acetone and then dried in a desiccator at ambient temperature. Inspection of the data in table 11 reveals that inhibition efficiency increases with increasing the concentration of PESA until 2 g/l. The addition of 2 mg/L Zn^{+2} improved the efficiency significantly. On the other hand, increase in temperature led to a decrease in the efficiency of PESA inhibitor without effect after the addition of 2mg/l zinc ions. This behavior can be explained similar to PASP case, that PESA molecules adsorbed on MS surface will be partially desorbed after the increase in temperature and lead to a decrease in the efficiency. Figures 59 (a & b) shows the corrosion rate and inhibition efficiency using PESA inhibitor only and with 2 mg/l Zn ions, respectively. Table 1 shows that PESA alone has moderate inhibition at high concentration. It was found that the efficiency at 2 g/L is 60% at 298 K, while it reached 92 % when 2 mg/l Zn^{+2} was added to PESA. The inhibition efficiency of PESA and Zn was concluded to be more efficient than PESA alone at all temperatures and dosages. This may suggest that

PESA has moderate adsorption on metal surface under the anodic mechanism, while Zn ions work as a cathodic inhibitor and synergize PESA mechanism to achieve high-efficiency results.

Temp.		298 K (25^0 C)				308 K (35^0 C)				318 K (45^0 C)			
Concentration		CR (mpy)	CR (mmy)	θ	η%	CR (mpy)	CR (mmy)	θ	η%	CR (mpy)	CR (mmy)	θ	η%
Blank		17.74	0.450	-	-	29.71	0.754	-	-	47.42	1.204	-	-
PESA (g/l)	Zn (mg/l)												
0.1	-	14.80	0.376	0.17	16.6	25.40	0.645	0.15	14.5	41.36	1.050	0.13	12.8
0.5	-	12.23	0.311	0.31	31.0	21.67	0.550	0.27	27.1	36.26	0.921	0.24	23.5
1.0	-	10.57	0.268	0.40	40.4	18.82	0.478	0.37	36.7	31.89	0.810	0.33	32.7
1.5	-	8.83	0.224	0.50	50.3	16.11	0.409	0.46	45.8	27.99	0.711	0.41	41.0
2.0	-	6.99	0.178	0.61	60.6	13.22	0.336	0.55	55.5	22.92	0.582	0.52	51.7
0.1	2	11.65	0.296	0.34	34.3	20.65	0.524	0.30	30.5	34.60	0.879	0.27	27.0
0.5	2	8.36	0.212	0.53	52.9	15.06	0.382	0.49	49.3	25.54	0.649	0.46	46.1
1.0	2	6.09	0.155	0.66	65.7	11.21	0.285	0.62	62.3	19.75	0.501	0.58	58.4
1.5	2	3.82	0.097	0.78	78.5	7.51	0.191	0.75	74.7	14.21	0.361	0.70	70.0
2.0	2	1.40	0.035	0.92	92.2	3.61	0.092	0.88	87.8	8.42	0.214	0.82	82.3

Table 11: Weight loss results at different inhibitors concentrations and temperatures

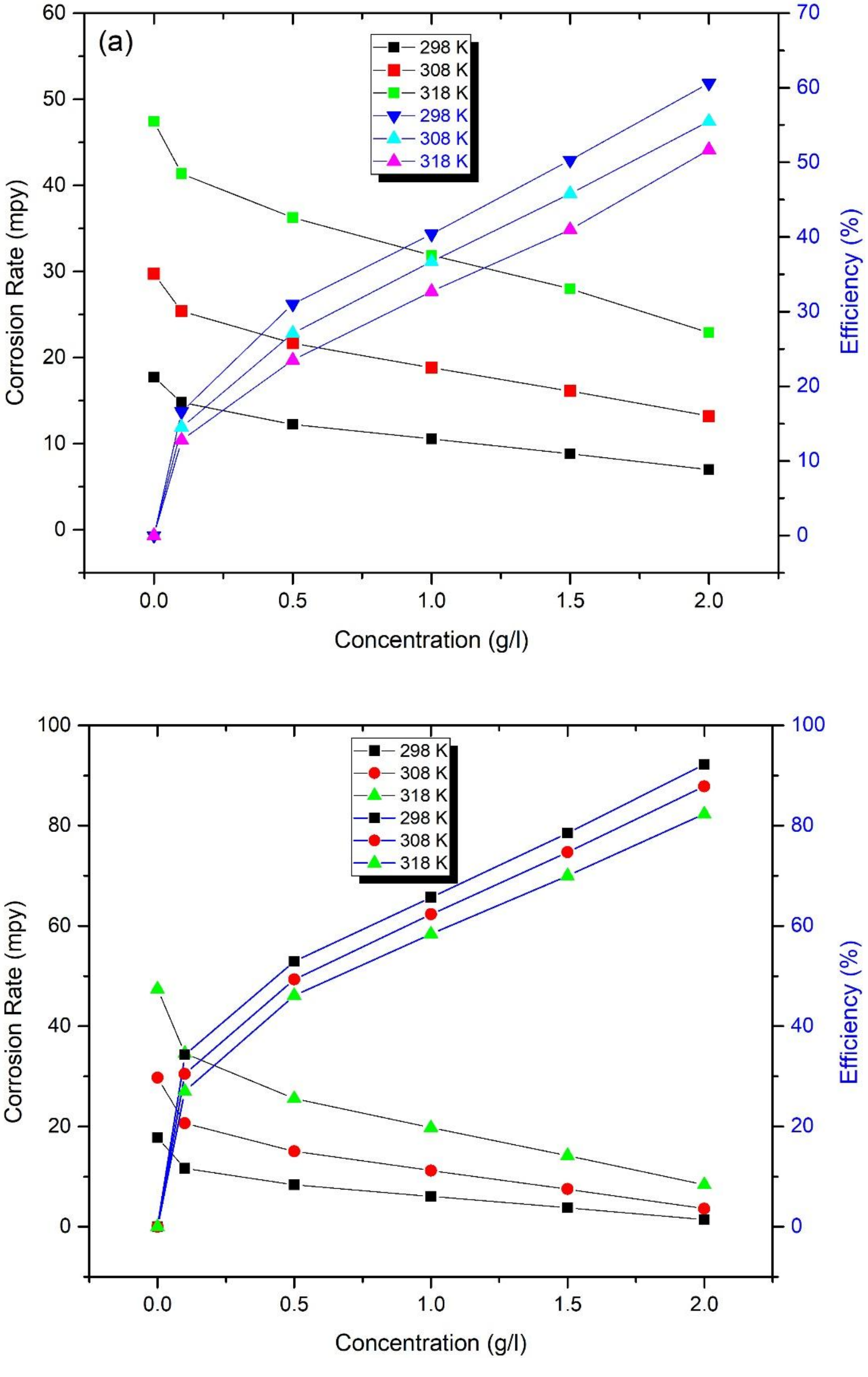

Figure 59: The corrosion rate and inhibition efficiency using (a) PESA inhibitor only (b) PESA + 2 mg/l Zn

4.2.2 Thermodynamic calculations

The activation energy (Ea) for MS dissolution in 3% NaCl was calculated by using the following Arrhenius equation:

$$\log CR = \frac{-E_a}{2.303\ RT} + \log A \tag{32}$$

Where R (8.314 J K^{-1} mol^{-1}) is the ideal gas constant, A is Arrhenius pre-exponential factor, and T is Kelvin temperature. Figure 60 (a & b) presents a plot of log CR versus 1/T in absence and presence of PESA only and with 2 mg/l Zn^{+2}, respectively. As shown in these figures, the activation energy (E_a) was calculated from the slope as summarized in Table 12. It is noticeable that activation energy values for the inhibited solutions are higher than the ones of the uninhibited solutions, and continue to increase as inhibitor concentration increases especially in the presence of zinc ions. The thermodynamic parameters including the standard enthalpy of activation (ΔH^*) and the standard entropy of activation (ΔS^*) for the formation of an activated complex in the transition state were calculated and listed in Table 12 as well. Plotting log (CR/T) versus 1/T gives straight lines of a slope [- ΔH^*/2.303R] and an intercept [log(R/Nh) + (ΔS^*/2.303R)] as in Figure 61 (a and b).

As tabulated in Table 12, for the both sets $E_a > \Delta H^*$ by a value which almost equal to RT. Thus, metal surface corrodes in 3% NaCl solutions in the absence and presence of inhibitors by what is called unimolecular reaction. The gradual increase of ΔS^* values for all cases indicates a decrease in disorder takes place during the course of the transition from reactants to the activated complex which reflects a decrease in the formation of activated complex and a decrease of overall corrosion reaction rate.

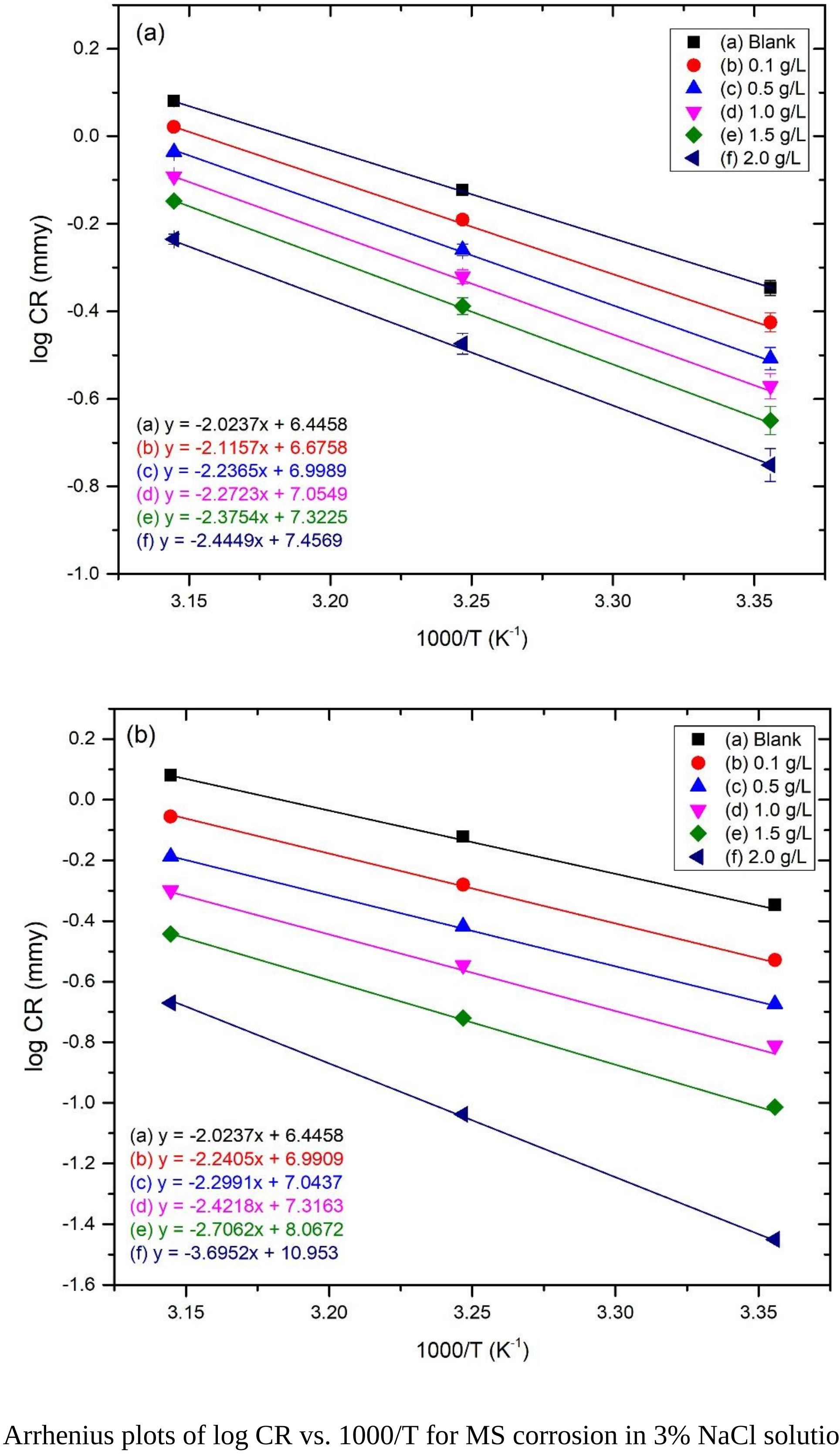

Figure 60: Arrhenius plots of log CR vs. 1000/T for MS corrosion in 3% NaCl solution (a) PESA (b) PESA + 2 mg/L Zn

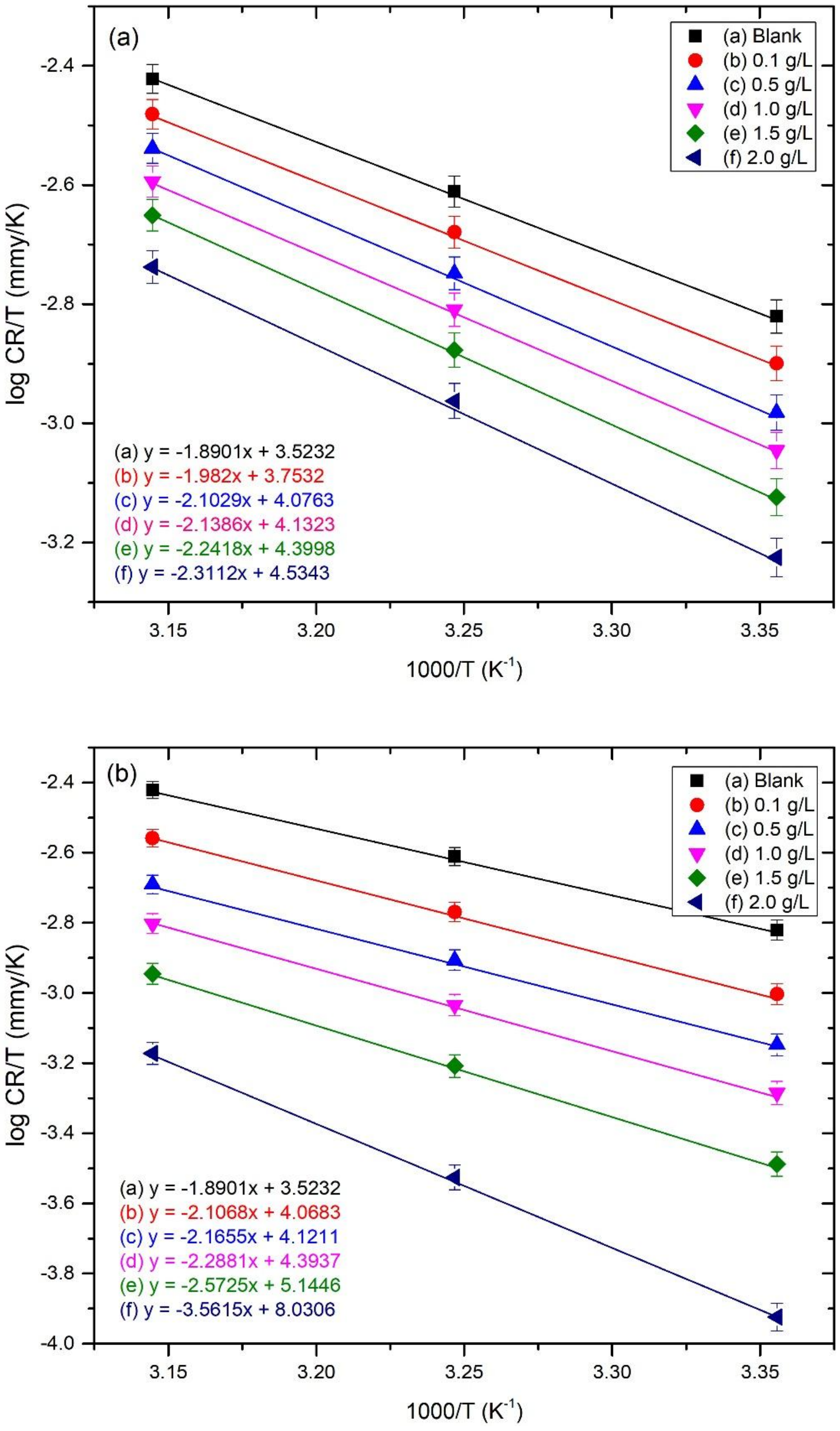

Figure 61: Transition state plots for MS in 3% NaCl solutions at different concentrations (a) PESA (b) PESA + 2 mg/L Zn

Inhibitors Concentration		**E_a (kJ mol^{-1})**	**ΔH^* (kJ mol^{-1})**	**ΔS^* (J mol^{-1} K^{-1})**
Blank		38.74	36.18	-130.12
PESA (g/l)	**Zn (mg/l)**			
0.1	**-**	40.50	37.94	-125.71
0.5	**-**	42.81	40.25	-119.53
1.0	**-**	43.50	40.94	-118.45
1.5	**-**	45.48	42.92	-113.33
2.0	**-**	46.79	44.23	-110.76
0.1	**2**	42.89	40.33	-119.68
0.5	**2**	44.01	41.45	-118.67
1.0	**2**	46.37	43.81	-113.45
1.5	**2**	51.82	49.26	-99.07
2.0	**2**	70.73	68.17	-43.81

Table 12: Activation thermodynamic parameters for MS in 3% NaCl in the absence and presence of inhibitors

4.2.3 Open circuit potential measurements

Open circuit potential (E_{ocp}) is an indicative factor in corrosion inhibition mechanism that is identified as the corrosion potential in the absence of net electrical current flowing through the metal surface. When corrosion reaction reaches equilibrium, E_{ocp} reaches a steady-state and it becomes equal to the corrosion potential (E_{corr}). The evolution of potential versus time constitutes a methodology for monitoring interface changes between a metal and its environment. The E_{ocp} curves of MS working electrode in aerated 3% NaCl solutions in the presence and absence of PESA synergistic inhibitors are shown as shown in Figure 62 (a and b). These figures represent the variation of the E_{ocp} under the experimental conditions as a function of time in presence of PESA alone and then with 2 mg/l Zn ions as a synergistic inhibitor. It could be observed that at steady-state, E_{ocp} was achieved after approximately 6000 seconds of immersion in the presence of PESA, while a steady state of E_{ocp} value was not achieved even after 6500 seconds of immersion in the absence of PESA which can be attributed to the porous nature of corrosion product layer. It is observable that - after reaching equilibrium - the potential is shifting toward negative values, which can be attributed to corrosion reactions on metal surface under this strong corrosive environment. In the presence of PESA, the E_{ocp} value at the steady state shifted to less negative values and reached steady-state conditions due to the adsorption of PESA on metal surface after the inhibition time which significantly reduces the porosity of the corrosion layer. It is also noted that the positive shift of corrosion potential was found to be concentration potential. Similar observations have been seen in Figure 62 (b) as the addition of Zn ions enhanced the inhibition efficiency and exhibited a synergistic effect on PESA under these test conditions.

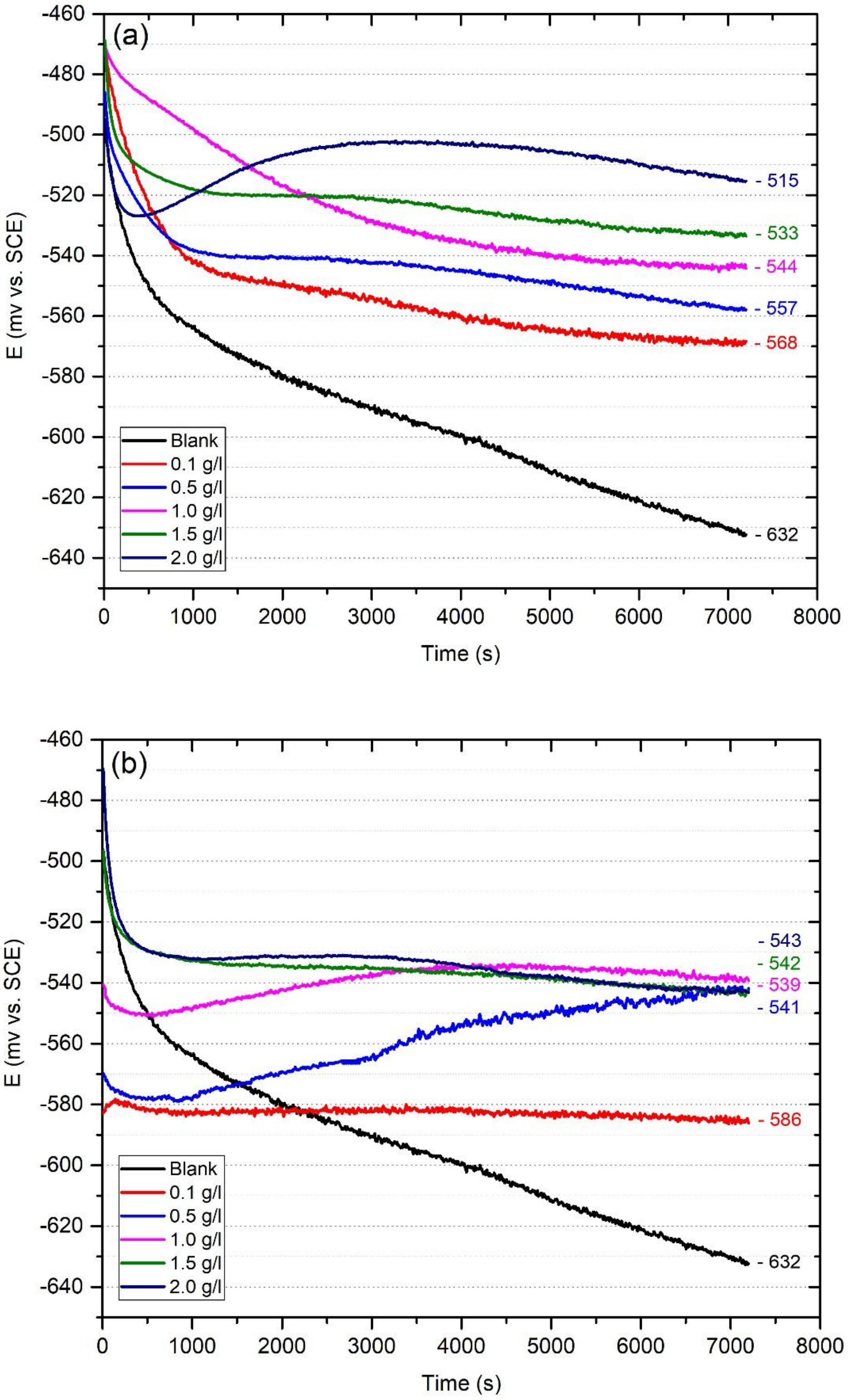

Figure 62: Open circuit potential for MS using (a) PESA inhibitor (b) PESA inhibitor + 2 mg/L Zn

4.2.4 Polarization measurements

Potentiodynamic polarization scans of PESA and its mixtures for mild steel in 3% NaCl solution were conducted at 25 °C (298 K) in presence and absence of inhibitors was undertaken in order to understand PESA inhibition mechanism whether it is anodic, cathodic or mixed-type organic inhibitor as shown in Figures 63 and 64. The electrochemical parameters including corrosion potential (E_{corr}), corrosion current density (i_{corr}), anodic Tafel slope (β_a), cathodic Tafel slope (β_c), corrosion rate (C_{rate}) and inhibition efficiency (η) values are listed in Table 13. This technique utilizes data obtained from cathodic and anodic polarization measurements by extrapolating the linear Tafel segments in a large domain of potential to the corresponding corrosion potential to obtain the corrosion currents. The calculation of inhibition efficiency (η%) was done from the polarization measurements and listed as well.

To understand the mechanistic behavior of PESA, it is good to highlight the corrosion mechanism of mild steel in nearly neutral aerated aqueous medium such as NaCl solution [73]. The reactions are as follows:

$$Fe \rightarrow Fe^{2+} + 2e^- \tag{34}$$

$$Fe^{2+} + Cl^- \rightarrow FeCl_2 \tag{35}$$

$$FeCl_2 + 2H_2O \rightarrow Fe(OH)_2 + 2H^+ + 2Cl^- \tag{36}$$

$$Fe^{2+} \overset{O_2}{\rightarrow} Fe^{3+} + 1e^- \tag{37}$$

The corresponding reduction reaction at cathodic sites is:

$$O_2 + 2H_2O + 4e^- \rightarrow 4OH^- \tag{38}$$

The products of the two anodic and cathodic reactions form $Fe(OH)_2$ which precipitates gradually on the metal surface and reacts with dissolved oxygen giving a complex corrosion product layer that consists of several iron oxide and hydroxide species which includes: FeO, FeOOH, and Fe_2O_3.

Tafel polarization curves, illustrated in Fig 63, show that the adsorption of PESA on the MS surface causes a moderate decrease in current density (i_{corr}) which conforms with results of OCP measurements. The addition of PESA to NaCl solution shifts corrosion potentials to a more positive direction. It can be observed that PASP suppresses the anodic reaction significantly while it has a limited effect on the cathodic reaction. The area of Tafel cathodic branch that appears from -600 to -1000 mV versus SCE can be attributed to neutral solutions to oxygen reduction reaction under diffusion control.

Various approaches have been reported to determine corrosion currents of processes controlled only by convective diffusion at a relatively low rotation speed (up to 1000 rpm), the corrosion rate can be considered equal to the limiting diffusion current [73][102]. In this case, the cathodic reaction is independent of PESA concentration. Therefore, the cathodic branch cannot be extracted to get i_{corr} [103]. Because PESA alone is anodic inhibitor since the anodic current exhibits a plateau, its extrapolation allows calculating inhibition efficiency but not accurately. Thus, i_{corr} was determined from the Tafel curves by extrapolation of both anodic and cathodic branches. In addition, electrochemical impedance spectroscopy was pursued findings that are more accurate.

Zinc is a well-known cathodic inhibitor synchronize in corrosion inhibition of mild steel with anodic adsorption inhibitors [104]. In Figure 64, the inhibition efficiency has increased noticeably with the addition of 2 mg/l Zn^{+2} with PESA. It is clear, that the inhibitive effect increases as PESA concentration increases in the presence of Zn. In additions, it is shown in polarization curves that both anodic and cathodic branches were changed through the inhibition of anodic and cathodic corrosion reactions. At dosages more than 0.1 g/L of PESA, the inhibition efficiency reached to a very good corrosion inhibition efficiency of 70%.

Inhibitor	E_{corr} (mV/SCE)	i_{corr} (mA/cm^2)	β_a (mV/dec)	β_c (mV/dec)	C_{rate} (mpy)	η (%)	θ
Blank - 3% NaCl	**-580**	**0.0876**	**170.2**	**188.3**	**40.03**	**-**	**-**
0.1 g/L PESA	**-559**	**0.0628**	**158.3**	**172.0**	**28.69**	**28**	**0.28**
0.5 g/L PESA	**-541**	**0.0492**	**144.2**	**165.4**	**23.20**	**42**	**0.42**
1.0 g/L PESA	**-527**	**0.0411**	**130.8**	**157.4**	**19.52**	**51**	**0.51**
1.5 g/L PESA	**-525**	**0.0343**	**114.9**	**151.1**	**15.58**	**61**	**0.61**
2.0 g/L PESA	**-504**	**0.02580**	**99.1**	**149.8**	**11.80**	**70**	**0.70**
0.1 g/L PESA + 2 mg/L Zn	**-552**	**0.0481**	**141.2**	**162.1**	**23.61**	**41**	**0.41**
0.5 g/L PESA + 2 mg/L Zn	**-532**	**0.0410**	**128.8**	**155.1**	**19.22**	**52**	**0.52**
1.0 g/L PESA + 2 mg/L Zn	**-525**	**0.0342**	**109.8**	**149.5**	**15.65**	**61**	**0.61**
1.5 g/L PESA + 2 mg/L Zn	**-511**	**0.0250**	**96.4**	**142.2**	**10.81**	**73**	**0.73**
2.0 g/L PESA + 2 mg/L Zn	**-502**	**0.0110**	**81.0**	**130.1**	**6.03**	**85**	**0.85**

Table 13: Potentiodynamic polarization results using Tafel plots

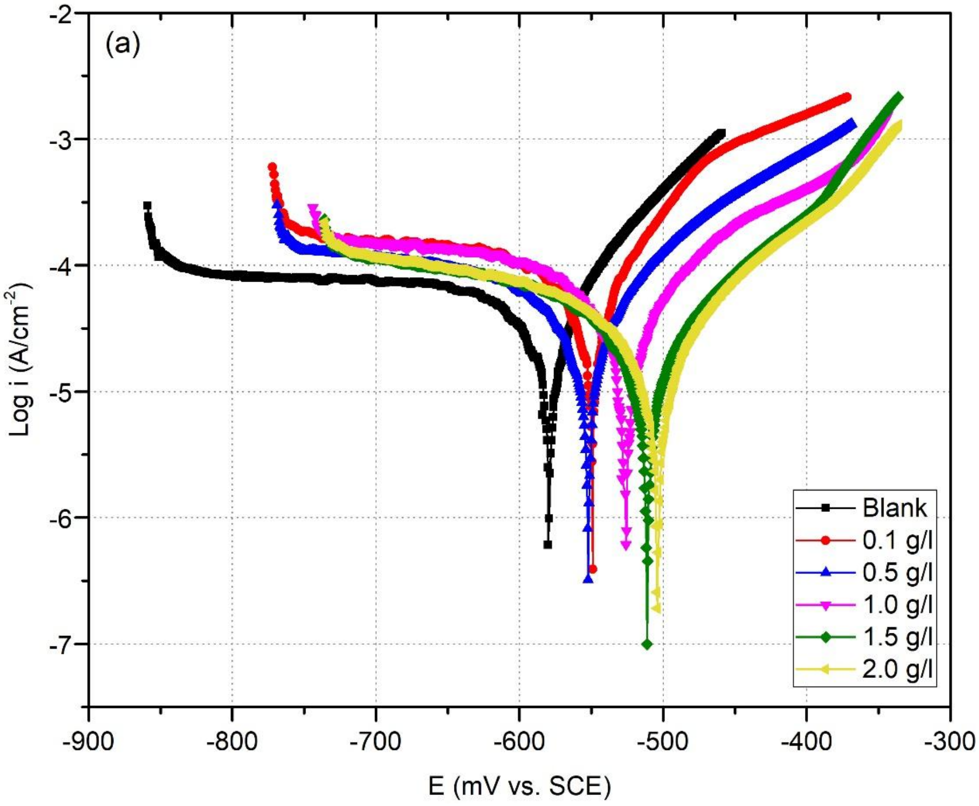

Figure 63: Tafel plots of using PESA inhibitor at different concentrations

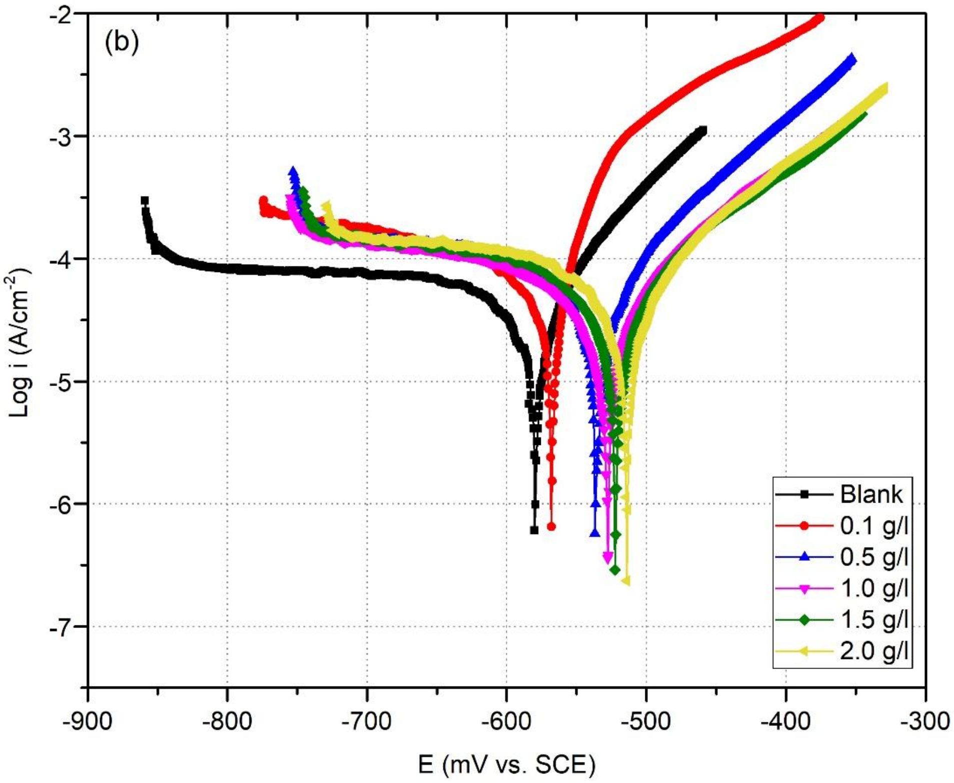

Figure 64: Tafel plots of using PESA + 2 mg/L Zn at different concentrations

4.2.5 EIS measurements

EIS technique is used to assess the mild steel corrosion inhibition efficiency of PESA in aerated 3.5% NaCl solution. Potentiostatic Electrochemical Impedance scans were conducted to provide insights on the process kinetics and the effect the adsorption of PESA on the metal surface has the double layer thickness and charge transfer process at the inhibitor-metal interface. Potentiostatic EIS data presented Bode and Nyquist diagrams for PESA and PESA-Zn mixtures in Figures 65 and 66 respectively, and corresponding results are illustrated in Table 14. EIS phase angle data are presented in Figure 67.

The appearance of capacitive semicircles as observed in all Nyquist spectra for both inhibited and the uninhibited specimen is believed to be due to charge transfer resistance and double layer capacitance. Typically, impedance spectra in the form of the depressed semicircle in the complex plane with center under the real axis are believed to be the behavior of solid electrodes. The appearance of inductive semicircles in Nyquist plot when no inhibitor is added can be attributed to the molecular diffusion of oxygen through a porous layer built up by corrosion which is the reaction limiting step.

The equivalent circuit by which the EIS plots were analyzed and presented in Figure 68 where, R_s is the solution resistance, R_{ct} is the charge transfer resistance, C_{dl} is the electrochemical double layer capacitance, R_f is the combined resistance of adsorbed inhibitor layer and the protective corrosion product layer (the protective layer) and C_f is the protective layer capacitance.

By comparing the Nyquist plot of an uninhibited solution with plots for inhibited solutions it is observed that uninhibited solution plot exhibits a complex combination of low-frequency inductive loop and high-frequency capacitive loops with two major time constants. When PESA is added to the solution, the effect of the inductive loop is reduced and at high concentrations, only one capacitive loop remains. It is also noticed that the polarization resistance significantly increases with increasing PESA concentration which is illustrated by the increase of the corresponding Nyquist semicircle plots. Bode plots exhibit increment in double layer impedance on both low frequency and high-frequency ranges by increasing PESA concentration which can be attributed to the reduction of the porosity of the corrosion product layer as well as increasing charge transfer resistance due to the reduction double layer capacitance as a result of PESA adsorption.

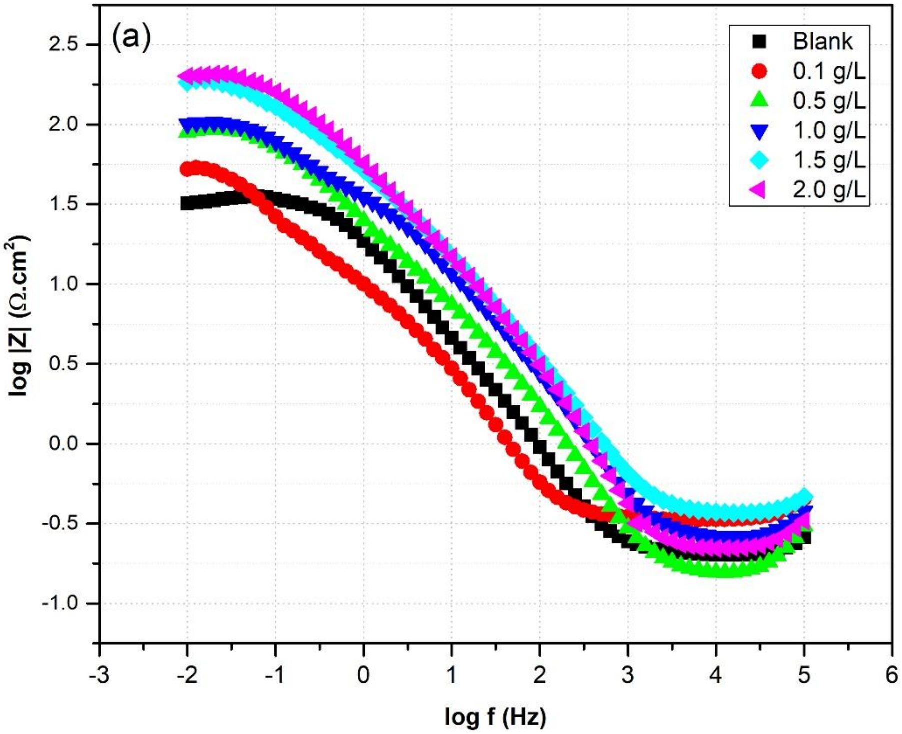
(a)
Blank
0.1 g/L
0.5 g/L
1.0 g/L
1.5 g/L
2.0 g/L
log |Z| (Ω.cm²)
2.5
2.0
1.5
1.0
0.5
0.0
-0.5
-1.0
-3
-2
-1
0
1
2
3
4
5
6
log f (Hz)

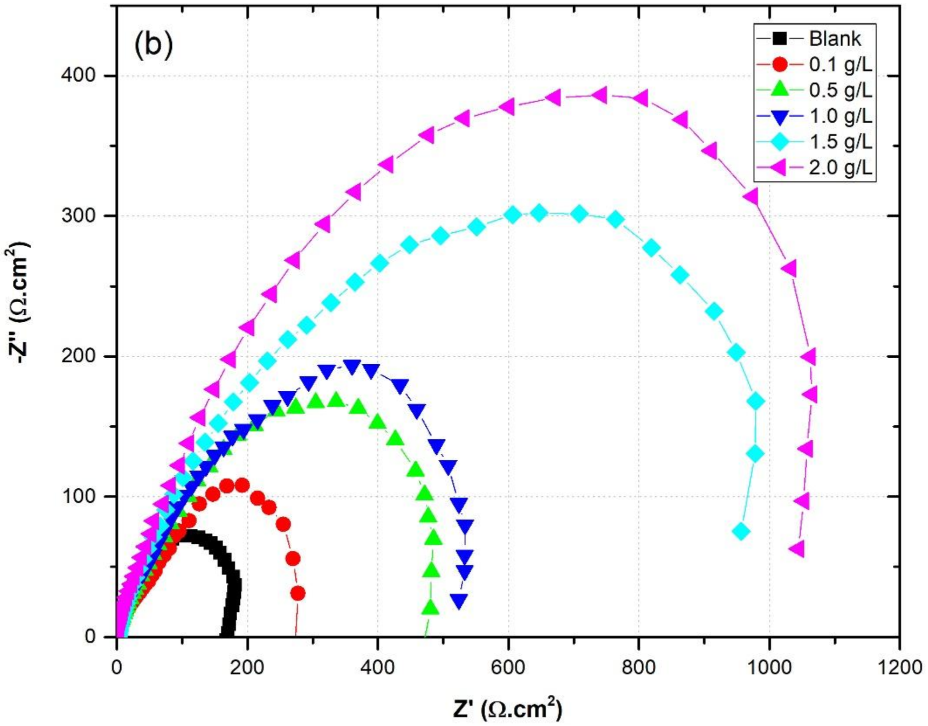

Figure 65: Plots for impedance spectra for mild steel in 3% NaCl in the presence and absence of PESA (a) Bode (b) Nyquist

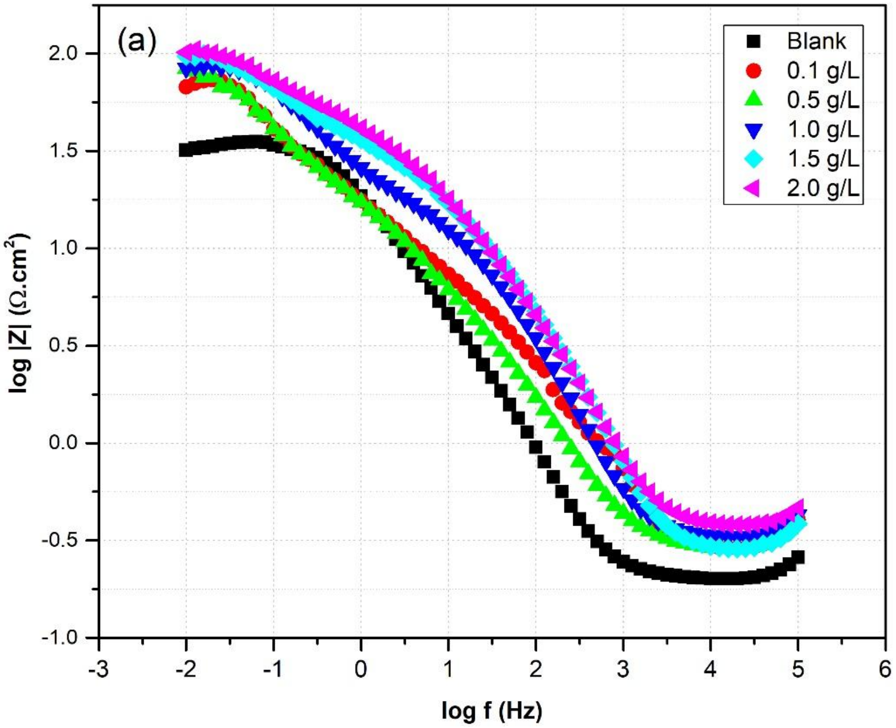

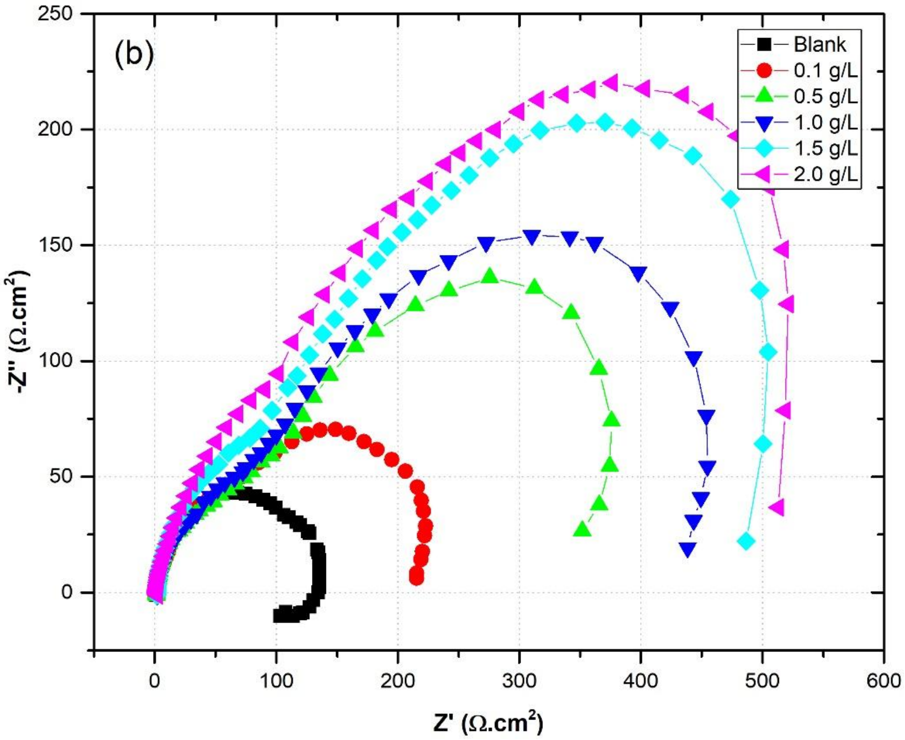

Figure 66: Plots for impedance spectra for mild steel in 3% NaCl in the presence and absence of PESA and 2 mg/l Zn (a) Bode (b) Nyquist

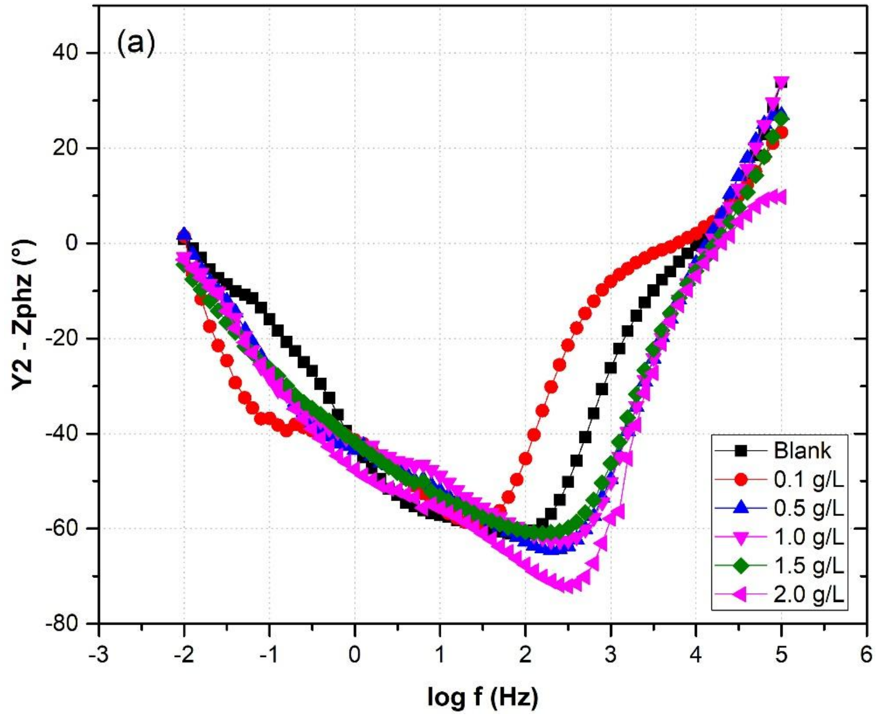

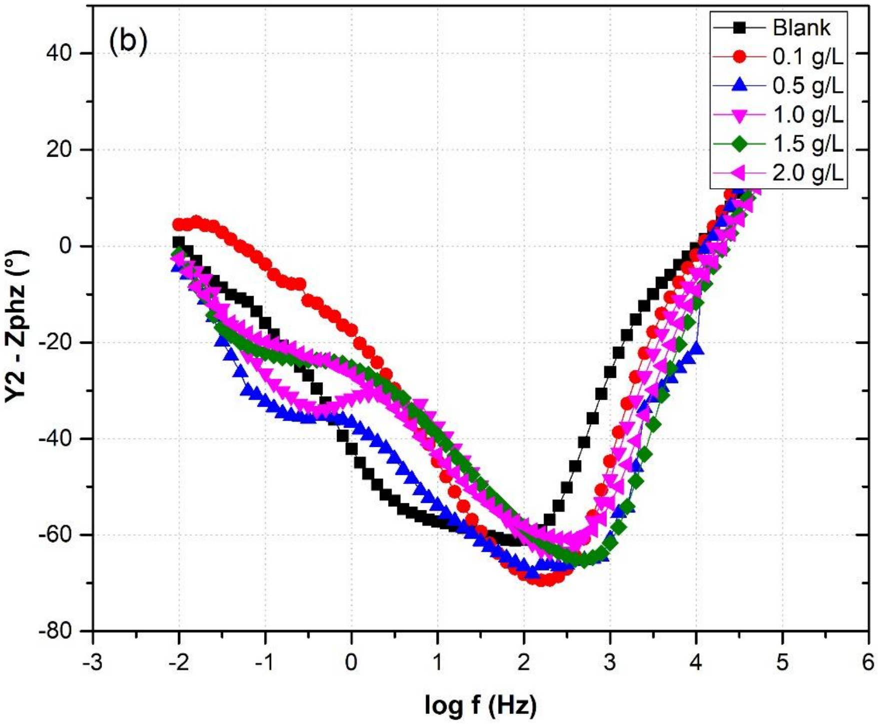

Figure 67: Phase angle of EIS for MS using (a) PESA inhibitor (b) PESA inhibitor + 2 mg/L Zn

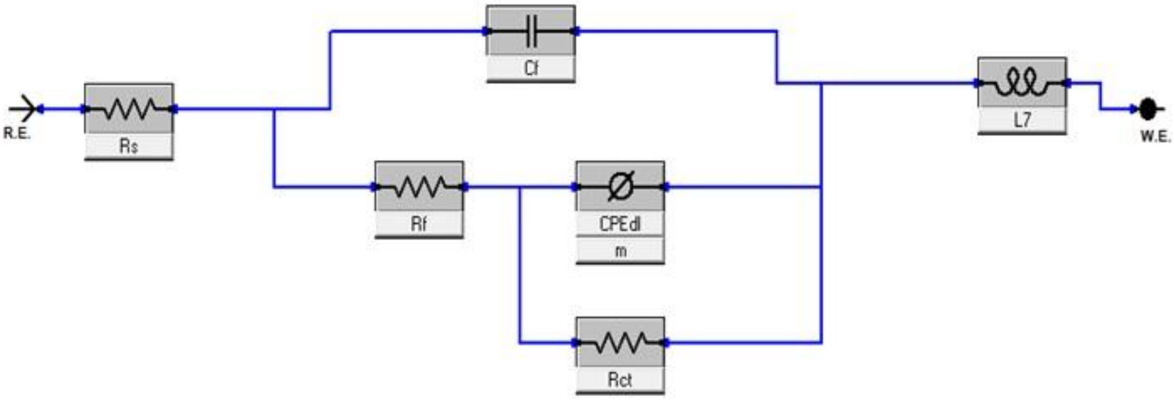

Figure 68: Equivalent circuit used to model impedance data of carbon steel in aerated 3% NaCl solution in the presence of PESA only and PESA with Zn ions

Inhibitor	Rs (ohm)	R_{ct} (ohm)	R_f (ohm)	Cdl	Cf	L7	η (%)
Blank - 3% NaCl	0.2064	14.82	2.0	0.009178	1.50E-03	2.23 E-7	**0.0**
0.1 g/L PESA	0.3473	62.07	4.1	0.036900	3.91E-03	2.96 E-7	**76.1**
0.5 g/L PESA	0.1681	106.70	2.5	0.010160	7.10E-04	2.35 E-7	**86.1**
1.0 g/L PESA	0.2677	130.60	2.0	0.008684	3.98E-04	3.37 E-7	**88.7**
1.5 g/L PESA	0.3756	231.30	1.7	0.005558	3.04E-04	3.33 E-7	**93.6**
2.0 g/L PESA	0.2282	229.00	7.7	0.004275	4.43E-04	1.18 E-7	**93.5**
0.1 g/L PESA + 2 mg/L Zn	0.2247	18.16	0.3910	0.004681	6.72E-04	3.39E-07	**18.4**
0.5 g/L PESA + 2 mg/L Zn	0.2769	118.30	0.3449	0.019970	2.72E-04	3.67E-07	**87.5**
1.0 g/L PESA + 2 mg/L Zn	0.3433	122.60	0.3930	0.013570	3.83E-04	3.28E-07	**87.9**
1.5 g/L PESA + 2 mg/L Zn	0.2919	138.30	0.6372	0.010860	2.07E-04	2.90E-07	**89.3**
2.0 g/L PESA + 2 mg/L Zn	0.3865	147.30	0.4660	0.007821	1.96E-04	3.16E-07	**89.9**

Table 14: Electrochemical parameters calculated from EIS measurements for mild steel in 3% NaCl in the presence and absence of different concentrations of inhibitors at 298 K.

4.2.6 Surface analysis results

4.2.6.1 Analysis of FTIR spectra

FTIR-ATR was utilized to characterize the adsorption of PESA on the metal surface. The steel specimen was immersed in 2.0 g/l PESA solution for 24 hours and then the surface was tested using ATR technique to evaluate the presence of adsorbed polymer on the steel surface. Figure 69 shows FTIR spectrums of PESA only and PESA on the metal surface. The spectrum of checking PESA presence on MS surface revealed that the metal has adsorbed PESA within 24 hrs contact time. The adsorption peaks at 3253 cm^{-1} correspond to the antisymmetric stretch of (-OH) group, while at 1705 cm^{-1} corresponds to (-COONa) groups. The peak of 1194 cm^{-1}

corresponds to (C-O) bending. These groups were contained in PESA, which were expected to enhance inhibition, stability and dispersion performance.

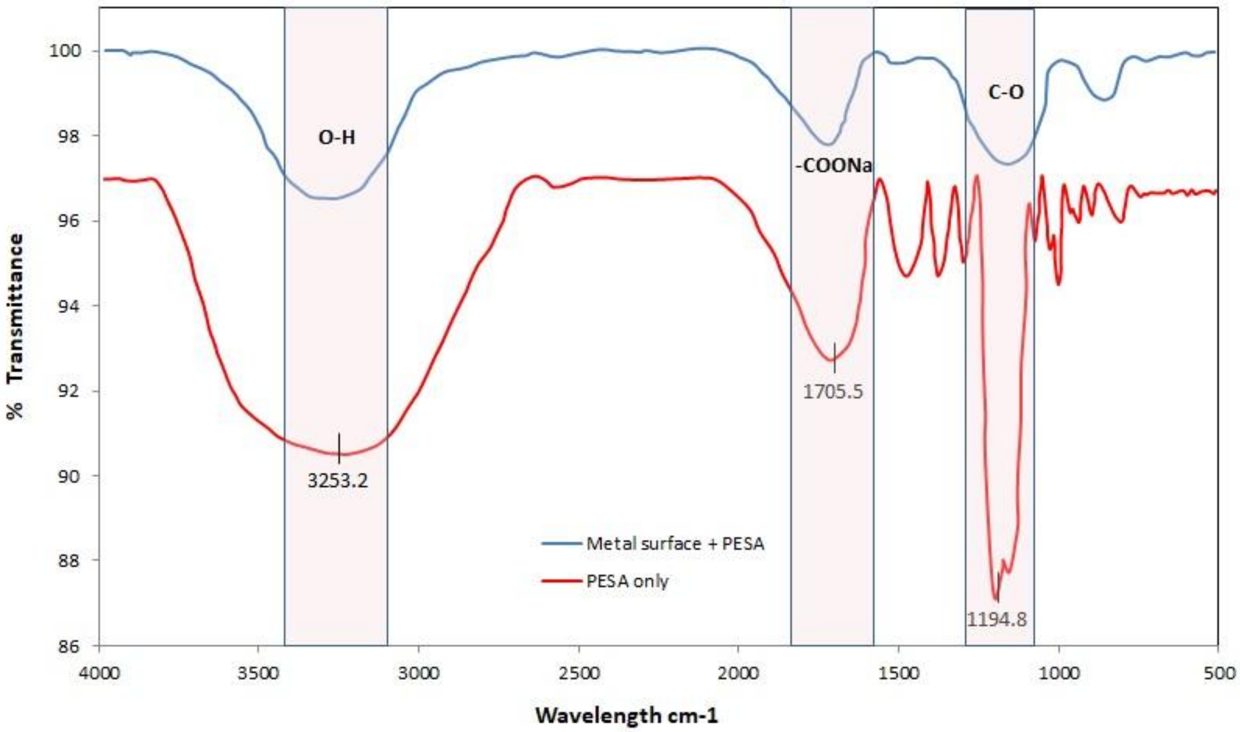

Figure 69: FTIR of PESA inhibitor and on MS surface at 2.0 g/L PASP

4.2.6.2 Scanning electron microscopy (SEM)

SEM micrographs of MS specimens before and after immersion in 3% NaCl solution as well as in the presence of 2.0 g/L PESA and 2.0 g/L PASP with 2 mg/l Zn^{+2} are shown in Figure 70 (a-d). The morphology of the MS specimen before immersion (a) is very smooth and shows no corrosion, while MS specimen immersed in 3% NaCl solution is the absence of inhibitor (b) is very rough and the surface is severely corroded. However, the addition of 2.0 g/l PESA suppresses the corrosion rate and surface damage has been diminished considerably, but there are localized are of pitting corrosion. The presence of 2 g/l Zn^{+2} with 2.0 g/l PESA as in Figure 70 (d) showed an excellent thin layer of a protective inhibitor film on MS surface. It is also noticeable that this protective film is thinner than the one formed in the case of PASP + Zn. This could reveal that the mechanism of PESA is adsorption precipitation layer (anodic inhibitor) rather than a cathodic inhibitor.

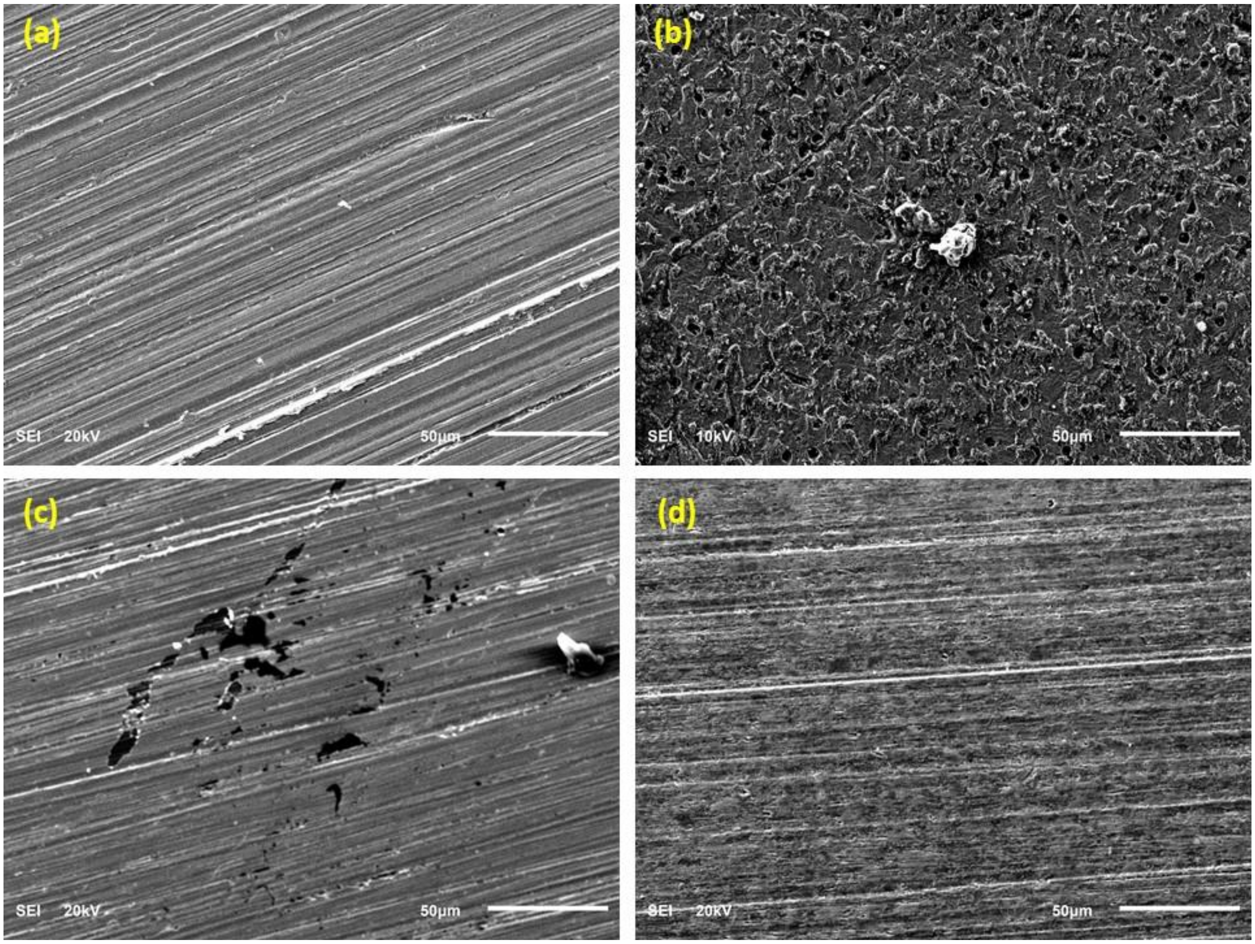

Figure 70: SEM micrographs of mild steel in 3% NaCl solution after 24 hrs immersion time at 298 K (a) polished before immersion, (b) after immersion without inhibitor, (c) after immersion with 2.0 g/L PESA (d) after immersion with 2.0 g/L PESA and 2 mg/L Zn

4.2.6.3 Energy dispersive X-ray spectroscopy (EDS)

The EDS technique was employed to get the information about the composition of MS surface in the absence and presence of inhibitors in 3% NaCl solution. The results of EDS spectra are presented in Figure 71 (a-d). The spectra of uninhibited specimen contain the peaks corresponding to the elements present in MS, whereas inhibited MS contains the peaks corresponding to the elements present in the inhibitor molecules, indicating the adsorption of inhibitor molecules at the surface. It is noticeable that the percentage of atomic content of Fe for MS before immersion was 85.8% and after immersion reached 89.5% due to surface cleaning. However, after the addition of PESA only and PESA with Zn inhibitors, the percentage of atomic Fe has decreased to 78.5% and 78.9%, respectively. The suppressed percentage of Fe in the inhibited specimens is due to the formation of an inhibitive film on MS surface. This can be noticed as well with an increase atomic carbon (C) representing the organic molecule and atomic zinc (Zn) in EDS spectra of the sample (d).

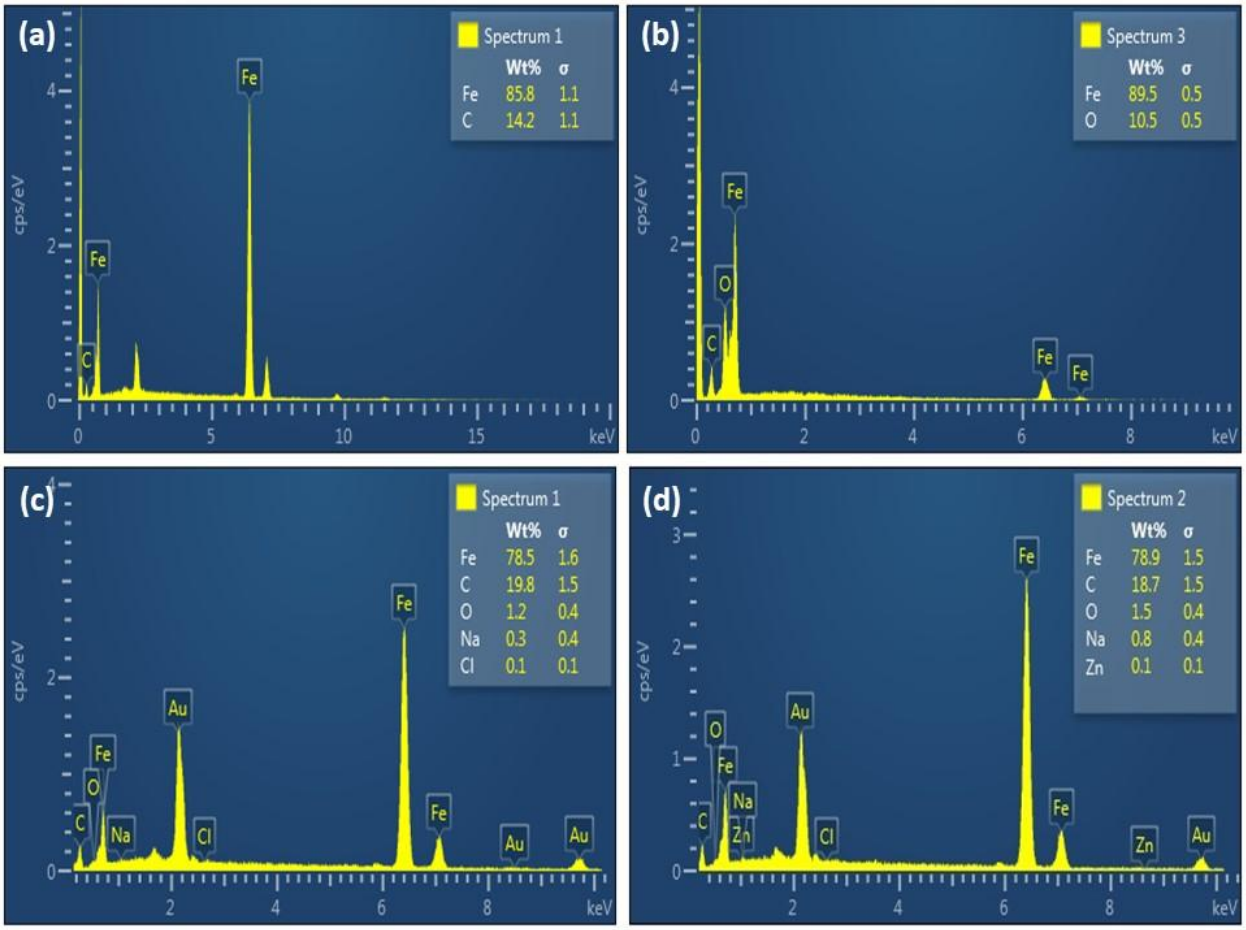

(a) Spectrum 1

	Wt%	σ
Fe	85.8	1.1
C	14.2	1.1

(b) Spectrum 3

	Wt%	σ
Fe	89.5	0.5
O	10.5	0.5

(c) Spectrum 1

	Wt%	σ
Fe	78.5	1.6
C	19.8	1.5
O	1.2	0.4
Na	0.3	0.4
Cl	0.1	0.1

(d) Spectrum 2

	Wt%	σ
Fe	78.9	1.5
C	18.7	1.5
O	1.5	0.4
Na	0.8	0.4
Zn	0.1	0.1

Figure 71: EDS spectra of MS specimens (a) polished before immersion, (b) after immersion without inhibitor, (c) after immersion with 2.0 g/L PESA, (d) after immersion with 2.0 g/L PESA and 2 mg/L Zn.

4.2.6.4 Atomic force microscopy (AFM)

The three-dimensional AFM images of polished (before immersion), uninhibited and inhibited mild steel specimens are shown in Figure 72 (a-d). The immersion time was only 4 hours in order to minimize pits depth and be able to get AFM micrographs. The roughness of polished mild steel specimen is computable with SEM images as shown earlier. The surface roughness of the corroded MS specimen in 3%NaCl is very high due to very fast corrosion especially pitting corrosion due to chloride ion as shown in AFM (b). While after the addition of 2 g/l PESA to the solution, the roughness and surface morphology has improved noticeably. However, there are areas having some pits due to pitting corrosion as shown in AFM (c). Adding only 2 mg/l of Zn ions has built a layer of PESA-Zn complex on the metal surface and inhibited the corrosion as shown in AFM (d). It can be expected that the mechanism of PESA alone is an adsorption type (anodic) corrosion inhibitor. While the PESA-Zn mechanism is expected to have dual properties of acting as an anodic and cathodic corrosion inhibition mechanism.

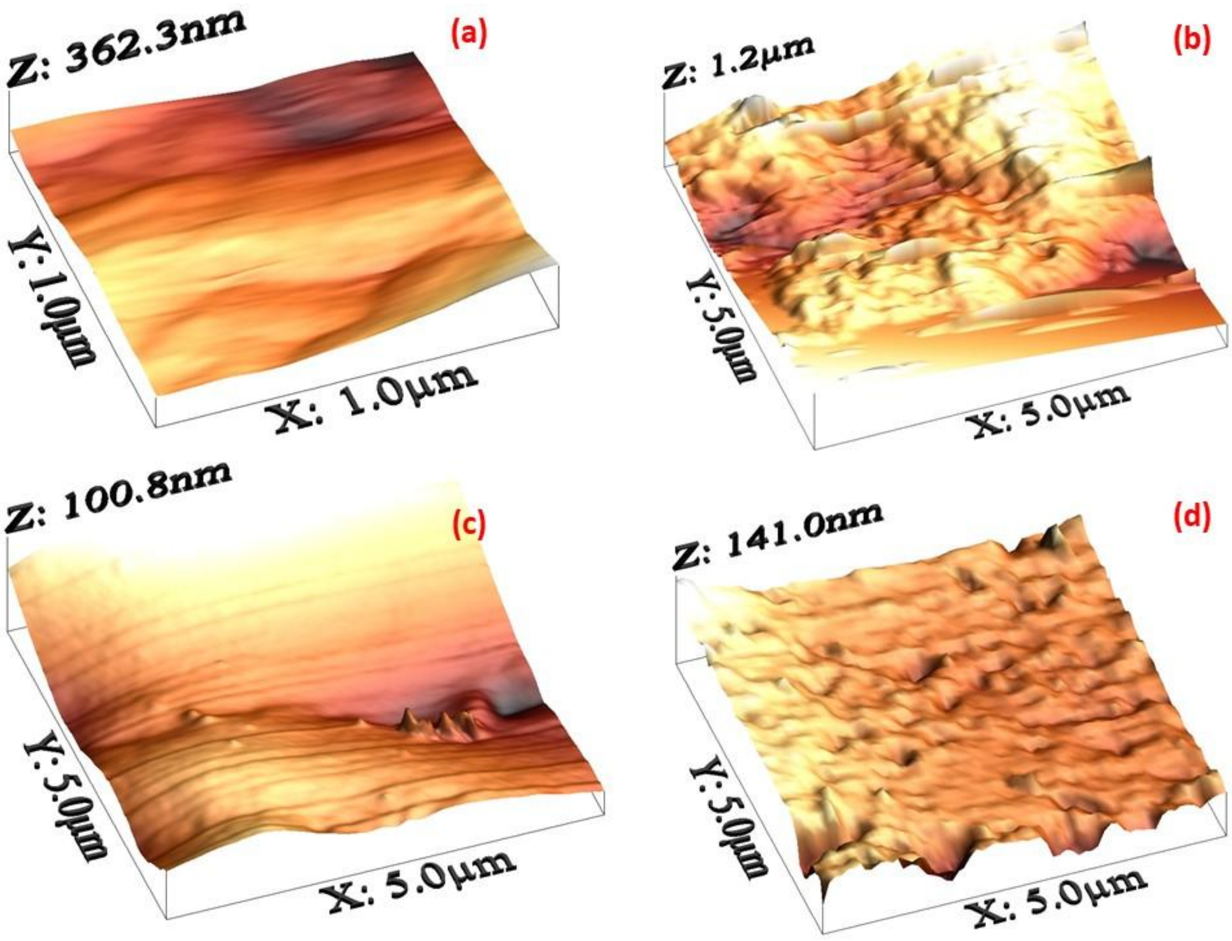

Figure 72: AFM micrographs of MS specimens (a) polished before immersion, (b) after immersion without inhibitor, (c) after immersion with 2.0 g/L PESA, (d) after immersion with 2.0 g/L PESA and 2 mg/L Zn.

4.2.7 Computational study

4.2.7.1 Quantum chemical calculations

The results obtained from quantum chemical calculations demonstrate that the electronic characteristics of the PESA are important parameters for prediction its reactivity on the steel surface.

Generally, HOMO and LUMO orbitals show the regions of the molecule which can donate or accept an electron, respectively. A molecule with large HOMO orbital is easy to donate an electron to unoccupied *d*-orbital of the metal atom. The one that has large LUMO orbital is easy to accept an electron from a metal atom. The optimized structure, HOMO, and LUMO diagrams of PESA molecule using AM1 model chemistry in VAMP module using the Materials Studio 8.0 software licensed to KFUPM. Figure 73 (a and b) shows the 3-D molecular structure of polyepoxysuccinic acid sodium form (PESA) and 3-D molecular structure of polyepoxysuccinic acid sodium form (PESA)with n = 4 repeating units, respectively. Figure 74 (a and b) shows the HOMO and LUMO orbitals distribution of PESA calculated using VAMP module at the AM1 level of theory in Material Studio 8.0 software. It is observed that the HOMO orbital localizes at –COONa groups in the polymer backbone. These are the regions donating an electron to unoccupied *d*-orbital of metal. On the other hand, LUMO orbital localizes at the same region around the carboxylate group on the polymer backbone. These regions can accept an electron from the metal surface. Thus, these analyses indicate that the carboxylate groups play an important role as active sites for the interaction of PESA with a steel surface.

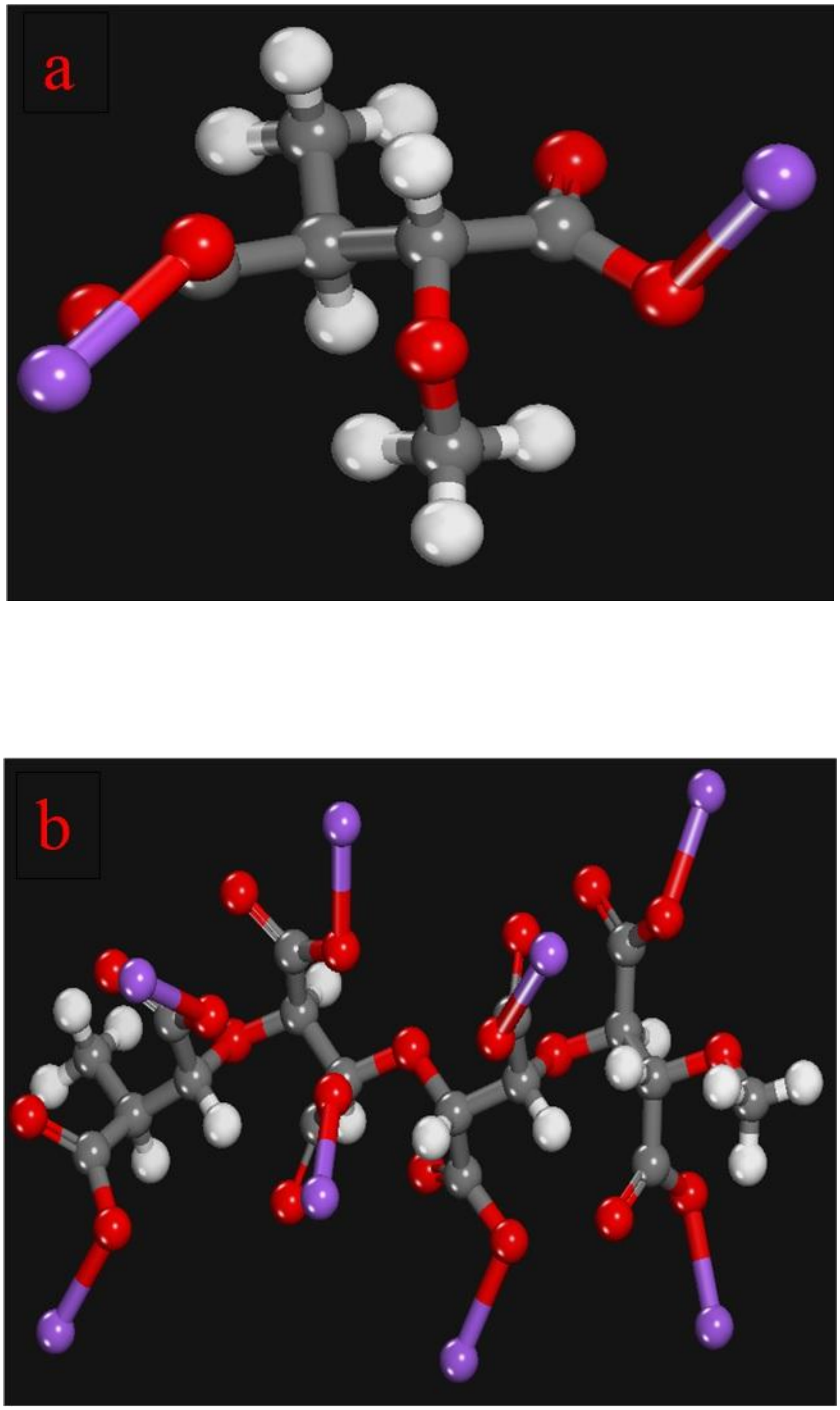

Figure 73: (a) 3-D molecular structure of polyepoxysuccinic acid sodium form (PESA) and (b) 3-D molecular structure of polyepoxysuccinic acid sodium form (PESA) with n = 4 repeat unit.

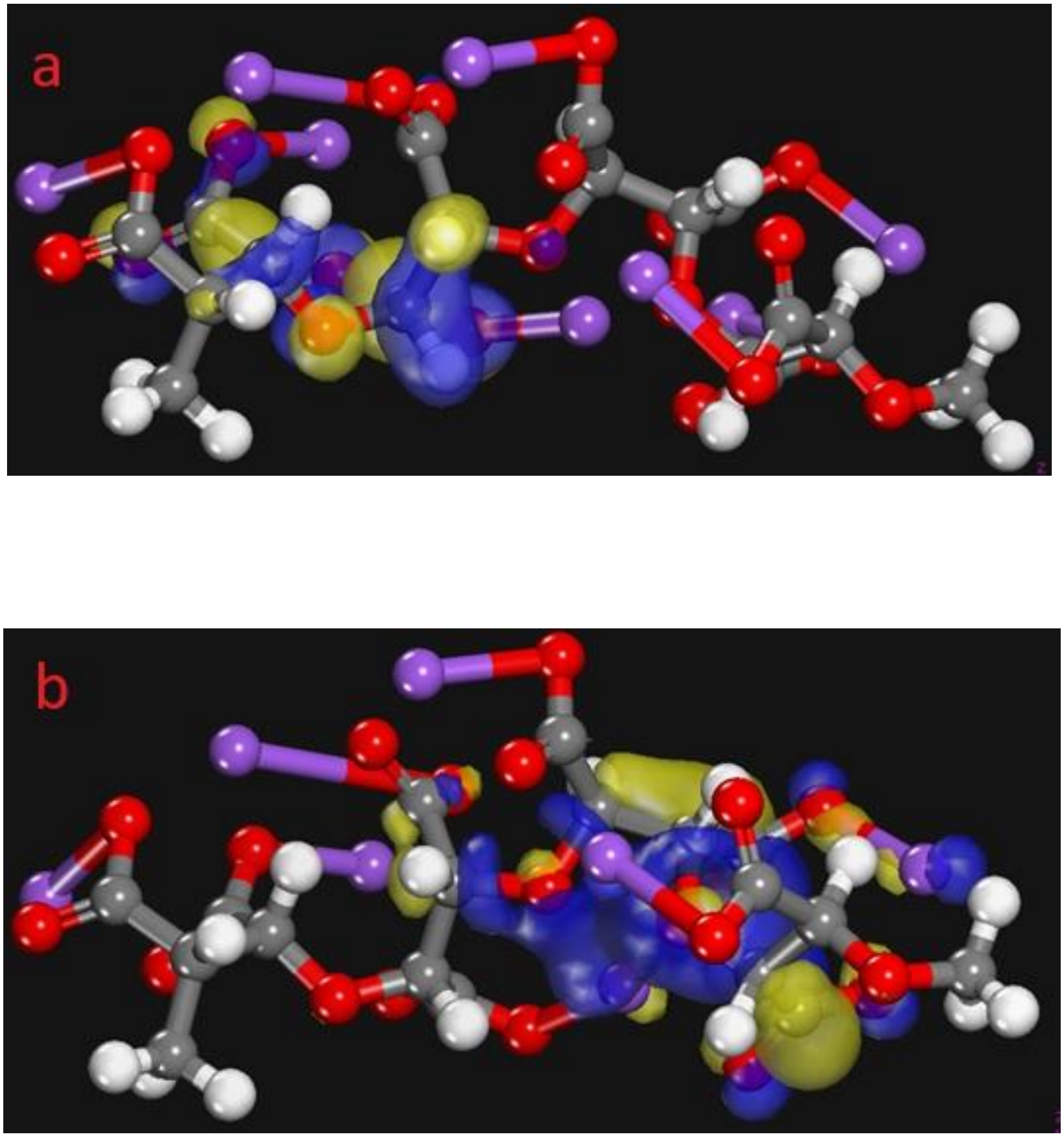

Figure 74: (a) HOMO and (b) LUMO orbital distribution of PESA calculated using VAMP module at the AM1 level of theory in Material Studio 8.0 software.

4.2.7.2 Monte Carlo simulation

Metropolis Monte Carlo simulations using simulated annealing procedure were further carried out to quantify the adsorption of PESA alone on the steel surface. Figure 75 shows (a) snapshot of the top view of the stable equilibrium configuration of PESA adsorption on Fe (110) surface and (b) is the side view side view of stable equilibrium configuration of PESA adsorption on Fe (110) surface in the gas phase using Monte Carlo simulation methodology. The simulation box consisted of 5 layers of iron atoms cleaved along the (110) plane. A supercell of (13 × 13) was created and vacuum layer of 50 nm height was fabricated. An optimized molecule of PESA was positioned near the surface of Fe (110) plane using the simulated annealing adsorption locator module with COMPASS force field. The simulations were performed under ultra-fine convergence conditions, while each simulation went through 10 cycles at 100,000 steps per cycle. Orientation and low adsorption figurations for the interaction of the systems on Fe (110) surface were obtained. It can be seen that PESA is adsorbed in a parallel orientation to the metal surface using the carboxylate groups and the hydrogen bonds present in the polymer chain. The calculated negative adsorption energy for PESA/Fe (110) surface is -944.97 kJ mol^{-} which is considered a very high adsorption energy. It has been reported that the higher the negative adsorption energies, the stronger the interaction of inhibitor molecules with metal surfaces. This result indicates that PESA is expected to inhibit steel corrosion in 3% NaCl solution as an adsorption-type (anodic) corrosion inhibitor. These results are in agreement with experimental results show that PESA has good corrosion inhibition efficiency under the tested stressed corrosion environment.

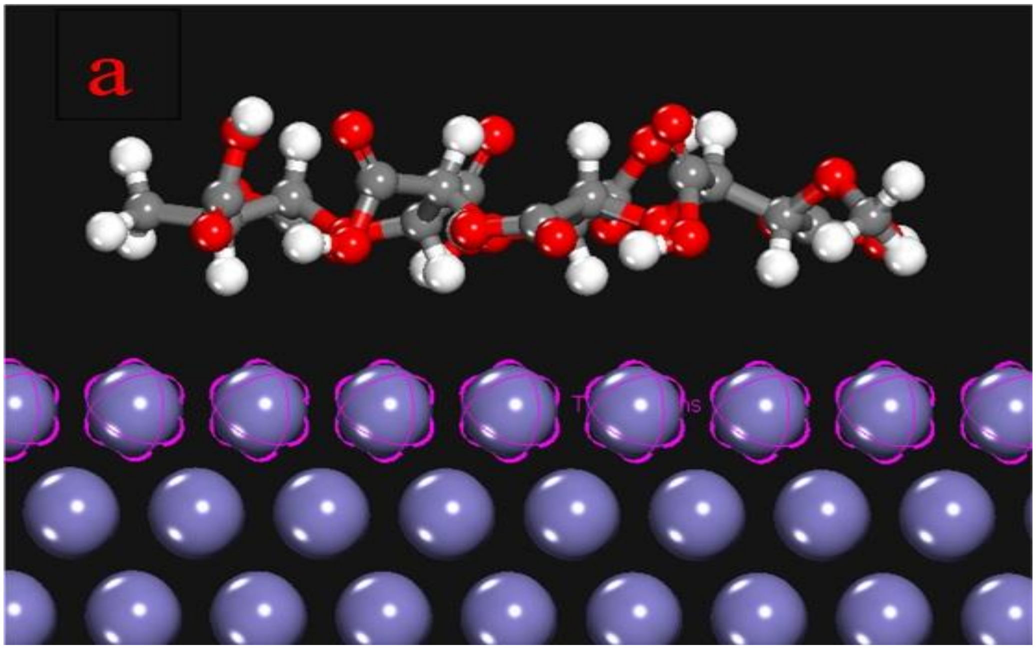
a

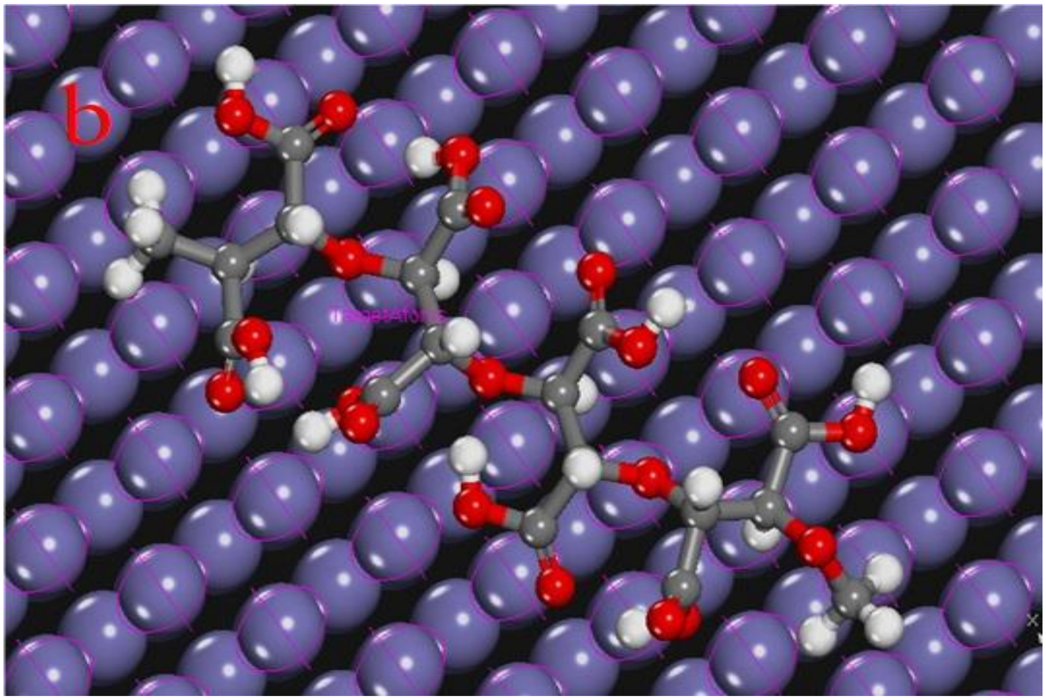

Figure 75: (a) Top view and (b) side view of stable equilibrium configuration of PESA adsorption on Fe (110) surface in the gas phase using Monte Carlo simulation methodology.

4.2.8 PESA mechanism

The inhibitive mechanism of PESA on mild steel in aerated 3% NaCl solution can be explained based on the above findings and adsorption results. The large electron-rich HOMO orbitals localized in -COONa groups and having lone pairs of electrons are getting adsorbed by donating electrons to d-orbitals of mild steel in a parallel position. Each 1 repeating unit of PESA has two carboxylic groups and they are the backbone of PESA structure. Furthermore, LUMO orbitals localized around carboxylic groups accept electrons from the metal surface. This model of adsorption of PESA on metal interface reduces the anodic reaction of the corrosion cell as observed in Tafel curves and thus PESA can be named as an anodic inhibitor. Additionally, PESA can be considered as a strong anodic inhibitor comparing to PASP because it has very high calculated negative adsorption energy. This adsorption layer was characterized proofed using FTIR-ATR on the metal surface. However, PESA polymer is large which hinders a smooth parallel adsorption of PESA on the metal-solution interface. The addition of Zn^{+2} at neutral pH has improved the inhibition efficiency noticeably by hindering the cathodic part of corrosion reaction through building a layer of PESA-Zn complex on the metal surface. Zn (II) is chelating with plenty carboxylic (-COOH) groups on PESA structure forming a precipitation complex adsobed on mild steel surface and reducing the cathodic corrosion reactions [107] [109]. So, PESA forms a PESA-Zn complex building a precipitation layer on mild steel surface and minimizing the overall corrosion rates. This was concluded from Tafel plots by observing a change in the cathodic part of Tafel plot. This layer was characterized using SEM, AFM, and EDX and showed a little thicker adsorption layer was formed after the addition of zinc ions. Therefore, zinc ions played a synergistic mechanism in mild steel inhibition at this stressed corrosive environment and formed a mixed-type of corrosion inhibition behavior in the corrosion cell. Figure 76 shows a schematic illustration of the suggested adsorption mechanism of PESA.

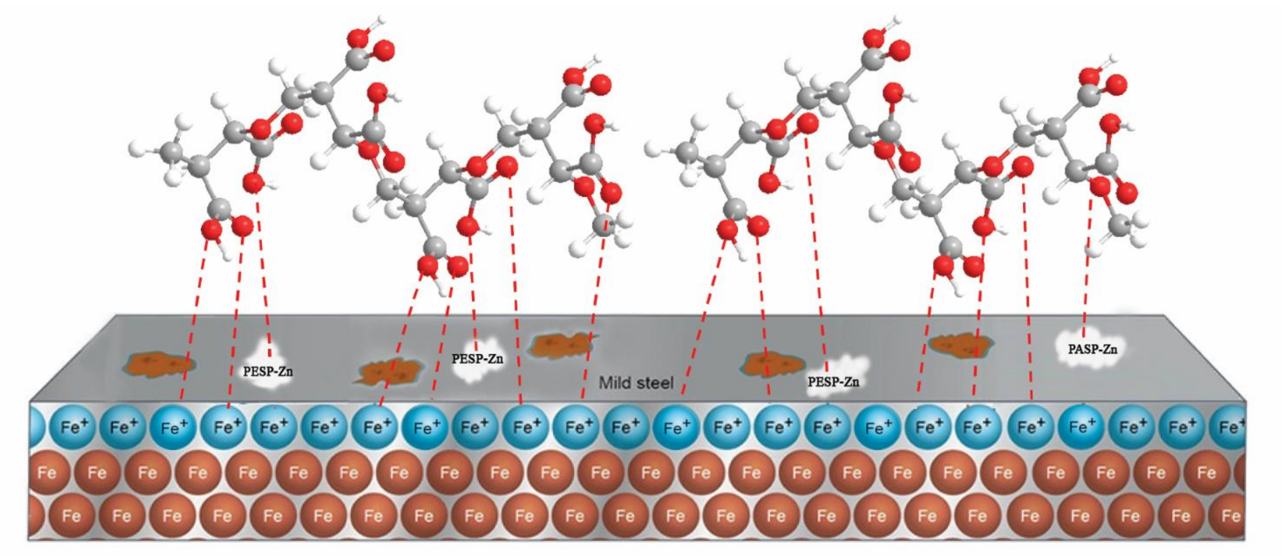

Figure 76: The schematic illustration of different modes of interactions on metal/solution interface in the presence of PESA and Zn inhibitors

4.2.9 PESA conclusion

Based on the result obtained from this study, the following conclusions may be drawn:

(1) The tested PESA is considered as a moderate adsorption-type (anodic) corrosion inhibitor for mild steel in 3% NaCl aerated solution because it is adsorbed on the metal surface.

(2) Potentiodynamic polarization study confirms the results obtained from weight loss method and revealed the electrochemical inhibition behavior of PESA and Zn.

(3) The molecular weight of PESA and the testing condition will quantify the dosage of inhibitor should be added. However, under potable water condition, the inhibitor dosage will be much lower than the tested corrosive environment.

(4) Zinc ions addition has shown good improvement of mild steel corrosion inhibition and has good synergistic effect with PESA.

(5) The micrographs obtained from SEM and AFM confirmed that there is a good protection film on metal surface minimizing the corrosion rate of mild steel in 3% NaCl.

(6) Computational quantum chemistry studies showed a correlation with the experimental results and findings where PESA has efficient adsorption sites and could be adsorbed on the metal surface.

4.2.10 Recommendations for future work

The above results show that the overall performance of PESA in mild corrosion inhibition was very good and potential in water treatment applications. There are a lot of works could be done on PESA in order to understand its performance under various industrial applications as the following:

1- Studying the performance of PESA on the corrosion inhibition of carbon steel under acidic conditions such as HCL or H_2SO_4 which can simulate industrial pickling processes.

2- Studying the dual mechanism of PESA as corrosion and scale inhibitor for cooling system application. This can be done by studying its scale inhibition performance of common mineral scales found in cooling systems such as $CaCO_3$ and $CaSO_4$. Also, its corrosion inhibition properties of carbon steel and copper in potable and waters.

3- Studying the performance of some PESA derivatives as green inhibitors for their corrosion inhibition on carbon steel in different types of water.

4- Studying the inhibition efficiency of PESA on different metallurgies commonly used in cooling systems such as copper, aluminum, and stainless steel.

REFERENCES

[1] E. McCafferty, *Introduction to Corrosion Science*. New York, NY: Springer New York, 2010.

[2] NACE International, “International Measures of Prevention, Application and Economics of Corrosion Technology (IMPACT),” 2016. [Online]. Available: https://inspectioneering.com/news/2016-03-08/5202/nace-study-estimates-global-cost-of-corrosion-at-25-trillion-ann. [Accessed: 14-Oct-2017].

[3] J. G. Speight, “Corrosion,” in *Oil and Gas Corrosion Prevention*, Elsevier, 2014, pp. e1–e24.

[4] I. B. Obot and A. Madhankumar, “Enhanced corrosion inhibition effect of tannic acid in the presence of gallic acid at mild steel/HCl acid solution interface,” *J. Ind. Eng. Chem.*, vol. 25, pp. 105–111, 2015.

[5] F. Zhang, “The Mussel Adhesive Protein (Mefp-1) A GREEN Corrosion Inhibitor,” KTH Royal Institute of Technology, 2013.

[6] R. W. (Robert W. Revie and H. H. Uhlig, *Corrosion and corrosion control : an introduction to corrosion science and engineering*. Wiley-Interscience, 2008.

[7] M. A. Amin, S. S. Abd El-Rehim, E. E. F. El-Sherbini, and R. S. Bayoumi, “The inhibition of low carbon steel corrosion in hydrochloric acid solutions by succinic acid: Part I. Weight loss, polarization, EIS, PZC, EDX and SEM studies,” *Electrochim. Acta*, vol. 52, no. 11, pp. 3588–3600, Mar. 2007.

[8] L. Sanders, X. Hu, E. Mavredaki, V. Eroini, R. Barker, and A. Neville, “Assessment of combined scale/corrosion inhibitors – A combined jar test/bubble cell,” 2014.

[9] M. Yadav, R. R. Sinha, S. Kumar, and T. K. Sarkar, “Corrosion inhibition effect of spiropyrimidinethiones on mild steel in 15 % HCl solution : insight from electrochemical and quantum studies,” *RSC Adv.*, vol. 5, pp. 70832–70848, 2015.

[10] B. E. A. Rani, B. B. J. Basu, B. E. A. Rani, and B. B. J. Basu, “Green Inhibitors for Corrosion Protection of Metals and Alloys: An Overview,” *Int. J. Corros.*, vol. 2012, pp. 1–15, 2012.

[11] V. S. (Vedula S. . Sastri and Wiley InterScience (Online service), *Green corrosion inhibitors : theory and practice*. Hoboken, NJ: Wiley, 2011.

[12] M. Bethencourt, F. J. Botana, J. J. Calvino, M. Marcos, and M. A. RodrÍguez-Chacón, “Lanthanide compounds as environmentally-friendly corrosion inhibitors of aluminium alloys: a review,” *Corros. Sci.*, vol. 40, no. 11, pp. 1803–1819, Nov. 1998.

[13] O. Olivares, N. V. Likhanova, B. Gómez, J. Navarrete, M. E. Llanos-Serrano, E. Arce, and J. M. Hallen, “Electrochemical and XPS studies of decylamides of α-amino acids

adsorption on carbon steel in acidic environment," *Appl. Surf. Sci.*, vol. 252, no. 8, pp. 2894–2909, Feb. 2006.

[14] S. A. Abd El-Maksouda and A. S. Fouda, "Some pyridine derivatives as corrosion inhibitors for carbon steel in acidic medium," *Mater. Chem. Phys.*, vol. 93, no. 1, pp. 84–90, Sep. 2005.

[15] D. E. Tallman, G. Spinks, A. Dominis, and G. G. Wallace, "Electroactive conducting polymers for corrosion control," *J. Solid State Electrochem.*, vol. 6, no. 2, pp. 73–84, Feb. 2002.

[16] D. E. Arthur, A. Jonathan, P. O. Ameh, and C. Anya, "A review on the assessment of polymeric materials used as corrosion inhibitor of metals and alloys," *Int. J. Ind. Chem.*, vol. 4, no. 1, p. 2, 2013.

[17] B. Müller, I. Förster, and W. Kläger, "Corrosion inhibition of zinc pigments in aqueous alkaline media by polymers," *Prog. Org. Coatings*, vol. 31, no. 3, pp. 229–233, Nov. 1997.

[18] S. S. Abd El Rehim, F. M. Tohamy, and M. M. Seleet, "Effect of some polyamino polycarboxylic acids on the corrosion of steel in sulphate solutions," *Surf. Technol.*, vol. 21, no. 2, pp. 169–177, Feb. 1984.

[19] K. S. Khairou and A. El-Sayed, "Inhibition effect of some polymers on the corrosion of cadmium in a hydrochloric acid solution," *J. Appl. Polym. Sci.*, vol. 88, no. 4, pp. 866–871, Apr. 2003.

[20] B. Zhang, C. He, C. Wang, P. Sun, F. Li, and Y. Lin, "Synergistic corrosion inhibition of environment-friendly inhibitors on the corrosion of carbon steel in soft water," *Corros. Sci.*, vol. 94, pp. 6–20, 2015.

[21] A. A. El Hosary, R. M. Saleh, and A. M. Shams El Din, "Corrosion inhibition by naturally occurringsubstances—I. The effect of Hibiscus subdariffa (karkade) extract on the dissolution of Al and Zn," *Corros. Sci.*, vol. 12, no. 12, pp. 897–904, Jan. 1972.

[22] A. Bouyanzer, L. Majidi, and B. Hammouti, "Effect of eucalyptus oil on the corrosion of steel in 1M HCl," *Bull. Electrochem.*, vol. 22, no. 7, pp. 321–324, 2006.

[23] M. Abdallah, "Guar Gum as Corrosion Inhibitor for Carbon Steel in Sulfuric Acid Solutions," *Port. Electrochim. Acta*, vol. 22, pp. 161–175, 2004.

[24] N. K. Gupta, P. G. Joshi, V. Srivastava, and M. A. Quraishi, "Chitosan: A macromolecule as green corrosion inhibitor for mild steel in sulfamic acid useful for sugar industry," *J. Biol. Macromol. Int. J. Biol. Macromol. Int. J. Biol. Macromol.*, 2017.

[25] F. S. de Souza and A. Spinelli, "Caffeic acid as a green corrosion inhibitor for mild steel," *Corros. Sci.*, vol. 51, no. 3, pp. 642–649, Mar. 2009.

[26] X. Wang, B. I. Lee, and L. Mann, "Dispersion of barium titanate with polyaspartic acid in aqueous media," *Colloids Surfaces A Physicochem. Eng. Asp.*, vol. 202, pp. 71–80, 2002.

[27] D. Hasson, H. Shemer, and A. Sher, "State of the Art of Friendly 'Green' Scale Control Inhibitors: A Review Article," *Ind. Eng. Chem. Res.*, vol. 50, no. 12, pp. 7601–7607, Jun. 2011.

[28] K. C. Low, A. P. Wheeler, and L. P. Koskan, "Commercial Poly(aspartic acid) and Its Uses," 1996, pp. 99–111.

[29] R. Cui, N. Gu, and C. Li, "Polyaspartic acid as a green corrosion inhibitor for carbon steel," *Mater. Corros.*, vol. 62, no. 4, pp. 362–369, Apr. 2011.

[30] S. M. Thombre and B. D. Sarwade, "Synthesis and Biodegradability of Polyaspartic Acid: A Critical Review," *J. Macromol. Sci. Part A*, vol. 42, no. 9, pp. 1299–1315, Sep. 2005.

[31] A. Ketsetzi, A. Stathoulopoulou, and K. D. Demadis, "Being 'green' in chemical water treatment technologies: issues, challenges and developments," *Desalination*, vol. 223, no. 1–3, pp. 487–493, Mar. 2008.

[32] R. A. Gross and B. Kalra, "Biodegradable Polymers for the Environment," *Science (80-.).*, vol. 297, no. 5582, pp. 803–807, Aug. 2002.

[33] I. Ostolska and M. Wiśniewska, "Comparison of the influence of polyaspartic acid and polylysine functional groups on the adsorption at the Cr2O3—Aqueous polymer solution interface," *Appl. Surf. Sci.*, vol. 311, pp. 734–739, Aug. 2014.

[34] Y. Gao, Z. Liu, L. Zhang, and Y. Wang, "Synthesis and Performance Research of Biodegradable Modified Polyaspartic Acid," in *2010 4th International Conference on Bioinformatics and Biomedical Engineering*, 2010, pp. 1–4.

[35] A. Martinod, A. Neville, M. Euvrad, and K. Sorbie, "Electrodeposition of a calcareous layer: Effects of green inhibitors," *Chem. Eng. Sci.*, vol. 64, no. 10, pp. 2413–2421, 2009.

[36] M. Euvrard, A. Martinod, and A. Neville, "Effects of carboxylic polyelectrolytes on the growth of calcium carbonate," *J. Cryst. Growth*, vol. 317, no. 1, pp. 70–78, Feb. 2011.

[37] Z. Liu, Y. Sun, X. Zhou, T. Wu, Y. Tian, and Y. Wang, "Synthesis and scale inhibitor performance of polyaspartic acid," *J. Environ. Sci.*, vol. 23, pp. S153–S155, Jun. 2011.

[38] D. Liu, W. Dong, F. Li, F. Hui, and J. Lédion, "Comparative performance of polyepoxysuccinic acid and polyaspartic acid on scaling inhibition by static and rapid controlled precipitation methods," *Desalination*, vol. 304, pp. 1–10, Oct. 2012.

[39] B. Zhang, D. Zhou, X. Lv, Y. Xu, and Y. Cui, "Synthesis of polyaspartic acid/3-amino-1H-1,2,4-triazole-5-carboxylic acid hydrate graft copolymer and evaluation of its corrosion inhibition and scale inhibition performance," *Desalination*, vol. 327, pp. 32–38, Oct. 2013.

[40] X. Gu, F. Qiu, X. Zhou, J. Qi, Y. Zhou, D. Yang, Q. Guo, and X. Guo, "Preparation and Application of Polymers as Inhibitors for Calcium Carbonate and Calcium Phosphate Scales," *Int. J. Polym. Mater.*, vol. 62, no. 6, pp. 323–329, Mar. 2013.

[41] Y. Xu, L. Zhao, L. Wang, S. Xu, and Y. Cui, “Synthesis of polyaspartic acid–melamine grafted copolymer and evaluation of its scale inhibition performance and dispersion capacity for ferric oxide,” *Desalination*, vol. 286, pp. 285–289, Feb. 2012.

[42] B. Senthilmurugan, B. Ghosh, and S. Sanker, “High performance maleic acid based oil well scale inhibitors—Development and comparative evaluation,” *J. Ind. Eng. Chem.*, vol. 17, no. 3, pp. 415–420, May 2011.

[43] W. J. Benton and L. P. Koskan, “Inhibition of carbon dioxide corrosion of metals,” US 5607623 A, 1995.

[44] J. C. Fan, L.-D. G. Fan, and J. Mazo, “Composition for inhibition of metal corrosion,” US 6620338 B2, 2002.

[45] B. Qian, J. Wang, M. Zheng, and B. Hou, “Synergistic effect of polyaspartic acid and iodide ion on corrosion inhibition of mild steel in H2SO4,” *Corros. Sci.*, vol. 75, pp. 184–192, 2013.

[46] Y. Xu, B. Zhang, L. Zhao, and Y. Cui, “Synthesis of polyaspartic acid/5-aminoorotic acid graft copolymer and evaluation of its scale inhibition and corrosion inhibition performance,” *Desalination*, vol. 311, pp. 156–161, Feb. 2013.

[47] H. P. Wang, Q. Wu, C. M. Li, and N. Gu, “Copper corrosion inhibition by polyaspartic acid and imidazole,” *Mater. Corros.*, vol. 64, no. 4, pp. 347–352, Apr. 2013.

[48] L. Yang, Y. Li, B. Qian, and B. Hou, “Polyaspartic acid as a corrosion inhibitor for WE43 magnesium alloy,” *J. Magnes. Alloy.*, vol. 3, no. 1, pp. 47–51, Mar. 2015.

[49] Y. Gao, L. Fan, L. Ward, and Z. Liu, “Synthesis of polyaspartic acid derivative and evaluation of its corrosion and scale inhibition performance in seawater utilization,” *Desalination*, vol. 365, pp. 220–226, 2015.

[50] M. A. Migahed, S. M. R. Rashwan, M. M. Kamel, and R. E. Habib, “Synthesis, characterization of polyaspartic acid-glycine adduct and evaluation of their performance as scale and corrosion inhibitor in desalination water plants,” *J. Mol. Liq.*, vol. 224, pp. 849–858, Dec. 2016.

[51] S. Shi, Y. Wu, Y. Wang, J. Yu, and Y. Xu, “Synthesis and characterization of a biodegradable polyaspartic acid/2-amino-2-methyl-1-propanol graft copolymer and evaluation of its scale and corrosion inhibition performance,” *RSC Adv.*, vol. 7, no. 58, pp. 36714–36721, Jul. 2017.

[52] M. A. Migahed, S. M. Rashwan, M. M. Kamel, and R. E. Habib, “Synthesized polyaspartic acid derivatives as corrosion and scale inhibitors in desalination operations,” *Cogent Eng.*, vol. 4, no. 1, p. 1366255, Aug. 2017.

[53] G. Wei, Y. Xu, and C. Xiong R, “A study on biodegradability of scale inhibitors.,” *J. BeiJing Univ. Chem. Technol.*, vol. 28, no. 1, pp. 59–62, 2001.

[54] X. Zhou, Y. Sun, and Y. Wang, “Inhibition and dispersion of polyepoxysuccinate as a

scale inhibitor," *J. Environ. Sci.*, vol. 23, pp. S159–S161, Jun. 2011.

[55] Y. SUN, W. XIANG, and Y. WANG, "Study on polyepoxysuccinic acid reverse osmosis scale inhibitor," *J. Environ. Sci.*, vol. 21, pp. S73--S75, 2009.

[56] D. Rose, G. Zaid, T. Burgoyne, and K. Brashear, "Synthesis of polyepoxy succinic acid compounds using free radical initiators," US 9109084 B1, 2014.

[57] Z.-L. ZHU, L.-H. ZHANG, H. ZHANG, Y.-L. QIU, R.-H. ZHANG, and J.-F. ZHAO, "Extraction of Cadmium from Sewage Sludge Using Polyepoxysuccinic Acid*1," *Pedosphere*, vol. 19, no. 2, pp. 137–142, Apr. 2009.

[58] L.-H. ZHANG and Z.-L. ZHU, "Chromium Extraction from Sewage Sludge Using Polyepoxysuccinic Acid," *Pedosphere*, vol. 22, no. 1, pp. 131–136, Feb. 2012.

[59] C. Wang, B. Gao, P. Zhao, R. Li, Q. Yue, and H. K. Shon, "Exploration of polyepoxysuccinic acid as a novel draw solution in the forward osmosis process," *RSC Adv.*, vol. 7, no. 49, pp. 30687–30698, Jun. 2017.

[60] W.-Y. Shi, C. Ding, J.-L. Yan, X.-Y. Han, Z.-M. Lv, W. Lei, M.-Z. Xia, and F.-Y. Wang, "Molecular dynamics simulation for interaction of PESA and acrylic copolymers with calcite crystal surfaces," *Desalination*, vol. 291, pp. 8–14, 2012.

[61] Y. Sasikumar, A. S. Adekunle, L. O. Olasunkanmi, I. Bahadur, R. Baskar, M. M. Kabanda, I. B. Obot, and E. E. Ebenso, "Experimental, quantum chemical and Monte Carlo simulation studies on the corrosion inhibition of some alkyl imidazolium ionic liquids containing tetrafluoroborate anion on mild steel in acidic medium," *J. Mol. Liq.*, vol. 211, pp. 105–118, 2015.

[62] J. Vosta and J. Eli~sek, "STUDY ON CORROSION INHIBITION FROM ASPECT OF QUANTUM CHEMISTRY*," *Corros. Sci.*, vol. 11, pp. 223–1, 1971.

[63] I. Lukovits, I. Bak6, A. Shaban, and E. Kglman, "Polynomial model of the inhibition mechanism thiourea derivatives," *Ekctrochimica Acra*, vol. 43, pp. 1–2, 1998.

[64] S. Ramachandran, B.-L. Tsai, M. Blanco, H. Chen, Y. Tang, and W. A. Goddard, "Atomistic Simulations of Oleic Imidazolines Bound to Ferric Clusters," *J. Phys. Chem. A*, vol. 101, no. 1, pp. 83–89, Jan. 1997.

[65] A. Zarrouk, B. Hammouti, A. Dafali, M. Bouachrine, H. Zarrok, S. Boukhris, and S. S. Al-Deyab, "A theoretical study on the inhibition efficiencies of some quinoxalines as corrosion inhibitors of copper in nitric acid," *J. Saudi Chem. Soc.*, vol. 18, pp. 450–455, 2014.

[66] I. B. Obot, D. D. Macdonald, and Z. M. Gasem, "Density functional theory (DFT) as a powerful tool for designing new organic corrosion inhibitors. Part 1: An overview," *Corros. Sci.*, vol. 99, pp. 1–30, 2015.

[67] L. Guo, S. Zhu, S. Zhang, Q. He, and W. Li, "Theoretical studies of three triazole derivatives as corrosion inhibitors for mild steel in acidic medium," *Corros. Sci.*, vol. 87,

pp. 366–375, 2014.

[68] K. F. Khaled, “Monte Carlo simulations of corrosion inhibition of mild steel in 0.5 M sulphuric acid by some green corrosion inhibitors,” *J. Solid State Electrochem.*, vol. 13, no. 11, pp. 1743–1756, Nov. 2009.

[69] E. Cor, “Standard Practice for Laboratory Immersion Corrosion Testing of Metals 1,” *Corrosion*, vol. 72, no. Reapproved, pp. 1–8, 2004.

[70] E. McCafferty, *Corrosion*. 1998.

[71] E. McCafferty, *Introduction to Corrosion Science*. New York, NY: Springer New York, 2010.

[72] I. Gamry Instruments, “Getting Started with Electrochemical Corrosion Measurement,” 2011.

[73] S. Saker, N. Aliouane, H. Hammache, S. Chafaa, and G. Bouet, “Tetraphosphonic acid as eco-friendly corrosion inhibitor on carbon steel in 3% NaCl aqueous solution,” *Ionics (Kiel).*, vol. 21, no. 7, pp. 2079–2090, 2015.

[74] N. A. Odewunmi, S. A. Umoren, and Z. M. Gasem, “Utilization of watermelon rind extract as a green corrosion inhibitor for mild steel in acidic media,” *J. Ind. Eng. Chem.*, vol. 21, pp. 239–247, 2015.

[75] N. Perez, *Electrochemistry and Corrosion Science*, 2nd ed. Cham: Springer International Publishing, 2016.

[76] H. Wang, “Electrochemical investigation of green film-forming corrosion inhibitors,” Royal Institute of Technology, 2011.

[77] M. Salasi, T. Shahrabi, E. Roayaei, and M. Aliofkhazraei, “The electrochemical behaviour of environment-friendly inhibitors of silicate and phosphonate in corrosion control of carbon steel in soft water media,” *Mater. Chem. Phys.*, vol. 104, no. 1, pp. 183–190, 2007.

[78] Z. Tao, S. Zhang, W. Li, and B. Hou, “Corrosion inhibition of mild steel in acidic solution by some oxo-triazole derivatives,” *Corros. Sci.*, vol. 51, pp. 2588–2595, 2009.

[79] G. A. Notes, “Basics of Electrochemical Impedance Spectroscopy,” Warminster PA, 2013.

[80] M. J. Walsh, S. E. Holton, A. Kajdacsy-Balla, and R. Bhargava, “Vibrational Spectroscopy Attenuated total reflectance Fourier-transform infrared spectroscopic imaging for breast histopathology,” *Vib. Spectrosc.*, vol. 60, pp. 23–28, 2012.

[81] E. B. Ituen, O. Akaranta, and S. A. Umoren, “N-acetyl cysteine based corrosion inhibitor formulations for steel protection in 15% HCl solution,” *J. Mol. Liq.*, vol. 246, pp. 112–118, 2017.

[82] G. K. H. Pang, K. Z. Baba-Kishi, and A. Patel, “Topographic and phase-contrast imaging in atomic force microscopy,” *Ultramicroscopy*, vol. 81, pp. 35–40, 2000.

[83] H. Zhang, J. Huang, Y. Wang, R. Liu, X. Huai, J. Jiang, and C. Anfuso, “Atomic force microscopy for two-dimensional materials: A tutorial review,” *Opt. Commun.*, vol. 406, pp. 3–17, Jan. 2018.

[84] M. R. Nellist, Y. Chen, A. Mark, S. Gödrich, C. Stelling, J. Jiang, R. Poddar, C. Li, R. Kumar, G. Papastavrou, M. Retsch, B. S. Brunschwig, Z. Huang, C. Xiang, and S. W. Boettcher, “Atomic force microscopy with nanoelectrode tips for high resolution electrochemical, nanoadhesion and nanoelectrical imaging,” *Nanotechnology*, vol. 28, no. 9, p. 95711, Mar. 2017.

[85] D. Stokes, *Principles and practice of variable pressure/environmental scanning electron microscopy (VP-ESEM)*. Chichester: Wiley, 2008.

[86] J. I. Goldstein, D. E. Newbury, P. Echlin, D. C. Joy, C. Fiori, and E. Lifshin, *Scanning Electron Microscopy and X-Ray Microanalysis*. Boston, MA: Springer US, 1981.

[87] A. L. Chong, J. I. Mardel, D. R. MacFarlane, M. Forsyth, and A. E. Somers, “Synergistic Corrosion Inhibition of Mild Steel in Aqueous Chloride Solutions by an Imidazolinium Carboxylate Salt,” *ACS Sustain. Chem. Eng.*, vol. 4, no. 3, pp. 1746–1755, Mar. 2016.

[88] J. I. Goldstein, D. E. Newbury, P. Echlin, D. C. Joy, C. E. Lyman, E. Lifshin, L. Sawyer, and J. R. Michael, *Scanning Electron Microscopy and X-ray Microanalysis*, 3rd ed. Boston, MA: Springer US, 2003.

[89] M. Cui, S. Ren, Q. Xue, H. Zhao, and L. Wang, “Carbon dots as new eco-friendly and effective corrosion inhibitor,” *J. Alloys Compd.*, vol. 726, pp. 680–692, 2017.

[90] ASTM International, “ASTM D2688 - 11 Standard Test Method for Corrosivity of Water in the Absence of Heat Transfer (Weight Loss Method),” West Conshohocken, PA, 2011.

[91] E. Naveen, B. V. Ramnath, C. Elanchezhian, and S. S. M. Nazirudeen, “Influence of organic corrosion inhibitors on pickling corrosion behaviour of sinter-forged C45 steel and 2% Cu alloyed C45 steel,” *J. Alloys Compd.*, vol. 695, pp. 3299–3309, 2017.

[92] H. Hamani, T. Douadi, D. Daoud, M. Al-Noaimi, R. A. Rikkouh, and S. Chafaa, “1-(4-Nitrophenylo-imino)-1-(phenylhydrazono)-propan-2-one as corrosion inhibitor for mild steel in 1M HCl solution_ Weight loss, electrochemical, thermodynamic and quantum chemical studies,” *J. Electroanal. Chem.*, vol. 801, pp. 425–438, 2017.

[93] A. Popova, E. Sokolova, S. Raicheva, and M. Christov, “AC and DC study of the temperature effect on mild steel corrosion in acid media in the presence of benzimidazole derivatives,” *Corros. Sci.*, vol. 45, pp. 33–58, 2003.

[94] V. Ramesh Saliyan and A. V. Adhikari, “Inhibition of corrosion of mild steel in acid media by N′-benzylidene-3-(quinolin-4-ylthio)propanohydrazide,” *Bull. Mater. Sci.*, vol. 31, no. 4, pp. 699–711, Aug. 2008.

[95] S. Kumar, H. Vashisht, L. O. Olasunkanmi, I. Bahadur, H. Verma, G. Singh, I. B. Obot, and E. E. Ebenso, “Experimental and theoretical studies on inhibition of mild steel corrosion by some synthesized polyurethane tri-block co-polymers,” *Sci. Rep.*, vol. 6, no.

1, p. 30937, Nov. 2016.

[96] Y. Lin, A. Singh, E. E. Ebenso, Y. Wu, C. Zhu, and H. Zhu, “Effect of poly(methyl methacrylate-co-N-vinyl-2-pyrrolidone) polymer on J55 steel corrosion in 3.5% NaCl solution saturated with CO2,” *J. Taiwan Inst. Chem. Eng.*, vol. 46, pp. 214–222, Jan. 2015.

[97] S. A. Umoren, “Synergistic inhibition effect of polyethylene glycol-polyvinyl pyrrolidone blends for mild steel corrosion in sulphuric acid medium,” *J. Appl. Polym. Sci.*, vol. 119, no. 4, pp. 2072–2084, Feb. 2011.

[98] G. Bahlakeh, M. Ramezanzadeh, and B. Ramezanzadeh, “Experimental and theoretical studies of the synergistic inhibition effects between the plant leaves extract (PLE) and zinc salt (ZS) in corrosion control of carbon steel in chloride solution,” *J. Mol. Liq.*, vol. 248, pp. 854–870, Dec. 2017.

[99] S. S. A. El-Rehim, M. A. M. Ibrahim, and K. F. Khaled, “4-Aminoantipyrine as an inhibitor of mild steel corrosion in HCl solution,” *J. Appl. Electrochem.*, vol. 29, no. 5, pp. 593–599, 1999.

[100] V. Ramesh Saliyan and A. V. Adhikari, “Inhibition of corrosion of mild steel in acid media by N′-benzylidene-3-(quinolin-4-ylthio)propanohydrazide,” *Bull. Mater. Sci.*, vol. 31, no. 4, pp. 699–711, Aug. 2008.

[101] I. Felhősi, J. Telegdi, G. Pálinkás, and E. Kálmán, “Kinetics of self-assembled layer formation on iron,” *Electrochim. Acta*, vol. 47, no. 13, pp. 2335–2340, 2002.

[102] Y. Zhu, M. L. Free, R. Woollam, and W. Durnie, “A review of surfactants as corrosion inhibitors and associated modeling,” *Prog. Mater. Sci.*, vol. 90, pp. 159–223, 2017.

[103] N. Ochoa, F. Moran, N. Pébère, and B. Tribollet, “Influence of flow on the corrosion inhibition of carbon steel by fatty amines in association with phosphonocarboxylic acid salts,” *Corros. Sci.*, vol. 47, no. 3, pp. 593–604, 2005.

[104] Y. Gonzalez, M. C. Lafont, N. Pebere, and F. Moran, “A synergistic effect between zinc salt and phosphonic acid for corrosion inhibition of a carbon steel,” *J. Appl. Electrochem.*, vol. 26, no. 12, pp. 1259–1265, Dec. 1996.

[105] B. J. Usman, S. A. Umoren, and Z. M. Gasem, “Inhibition of API 5L X60 steel corrosion in CO 2 -saturated 3.5% NaCl solution by tannic acid and synergistic effect of KI additive,” 2017.

[106] J. Zeng, J. Zhang, and X. Gong, “Molecular dynamics simulation of interaction between benzotriazoles and cuprous oxide crystal,” *Comput. Theor. Chem.*, vol. 963, no. 1, pp. 110–114, Jan. 2011.

[107] N. Palanisami, P. Rajakannu, and R. Murugavel, “Non-covalently aggregated zinc and cadmium complexes derived from substituted aromatic carboxylic acids: Synthesis, spectroscopy, and structural studies,” *Inorganica Chim. Acta*, vol. 405, pp. 522–531, Aug. 2013.

[108] J. Li, C. Yin, and F. Huo, “Development of fluorescent zinc chemosensors based on various fluorophores and their applications in zinc recognition,” *Dye. Pigment.*, vol. 131, pp. 100–133, Aug. 2016.

[109] G. Z. Kyzas, P. I. Siafaka, E. G. Pavlidou, K. J. Chrissafis, and D. N. Bikiaris, “Synthesis and adsorption application of succinyl-grafted chitosan for the simultaneous removal of zinc and cationic dye from binary hazardous mixtures,” *Chem. Eng. J.*, vol. 259, pp. 438–448, Jan. 2015.

VITAE

Name	Aasem Muhammed Nour Zeino
Nationality	SYRIAN
Date of Birth	07/11/1984
Email	aasem.zeino@gmail.com
Address	Chemistry Department, KFUPM, Dhahran, Saudi Arabia

Academic Background:

- **(June 2006)** B.Sc. in Applied Chemistry, Department of Chemistry, Faculty of Science, Damascus University, Syria.

- **(September 2009 - November 2011)** MS. Student at the Department of Chemistry, Faculty of Science, KFUPM, KSA.

- **(February 2012 - November 2017)** Ph.D. student at the Department of Chemistry, Faculty of Science, KFUPM, KSA.